Universitetet i Stavanger

FACULTY OF SCIENCE AND TECHNOLOGY

MASTER'S THESIS

Study program/Specialization: Master of Science in Petroleum Engineering Specialization - Reservoir Engineering	Spring semester, 2019 Open
Author: Yosra Cherif	 (signature of author)

Program coordinator: Merete Vadla Madland Supervisor(s): Edvard Omdal Reidar Inge Korsnes Pål Østebø Andersen	

Title of master's thesis: Water flooding of Eldfisk reservoir cores

Credits: 30 points

Keywords: Chalk Eldfisk reservoir Water weakening Mechanical tests (Hydrostatic test + Creep) Chemical analyses Scanning Electron Microscopy	Number of pages: 99 + supplemental material/other: 1 Stavanger, 21/06/2019

Abstract

Enhanced Oil Recovery (EOR) and the effect of the aqueous chemistry on the mechanical strength of chalk have been extensively studied over the years. This is simply because the stability of the reservoir system is affected by several interdependent factors such as the mineralogical composition, temperature, pressure, and brine ionic composition. For instance, seawater injection in North Sea chalk reservoirs has the ability to decrease the mechanical properties of the reservoir rocks, known as water weakening. This phenomenon leads to compaction which is on one side a significant method for Improved Oil Recovery (IOR) but is on the other side a cause of seabed subsidence. Then, in order to study and separate the effect of specific ions, seawater has been substituted by brines with simpler aqueous chemistry, like NaCl, $MgCl_2$ and $MgCl_2$ combined with $CaCl_2$.

A vast amount of research have been conducted on outcrop chalks to predict the properties of reservoir chalk when exposed to different EOR brines. This is because onshore chalk analogues to that of the North Sea are easily obtainable and less expensive to sample. However, in this study the geo-mechanical behaviour of chalk is investigated by performing a series of preliminary tests on real reservoir chalk sampled from the North Sea. Then, the obtained results are compared with previous test results gained from outcrop chalks.

The mechanical behaviour and the phenomenon known as water weakening of chalk is studied by flooding cores under isotropic stress at 130°C with nonreactive brines such as NaCl and reactive brines like synthetic seawater (SSW), $MgCl_2$, and $MgCl_2$ combined with $CaCl_2$. Chemical- and microscopic analysis were also employed to further investigate the compositional variation of fluids and mineralogical alteration of chalk, and hence study the interplay between chalk and injected fluids referred to as water weakening.

Experimental results show that the chemical effect of 0.219 M $MgCl_2$ or SSW injection into reservoir cores have a significant influence on the mechanical behaviour compared to that observed with 0.657 M NaCl brine. This was clearly noticed from the creep development when changing brines from NaCl to $MgCl_2$ in the first test and to SSW in the second test. These results are in agreement with previous work performed on outcrops. The creep compaction in core flooding experiments was explained by precipitation of secondary Mg-bearing minerals and dissolution of primary calcite.

This work is part of a study showing that results gained from previous studies on water wet outcrop chalks are also valid for reservoir cores thus improving the understanding of reservoir chalk behaviour.

Acknowledgment

Table of Contents

List of Figures

List of Tables

Chapter 1 Introduction

1.1 Background

On the Norwegian Continental Shelf (NCS), several oil and gas fields are producing hydrocarbons from chalk formations. The most known formations are Ekofisk, Tor and Hod of Danian, Maastrichian and Turonian to Campanian ages respectively. These formations host the majority of resources in the North Sea.

Unfortunately, oil and gas recoveries from chalk reservoirs still limited, and production trends are decreasing. A large amount of hydrocarbons originally in place is remained in the reservoirs even though nowadays production strategies are implemented, and this is because of the complexity of chalk. Thus, improving the oil recovery in chalk reservoirs by developing more effective production technologies and finding solutions to increase the recoverable resources in the existing and upcoming chalk fields has been of major interest to the industry and in scientific research. Among different Improved Oil Recovery (IOR) techniques, seawater injection has proven to be a successful measure to provide pressure support and to maximize recovery of hydrocarbons.

The Ekofisk field, as well as many neighbouring fields in the Greater Ekofisk area, were originally produced by pressure depletion in the primary production phase. However due to reduced pore pressure, the overburden load supported by the porous chalk reservoirs increased leading to severe compaction, which in turn was transmitted to the seafloor resulting in several meters of seabed subsidence (Hermansen, Landa, Sylte, & Thomas, 2000; Hermansen, Thomas, Sylte, & Aasboe, 1997; Sulak & Danielsen, 1988; Lawrence W. Teufel, Rhett, & Farrell, 1991).

To provide pressure support and to reduce compaction, seawater injection was implemented. It was a great success and the recovery factor is expected to reach 50% (Sheng, 2010). However, even though the injection process managed to build up the pore pressure, it was recognized that compaction continued (Delage, Schroeder, & Cui, 2008; Sheng, 2010; Sulak & Danielsen, 1988), and seawater injection has shown to have an additional effect which is compaction.

Studies to evaluate the potential of seawater for compaction showed that high compaction rates were observed in reservoir zones experiencing increased water saturation even if the pressure

was kept constant, whereas intervals of the reservoir under re-pressurization or pressure maintenance in the absence of water maintained tiny compaction rates (Hermansen et al., 1997). Compaction is an important drive mechanism affecting the performance of the reservoir and increasing the oil recovery, and it was explained by the chemical interplay between ions in the injected seawater and the rock itself, referred to as "water weakening".

The effect of the chemical composition of injected seawater on mechanical properties of chalk have been extensively investigated (R. Korsnes, Madland, & Austad, 2006; M. V. Madland & Risnes, 2005). During the continuous flooding of non-equilibrium brines such as synthetic seawater (SSW), dissolution and precipitation of minerals take place by the effect of reactive ions that interact with the host rock. As a result, the morphology and texture of the chalk material are changed, thereby the mechanical strength is also affected. Furthermore, a large amount of experiments have been studied to understand the effect of brines with modified chemistry on chalk deformation under creep, meaning under constant stress conditions (M. Madland et al., 2011; Anders Nermoen, Korsnes, Madland, & Hiort, 2015).

In line with water weakening, numerous researches have been conducted to get a better understanding of the relation between the brine composition of injection fluids and the geo-mechanical properties of chalk reservoirs. Yet, most of the studies done previously seem to be performed commonly on onshore outcrop chalks and rarely on reservoir rocks from the North Sea. This is due to shortage of the core material and the high costs of extracting reservoir samples. Also, issues related to core-to-core heterogeneity, cleaning and conservation of the reservoir cores are both difficult and expensive.

Chalk from exposures with a comparable mineralogy, permeability, porosity environment and sedimentary age as reservoir chalk are suited to be used during systematic investigations to understand the mechanical behaviour of reservoir rocks and chemical interactions when different brines are injected. Hence, by selecting the most convenient reservoir chalk substitutes in combination with similar pressure, temperature and fluid composition as found in the reservoir, reservoir conditions can be imitated. For instance, Liège chalk represents a possible mechanical analogue to Ekofisk field (Collin, Cui, Schroeder, & Charlier, 2002; M. L. Hjuler & Fabricius, 2009; Jarvis, 2006) and Aalborg chalk is comparable to Valhall reservoir chalk in terms of geo-mechanical properties (M. L. Hjuler & Fabricius, 2009). Hence, laboratory tests carried out on outcrop chalk research may provide adequate information paramount for further research.

However, prediction of reservoir chalk properties by testing outcrop chalk is not always feasible since the correlation between the pore pressure, effective stress and temperature encountering onshore outcrop chalks is by no means similar to that experienced by reservoir chalks (M. L. Hjuler & Fabricius, 2009). The different diagenetic histories undergone by outcrop and reservoir chalks results expectedly in varying chalk properties. North Sea offshore chalks are deeply buried with depths exceeding 3 km in many places, whereas onshore chalks such as Danish chalks have relative low burial depths ranging from 500 to 750 m (P. Japsen, 1998; P. Japsen & Bidstrup, 1999; P. J. C. Japsen, 2000) as shown in Figure 1.1.
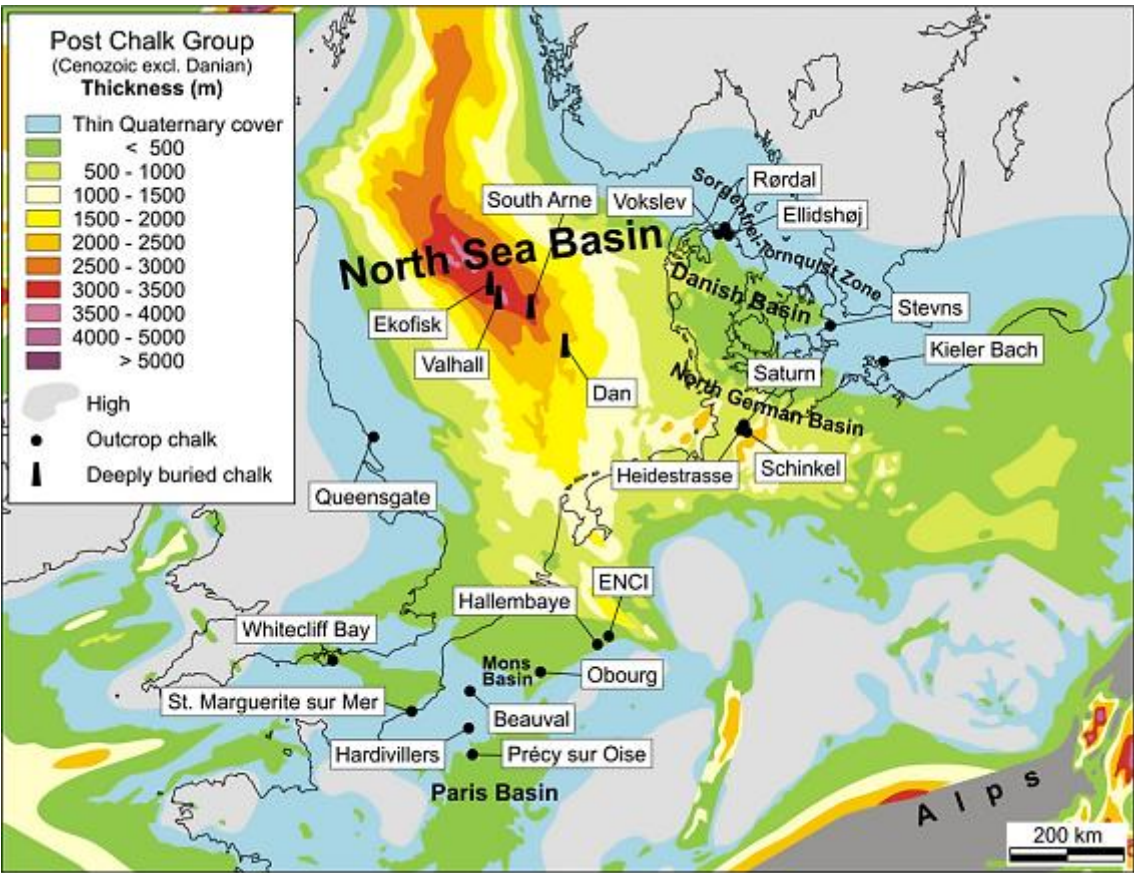
Figure 1.1 Map of the North Sea area showing the present-day burial depths of sampled localities from Engineering properties of chalk (M. L. Hjuler & Fabricius, 2009)

In offshore reservoirs, the effective stress is given by the overpressure related to the weight of the overburden rocks, which results in different degrees of diagenetic alteration. Reservoir chalks display significant mineralogical changes affecting the calcite redistribution, specific surface area, permeability (M. L. Hjuler & Fabricius, 2009), as well as the wettability of the grain surfaces (Mona Wetrhus Minde, 2018a). Furthermore, the presence of hydrocarbons in reservoir chalks combined with overpressuring effects have the ability to delay precipitation and dissolution of calcite and preserve the porosity by delaying the cementation mechanism.

3

Hence, porosity is preserved due to retarded mechanical compaction compared to outcrop chalk (P. Japsen, 1998) . However, this is not always the case on account of cementation.

Selecting right reservoir chalk substitutes during mechanical testing and modelling is quite challenging. It requires understanding and knowledge of characteristics of outcrop chalks and properties of reservoir chalks to be characterized if possible. Awareness and care should also be taken in order to avoid ending up with an outcrop chalk having deviating characteristics. Thus, using actual reservoir cores during testing will enhance the accuracy of prediction of the reservoir behaviour, and eventually contribute to find more efficient and smarter techniques to produce hydrocarbons from future reservoirs.

1.2 Objectives

In this thesis, chalk reservoir cores from the North Sea under hydrostatic stresses are flooded with Synthetic Sea Water (SSW) and simplified brines having the ionic strength of seawater at 130°C to detect deformation of chalk when loaded hydrostatically and during creep. Thus, the primary focus of the present study is to:

- Investigate the geo-mechanical behaviour of Eldfisk reservoir cores during brine injection.

- Understand chemical effects for water weakening of chalk that are in line with the experimental results.

- Study the effect of individual ions by simplifying the aqueous chemistry.

Many experiments at the University of Stavanger have been performed on outcrop chalk previously under isotropic conditions using triaxial cells at high temperature of 130°C. This allows to evaluate the feasibility of studies on onshore chalks when comparing to reservoir chalks. The last objective is then to:

- Compare geo-mechanical behaviour of tested reservoir cores with previous results gained from onshore outcrop chalks.

1.3 Outline of the thesis

In Chapter 2, a literature review of North Sea reservoir chalk is covered. Then, characteristics of Eldfisk field and challenges related to its production are highlighted. Basic concepts of rock mechanics and previously proposed mechanisms for rock-fluid interactions are also presented.

Chapter 3 covers the experimental methodology of performed geo-mechanical and chemical tests. In this chapter, a detailed description of experimental procedures and the instruments in use is followed by data processing and calculation methods.

Experimental results for each test are displayed in Chapter 4. The chalk geo-mechanical behaviour of each core is studied during hydrostatic loading- and creep phases. Besides, the analysis of chemical compositions of effluents and analysis of flooded chalk material are exhibited for further discussion.

Discussion of the obtained results in terms of chalk geo-mechanical behaviour and chemical interactions with injected brines is given in chapter 5. Last but not least, concluding remarks are presented in chapter 6 and recommendation for future work are listed in chapter 7.

Chapter 2 Literature and Theory Review

2.1 Chalk reservoirs

The main hydrocarbon deposits in the central and southern part of the North Sea (Norway, United Kingdom, and Denmark) are present in Chalk reservoirs. Hydrocarbon fields in the North Sea are located over thick areas of Kimmeridge and Oxford clay source rocks on growing structures that induced fractures in chalk. Thus, hydrocarbons were able to enter the pore space in chalk reservoirs through fractures due to buoyancy and pressure effects (Hardman, 1982).

Geology categorize chalk of the North Sea as a fine-grained, sedimentary rock belonging to the carbonate rock family with a major calcite content and a minor content of other minerals that ranges from few and up to 15 weight percent depending on age, degree of diagenesis and location (M. L. Hjuler & Fabricius, 2009).

The chalk matrix is mainly composed of the skeletons originating from planktonic algae that lived in pelagic, oceanic environment. The skeletal debris consists of a major constituent being coccoliths and a minor occurrence of foraminifera, calcite spheres, and microfossil fragments (Hardman, 1982).

Coccoliths are typically of the size 2 to 15 µm, and each coccolith composed of hundreds to thousands of calcite crystals with sizes ranging between 0.2 and 3µm. A typical microscopic picture of chalk grain structure is presented in Figure 2.1. This Scanning Electron Microscope (SEM) image shows the mixed composition of more or less intact skeleton fragments. It can also be seen that the dimensions of individual grains are noticeably smaller than the dimensions of the pores.
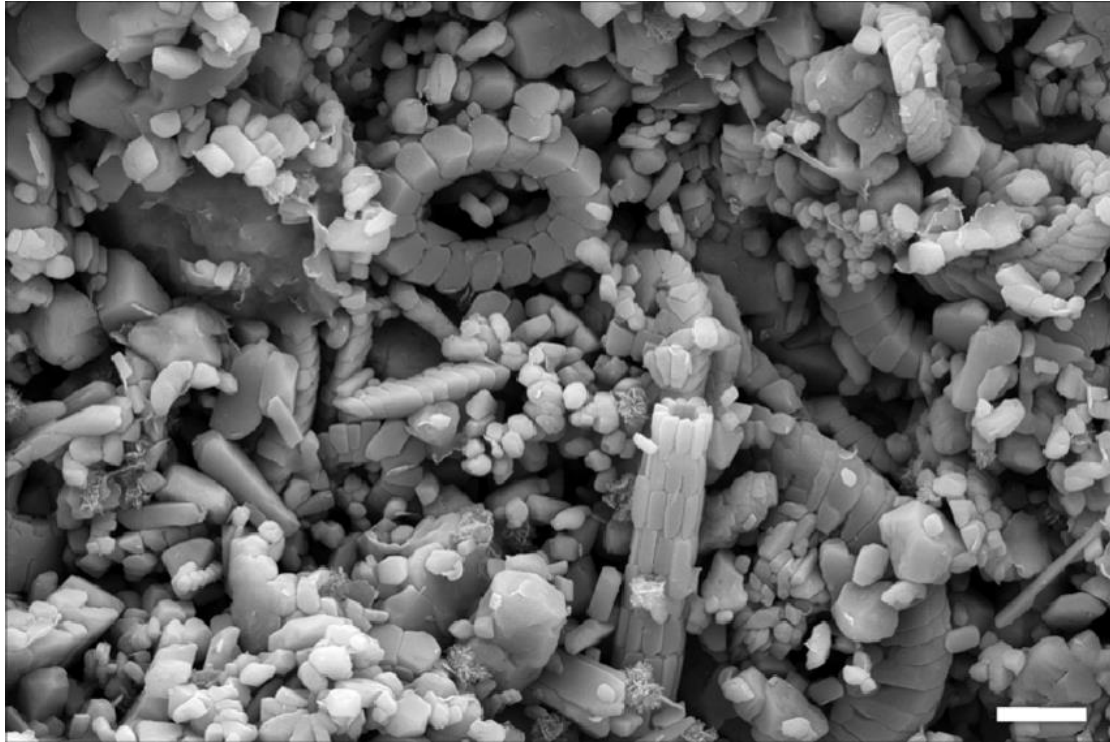
Figure 2.1 Scanning electron microscope (SEM) of chalk from Liège (Wang et al., 2016)

The relatively open structure of the chalk material may clarify the high porosity of chalk reservoirs. A typical nannofossil chalk have an initial porosity up towards 70% (P. A. Scholle, 1977) and this is commonly reduced to values between 10 and 50% (M. L. Hjuler & Fabricius, 2009; Peter A. Scholle & Kinsman, 1973), depending on burial conditions and mechanical and chemical compactions during and after burial of microfossils. Chalk reservoirs at great depths may remarkably preserve their high porosities. According to Scholle (1977), these unexpected porosities may be the result of the retardation of mechanical and chemical compaction processes. Overpressured hydrocarbons reduce the differential stresses and thus maintain the porosity physically. In addition, oil that is introduced into the rock at early stages and its high saturation may exclude water and hence inhibit chemical compaction.

Despite the high porosity of chalk reservoirs, the matrix permeability is generally low and it is ranging from 1-10 mD in the North Sea (Lykke, 2005). Fractures induced by diapirism, fault movement, or folding play therefore an important role in oil migration to hydrocarbon traps.

2.2 Eldfisk field and production challenges

Eldfisk is one of the largest fields in the Norwegian Continental Shelf (NCS) and the second largest of the three producing fields in the Ekofisk area. Eldfisk field is located in the southern part of the Norwegian sector in the North Sea, approximately 10 kilometres south of the Ekofisk field, not far from the British and Danish sectors as shown in the location map in Figure 2.2, and it has a water depth between 70 and 75 meters (NPD factpages, Eldfisk, 2019).
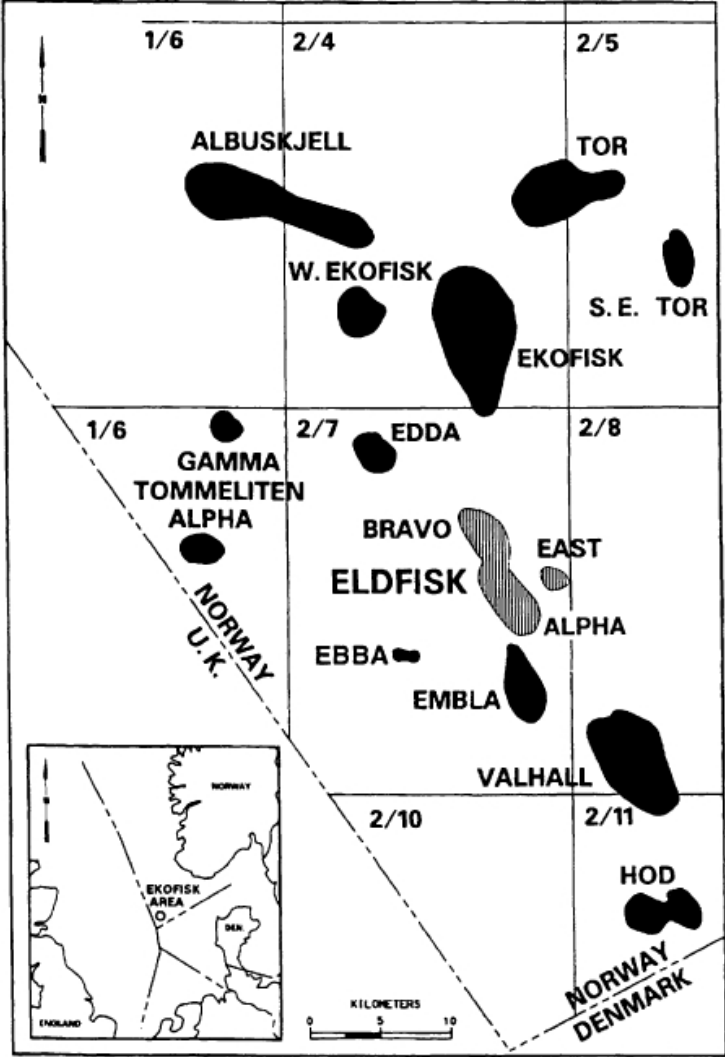
Figure 2.2 Location map of Eldfisk Field in relation to the Greater Ekofisk area and the southern Norwegian North Sea (Stoddart et al., 1995)

As a result of compression of a regional fault, Eldfisk field is contained in a salt-related anticline consisting of a northern structure (Bravo) and a southern structure (Alfa) (Zhu et al., 2012). Eldfisk field produces from chalk layers belonging to Ekofisk, Hod, and Tor formations of early Palaeocene and late Cretaceous ages. The Bravo structure produces only from Ekofisk and Tor formations, however Alfa structure is productive in all three reservoirs (Wade, Hough, Harrington, Valdal, & Pedersen, 1998).

The reservoirs rocks, located at depths of 2700 to 2900 meters, have porosities ranging from 17% in the Hod formation up to 45% in the Tor formation. Matrix and effective permeabilities are varying as well between 1 and 3 md and between 1 and 15 md respectively (Wade et al., 1998). The effective permeability is much higher than the matrix permeability due to the natural fracture system that allows the reservoir fluid content to flow more easily (Sulak & Danielsen, 1988).

According to a diagenesis study carried out on Eldfisk chalk samples from the upper Tor formation belonging to the Bravo structure (Madsen, 2010), the chalk is usually almost pure carbonate with a calcite content between 96 and 97%. The non-carbonate content consists mainly of quartz, kaolinite and minor occurrence of dolomite, feldspar, pyrite, fluorite, illite-smectite, fluor-apatite and crandelite. However, intervals with high non-carbonate content, up to 12%, may be found in the studied well. These intervals in the Eldfisk field contain abundant quartz and kaolinite minerals Figure 2.3, that probably derive from weathering products such as quartz, kaolinite, feldspar and smectite from the nearby Baltic Shield (Kennedy, Brooks, & Glennie, 1987). The porosity in quartz- and kaolinite rich intervals have been investigated using neutron- and density logs, and it have been estimated to range from 20 to 25% (Madsen, 2010)
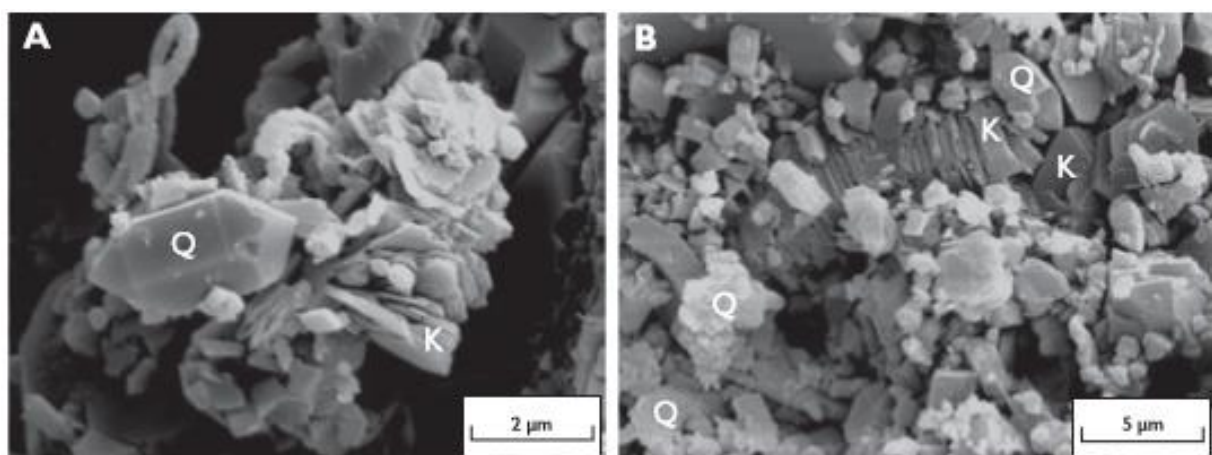
Figure 2.3 Scanning electron microphotographs of chalk samples from the Eldfisk field from the Tor Formation showing kaolinite (K) and quartz (Q) content (Madsen, 2010)

The Eldfisk field was discovered in 1970, approved for development in 1975 and started production in 1979. Ever since that time, Eldfisk has been under production for almost four decades until now. The Eldfisk field, similar to many fields in the Norwegian North Sea, was originally produced by pressure depletion as the primary drive mechanism. However, due to reduced pore pressure caused by hydrocarbon production, the reservoir experienced severe compaction, which in turn resulted in several meters of seabed subsidence. Then in 1999, water injection was implemented through horizontal wells to provide pressure support to the reservoir, in order to compensate for the additional surface subsidence and reduce compaction (NPD factpages, Eldfisk, 2019). Even if the injection process managed to build up the pore pressure and reduce the compaction rate, the compaction continued, and this is probably due to the water weakening effect induced by water injection at later stages of the field life.

2.3 Mechanical concepts and definitions

2.3.1 Stress

Stress is the force acting on a given area, and when it acts within a deformable rock, it causes the change of its size or shape leading consequently to deformation. Assuming that F is the force acting through a cross-section, then the stress σ is defined as:

$$\sigma = \frac{F}{A} \tag{2.1}$$

where

σ Stress, $Pa = {N}/{m^2}\ or\ psi$

F   Force, N

A   Cross-section area, m^2

The force acting on a surface can be decomposed into two components. One component is normal to the cross-section area, denoted F_n, and the other component is tangential to the plane of the area, F_p. Thus, there are two types of stresses acting on a surface, which are the normal stress and the shear stress. The normal stress arises from the normal net force as expressed by equation (2.2).

$$\sigma_n = \frac{F_n}{A} \qquad (2.2)$$

where

σ_n Normal stress, $Pa = {N}/{m^2}\ or\ psi$

F_n Force, N

A   Cross-section area, m^2

The normal stress can be tensional, also said extensional, because it stretches or lengthens the rock. It can also be compressive tending to squeeze the rock material by collinear normal forces acting in opposite direction towards the concerned cross-section area as illustrated in Figure 2.4. The sign convention states that compressive stresses are represented by positive values in rock mechanics.
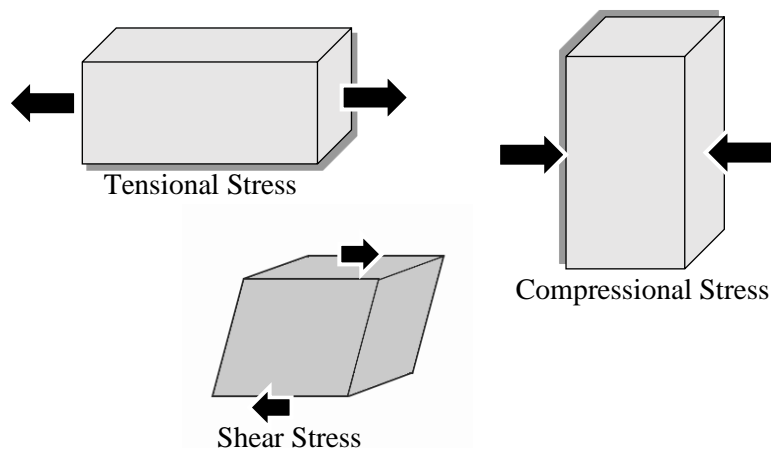
Figure 2.4 Illustration of differential stresses

As mentioned previously, the stress is not only normal, but it can also be shearing. This is when the stress is acting parallel to the plane due to tangential net force. Shear stress tends to cause deformation of the rock by slippage and translation. Equation (2.3) is a mathematical expression for shear stress.

$$\tau = \frac{F_p}{A} \qquad\qquad (2.3)$$

where:

τ Shear stress, $Pa = {N}/{m^2}\ or\ psi$

F_p Parallel force component, N

A   Cross-section area, m^2

When tensional, compressional, or shear stresses occur, the stress is not equal from all directions and is greater in some directions than others. Stress is then said to be differential (deviatoric). Rocks are in many cases subject to differential stresses because of tectonic forces. In other cases, rocks experience equal stress exerted from all directions as shown in Figure 2.5. This kind of stress is known as isotropic or hydrostatic stress.
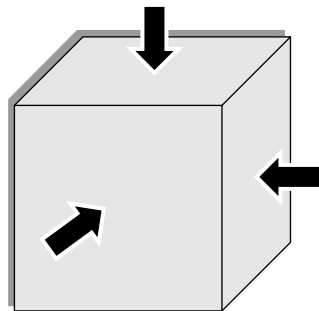
Lithostatic Stress

Figure 2.5 Illustration of hydrostatic stress condition

2.3.2 Effective stress

The way the force is distributed and transferred in rocks is an unpredictable and complicated physical process. One of the major factors leading to the complexity of stress distribution is the fact that rocks are porous media consisting of a cross between solids and fluids within the pores. Solids made up by the matrix grains of the rock carry the applied load alone. Although, fluids are commonly present in the pore space of the rock, and they provide a hydraulic pressure which balances the exerted loads. The relationship between the total stress applied by an external load and pore pressure is then defined in terms of effective stress. The concept of effective stress was proposed by Terzaghi (1923) based on studies of the behaviour of soil exposed to stresses exerted externally and to pressure within the pore volume.

The effective stress was then defined as the stress that the matrix of the rock is subject to and it was expressed mathematically as the difference between the total external stress and the pore pressure.

$$\sigma' = \sigma - P_p \tag{2.4}$$

where:

σ' The effective stress, $Pa = {}^N/_{m^2}$ or psi

σ The total stress, $Pa = {}^N/_{m^2}$ or psi

P_p Pore pressure, $Pa = {}^N/_{m^2}$ or psi

The effective stress of a porous material was further studied by M. A. Biot (1941) and Skempton (1961). A correction factor α for the pore fluid pressure was then introduced as represented in equation (2.5), thus the total stress is reduced by a fraction of the pore pressure (M. A. Biot, 1941; Charlez, 1991).

$$\sigma' = \sigma - \alpha * P_p \tag{2.5}$$

α is also called Biot's factor, effective stress coefficient as well as poroelastic coefficient. According to M. Biot and Willis (1957) the correction factor depends on the poroelastic behaviour of the rock. In other words, it depends on the stiffness of the rock matrix. Besides, a study performed on chalk (Lawrence W Teufel & Warpinski, 1990) revealed that the effective stress law is linear and that Biot's coefficient decreases with decreased porosity. In this study, it has been shown that for chalk with porosities ranging from 15-36% there is a decrease in the Biot's coefficient from unity to values around 0.8.

2.3.3 Strain

When rocks deform in response to external forces, they are said to be strained. Strain is the change in the original rock's shape, size or volume when subjected to hydrostatic or differential stresses. Strains in a rock sample are then calculated from the measured linear and volumetric deformations with reference to the original dimensions according to equations (2.6), (2.7) and (2.8).

$$\varepsilon_{ax} = -\frac{L - L_0}{L_0} = \frac{\Delta L}{L_0} \qquad (2.6)$$

where:

ε_{ax} Axial strain, dimensionless

L Length after deformation, m or ft

L_0 Original length, m or ft

ΔL Change in length, m or ft

$$\varepsilon_{rad} = -\frac{D - D_0}{D_0} = \frac{\Delta D}{D_0} \qquad (2.7)$$

where:

ε_{rad} Radial strain, dimensionless

D Diameter after deformation, m or ft

D_0 Original Diameter, m or ft

ΔD Change in diameter, m or ft

$$\varepsilon_{vol} = -\frac{V - V_0}{V_0} = \frac{\Delta V}{V_0} \qquad (2.8)$$

where:

ε_{vol} Volumetric strain, dimensionless

V Volume after deformation, $m^3 or$ ft^3

V_0 Original volume, $m^3 or$ ft^3

ΔV Change in volume, $m^3 or$ ft^3

During mechanical tests, the unit volume change of a cylindrical test specimen is calculated from axial and radial strains by equation (2.9) (Anders Nermoen et al., 2015).

$$\varepsilon_{vol} = \varepsilon_{ax} + 2\varepsilon_{rad} + 2\varepsilon_{ax}\varepsilon_{rad} + \varepsilon_{rad}^2 + \varepsilon_{ax}\varepsilon_{rad}^2 \qquad (2.9)$$

2.3.4 Stress-strain relationship

As defined in section 2.3.3, strain is the deformation of rocks as response to applied stresses. As rocks are subjected to increased stress, they pass through three stages of deformation: Elastic, ductile and brittle deformation as depicted in Figure 2.6.
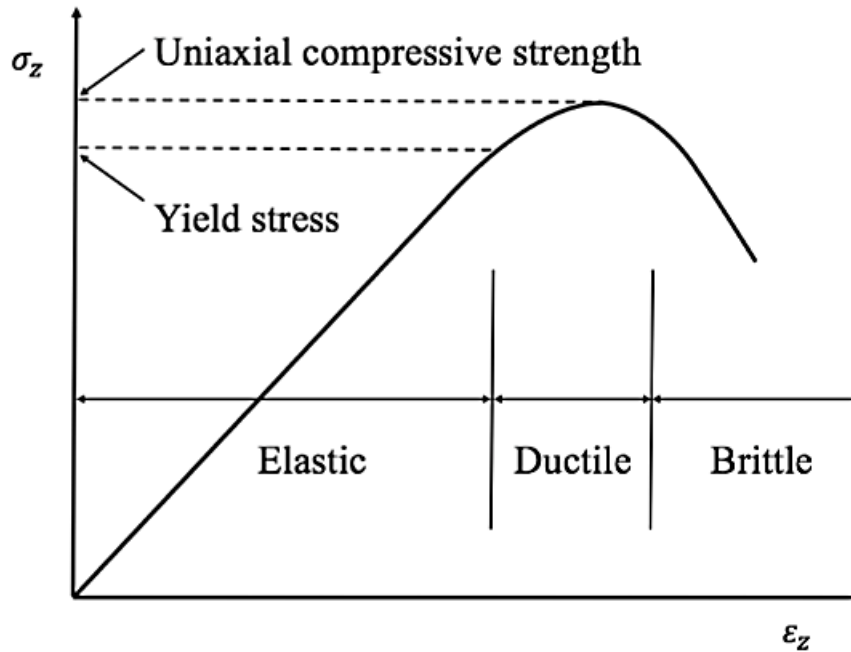
Figure 2.6 Typical stress-strain curve during uniaxial or triaxial test (Fjaer, Holt, Horsrud, Raaen, & Risnes, 2008)

At the first deformation stage, the rock is strained elastically meaning that it may be deformed enough that its size or shape changes, but the change is not permanent. Thus, the strain is reversible, and the rock would tend to return to its original state upon stress relief. According to Fjaer et al. (2008), axial strain (ε_a) is proportional to stress within the elastic deformation stage, and the stress-strain relation can be expressed by Hook's law as:

$$\sigma = E * \varepsilon_a \qquad (2.10)$$

E is an elastic modulus known as Young's modulus. It measures the stiffness of the rock, more specifically it estimates the rock's ability to resist deviatoric loading. For isotropic loading states, where all stresses from all directions are equal, another important elastic modulus is introduced, which is the bulk modulus (K). It is the constant of proportionality between the hydrostatic stress (σ_{conf}) and volumetric strain (ε_v) obeying Hook's law as:

$$\sigma_{conf} = K * \varepsilon_v \qquad (2.11)$$

When sufficiently high stresses beyond the yield point are exerted, rock's deformation becomes plastic, and the deformation is said to be ductile. The yield point denotes the stress level beyond which permanent deformations will occur. Thus, upon the ductile deformation stage, rocks undergo irreversible changes and they will no longer return to their original states. However, they keep their ability to support loads.

The third stage of deformation is the brittle deformation. When the limit of the ductile region is exceeded under deviatoric stress states, the rock's ability to resist stress decreases significantly leading to increased strain and fracturing or failure consequently.

2.3.5 Time-dependent deformation

Creep is a time dependent deformation which occurs in a material when it is under constant stress. Creep may take place in both dry and saturated rocks since it originates from viscoelastic effects in the solid framework (Fjaer et al., 2008). Several factors related to compaction of chalk and management of reservoirs that give rise to creep have been reported. For instance, creep associated with chemical water weakening (R. Korsnes et al., 2006).

Creep development with time, represented in Figure 2.7, is divided into three phases.

- Primary creep or transient creep: It is characterized by an initial period of a rather high rate of strain followed by a decreasing deformation rate. According to Fjaer et al. (2008), when the loaded stress is decreased to zero, the deformation will reduce to zero as well. Hence, the deformation of the material is reversible and is related to creep in the elastic state.

- Secondary creep, also called steady state creep: It is when the strain rate is relatively stable. In this phase, the deformation is permanent since materials are not able to return to their original shapes even if the applied stress is reduced to zero.

- Tertiary creep or accelerating creep: It occurs under deviatoric stress conditions, and it is characterized by an accelerated strain rate causing rock failure. This behaviour is generally associated to high shear stresses. Tertiary creep is not common for chalk rocks due to their high compressibility (Omdal, 2010). Indeed, large amount of creep is related to chalk porosity reduction and hence hardening, which makes the material more stable towards shear stress.
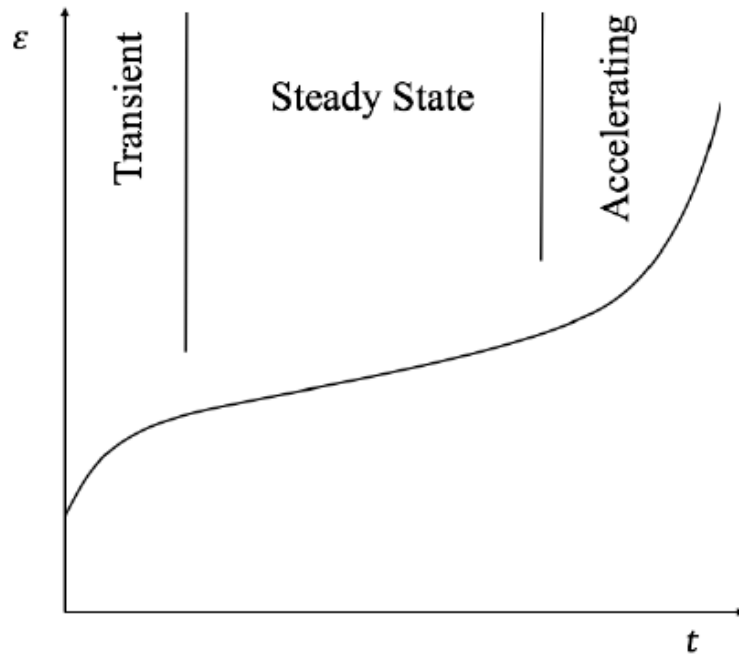
Figure 2.7 strain versus time for a creeping material (Fjaer et al., 2008)

Creep has a stress-dependent behaviour i.e. it depends on the stress magnitude. For low stresses, the rock becomes stable after a period of primary creep (Fjaer et al., 2008). For moderate stresses, the material is less stable, and it undergoes all creep phases. Whereas, the material may fail after rapidly running through all three creep phases when it is subjected to high stresses. Creep is also a molecular process with a time scale that is temperature dependent. The process accelerates generally with temperature according to the same reference.

2.4 Failure mechanics

As rocks are exposed to relatively large stress loads, they may deform in a permanent and irreversible manner, loose their ability to carry loads, and eventually fall apart. Failure of reservoir rocks is considered as the origin of several serious problems like seabed subsidence, production of solids and borehole instability. Hence, to ensure continuous safe and efficient production operations, it is of great significance to predict and prevent the conditions under which rocks are likely to fail.

2.4.1 Failure modes

In chalk, the rock material is sensitive to applied stress due to its microstructure composed of intact coccoliths and calcite platelets that are arranged in a non-uniform structure. Moreover, the grain contacts that carry the loads may consist of solid-solid contacts, or may be purely

frictional (Risnes, 2001). Thus, the complex structure of chalk and the irregularities at the calcite surfaces give rise to failure such as shear failure, pore collapse, and tensile failure.

Shear failure is regarded as the basic failure mechanism during uniaxial or triaxial tests. It occurs when the shear stress exceeds the shear strength of the rock. Eventually, a fracture will form along the failure plane, and friction will develop as the two sides of the fracture move relative to each other as illustrated Figure 2.8.
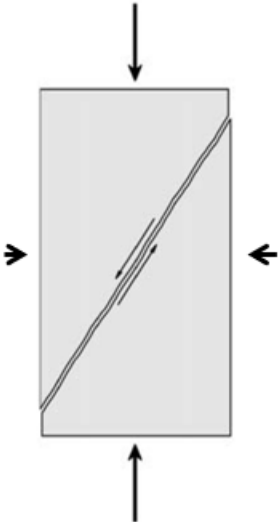
Figure 2.8 Shear failure (Fjaer et al., 2008)

Shear failure under different stress conditions may give rise to other failure modes such as pore collapse. Mechanically, chalks with high porosities act as frictional material which fails in shear failure mode. Yet, the open structure of the chalk matrix, where the dimension of the pore spaces is greater than the size of the grains, promotes another failure mechanism, referred to as pore collapse. When chalk grains are compressed, they may loosen or break and then be forced into the pore space, resulting in closer packing as illustrated in Figure 2.9.
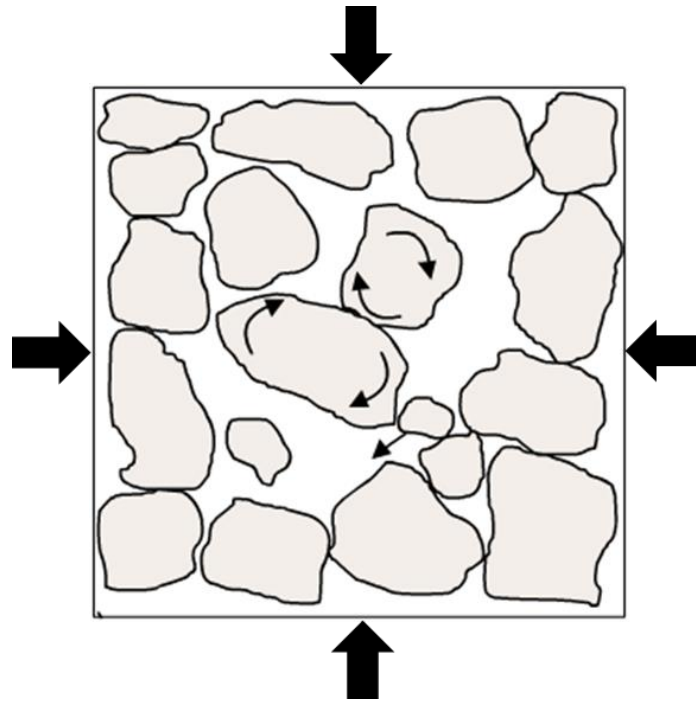
Figure 2.9 Grain reorientation due to excessive compressive stresses resulting in a closer packing modified after (Fjaer et al., 2008)

Even if no macroscopic shear stresses are present under pure isotropic loading, pore collapse still can occur. At the microscopic level, this is due to local excessive shear forces between grains and grain contacts caused by grain sliding possibly when the bonds are broken or due to sliding on frictional contact (Risnes, 2001). Thus, pore collapse may be considered as distributed shear failure within the rock. This failure mechanism may also take place under non-hydrostatic loading conditions (Fjaer et al., 2008), and under both stress conditions hydrostatic and non-hydrostatic, it causes permanent damages by reducing the stiffness of the rock and promoting yielding of chalk.

Tensile failure is also another failure mode initiated by shear failure. It occurs when excessive tensile stress exceeds the tensile strength, which is a characteristic property of the rock (Fjaer et al., 2008). As a result, the rock splits along the fracture planes that are developed by pre-existing cracks. The tensile strength is then strongly affected by the presence of fractures in the rock. The tensile strength of most sedimentary rocks is relatively low, roughly a few MPa or less (Lockner & constants, 1995), and it is even assumed to be zero in various applications.

2.5 Possible water weakening mechanisms

2.5.1 Physical effects

Capillary forces arise from the combined effect of fluid-surface tension at partially saturated grain surfaces and the presence of immiscible wetting and non-wetting phases in the pore throats. Capillary forces have been regarded as one of the most important mechanisms of water weakening in chalk. One explanation is that water, at low saturations, forms a capillary meniscus which induces an apparent cohesion in form of bridges between chalk grains as illustrated in Figure 2.10.
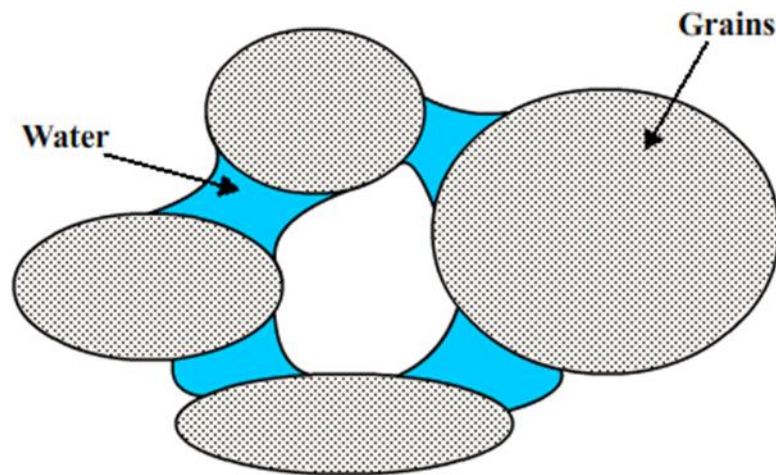
Figure 2.10 Chalk grains hold together by capillary forces modified after (Risnes, Flaageng, science, & technology, 1999)

When chalk is either saturated with oil or dry, assuming that a dry chalk still contains some water, the capillary bonds will retain the strength of the rock material. However, when the water saturation is increased such that it reaches a threshold value, the capillary menisci collapses and thus the capillary forces disappear which results in weaker chalk (Gutierrez, Øino, Høeg, & Engineering, 2000).

Yet, it has been shown (Risnes et al., 1999; Risnes, Haghighi, Korsnes, & Natvik, 2003; Risnes, Madland, Hole, Kwabiah, & Engineering, 2005) that upon introduction of other fluids, such as methanol or glycol mixtures, chalk becomes considerably stronger than when it is water saturated. Methanol and glycol are miscible with water in all proportions, thereby there will be no capillary forces which provide contribution to strengthen the rock. This indicates that

capillary forces can only play a minor role in chalk-fluid interactions and it is not the only mechanism in explaining water weakening.

2.5.2 Physio-chemical effects

Several physio-chemical effects have been considered as possible mechanisms for water weakening of chalk, one of which is adsorption (Risnes et al., 2005). Water have the ability to change the surface properties of chalk by adsorption into the layers of the grain surface. Due to adsorption, the overlap of charged layers induces electrostatic potentials in the diffusive double layer. Then these potentials set up disjoining pressures in the intergranular contacts leading to altered adhesive van der Waals forces (M Megawati, Hiorth, Madland, & engineering, 2013). Adsorption of surface-active ions present in injected brines give rise to increased compaction rates (A Nermoen, Korsnes, Haug, Hiorth, & Madland, 2014) and yielding at lower effective stresses compared to dry or oil-saturated chalks (Liteanu, Spiers, & De Bresser, 2013) by reducing the internal friction and letting the grains to slide and reorganize more freely (Anders Nermoen et al., 2015).

Risnes et al. (2003), studied the effect of concentrated brines on chalk-fluid interactions when changing the ion concentration of the pore fluid, and suggested eventually another key parameter within the physio-chemical effects, which refers to the water activity.

2.5.3 Chemical effects

Compaction behaviour of chalk reservoirs is not inferred solely from physical and physio-chemical effects, contrariwise, the chemical effects should be taken into account (Bjørlykke, 2014; Bjørlykke, Høeg, & Geology, 1997; Croize, Renard, & Gratier, 2013; Hellmann, Renders, Gratier, Guiguet, & Crerar, 2002). Newman (1983) concluded that the water chemistry of the pore fluid can dramatically affect the mechanical strength of chalks. This was attributed to the difference in the ionic composition of the original reservoir fluid and the injection brine that is not in chemical equilibrium with chalk. Equilibrium chemistry is concerned with a closed system that have reached a balanced condition termed thermodynamic equilibrium after that different chemical reactions have occurred (Omdal, 2010). Assuming that formation water is in chemical equilibrium with the reservoir chalk, then introducing a new brine having a different ionic composition will induce chemical reactions until new equilibrium is established.

Dissolution-Precipitation

In a mechanical study by Newman (1983), oil saturated chalks under stress did not undergo enhanced compaction when flooded by equilibrium formation brine. However, the reservoir cores experienced immediate compaction when non-equilibrium seawater was injected. The main conclusion from this study was that compaction is linked to mechanical failure by dissolution of calcium carbonate at low stresses and to dissolution and pressure solution at elevated stresses.

Experiments on chalk cores exposed to either artificial Ekofisk formation water or seawater-like brines with four times the concentration of sulphate at 130°C (Heggheim, Madland, Risnes, Austad, & Engineering, 2005), showed that chalk samples saturated with modified seawater were 20-25% mechanically weaker than those saturated with artificial Ekofisk formation water. The water weakening of chalk was interpreted in terms of dissolution/precipitation and the chemical nature of the thin water film close to the intergranular contacts.

More recent studies have been performed at the University of Stavanger in attempt to highlight the impact of chemical aspects in term of dissolution/precipitation on the mechanical behaviour of chalk (Hiorth, Cathles, & Madland, 2010; Hiorth, Jettestuen, Cathles, & Madland, 2013; M. Madland et al., 2011; M. Madland et al., 2008; M. Megawati, Madland, & Hiorth, 2015). Experimental results pointed towards the precipitation of new magnesium-bearings minerals and the dissolution of calcite in chalk cores exposed to magnesium-rich brines. Dissolution and precipitation in chalk flooded with Mg-rich brines can be described by the following reactions:

$$CaCO_3(s) \leftrightarrow Ca^{2+} + HCO_3^- - H^+ \qquad (2.1)$$

$$MgCO_3 \leftrightarrow Mg^{2+} + HCO_3^- - H^+ \qquad (2.2)$$
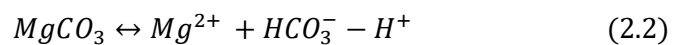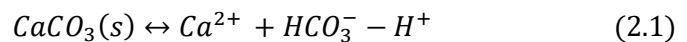
The mechanical properties of chalk are influenced by the morphological changes induced by the precipitation and dissolution processes. To specify, the mechanical friction is affected by the preferential dissolution of calcite in the granular contacts that are under high stress (Megawati Megawati, 2015a). As the grains are displaced by sliding and rotating, they lead to a local collapse (Powell & Lovell, 1994). However, when new minerals precipitate, the resistance of the frictional chalk material against mechanical deformation increases on a long-term perspective due to increased intergranular friction (Megawati Megawati, 2015a)

In studies by Reidar Inge Korsnes (2007), it is reported that the chemical water weakening of chalk subjected to seawater is likely to be associated with the substitution process of calcium ions at the chalk surface by magnesium ions from seawater in the presence of sulphate. He also investigated the effect of temperature on the mechanical weakening by seawater (Reidar I Korsnes et al., 2008), and the laboratory tests documented that magnesium ions were able to displace calcium ions from the calcite grains at high temperatures.

However, the substitution process decreases with decreased temperature as the affinity of calcium towards chalk is higher than that of magnesium ions at ambient temperature (R. Korsnes et al., 2006a). Moreover, core flooding experiments with synthetic seawater at high temperatures as 130°C (R. Korsnes et al., 2006), showed that the mechanism in focus affected the mechanical properties of chalk significantly in the presence of sulphate.

At the natural pH, due to the electrostatic forces and the positive surface charge, sulphate ions are adsorbed to the inter-grain contacts as illustrated schematically in Figure 2.11. This process is intensified at high temperature since the affinity of sulphate towards the chalk surface increases with temperature, and the affinity increases even more significantly beyond 100°C (Strand, Høgnesen, & Austad, 2006).

Moreover, it have been confirmed that magnesium and sulphate make up ion-pairs in aqueous solutions at elevated temperature (Carlberg, 1973). Similarly, the reactivity and affinity of magnesium ions towards the chalk surface and sulphate ions increases with increased temperature as suggested by the high exothermic hydration reaction of magnesium and the partly dehydrated ion (Reidar I Korsnes et al., 2008). Thus, substitution reactions necessitate the presence of sulphate. Another important conclusion drawn from the performed studies, was that ion substitution influences the mechanical strength of chalk considerably, and that a possible explanation for the chalk weakening induced by the chemical effect is the size difference between magnesium and calcium which engender structural changes in the intergranular contacts during substitution process.
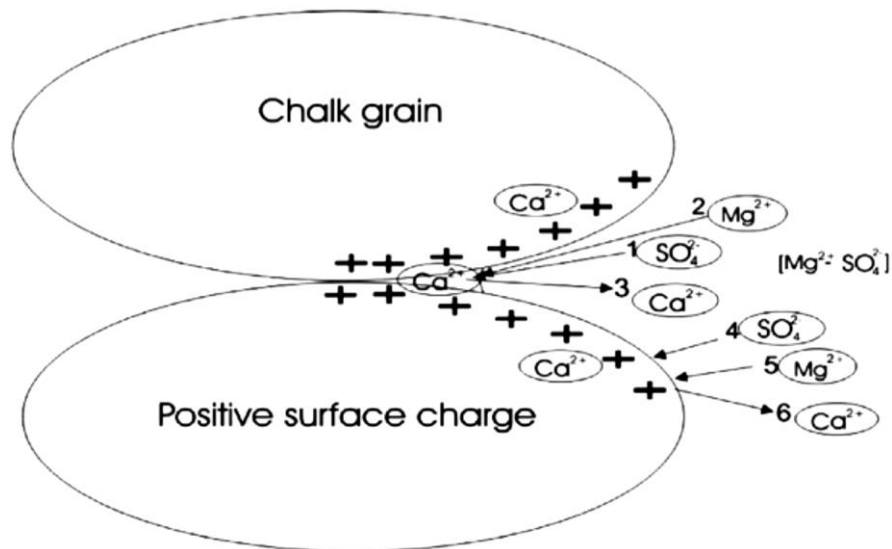
Figure 2.11 Substitution of Mg^{2+} with Ca^{2+} in the presence of SO_4^{2+} (R. Korsnes et al., 2006)

Pressure solution

Pressure solution in chalk was another mechanism proposed to explain the water weakening effect (Croize et al., 2013; Risnes et al., 2003; Risnes et al., 2005). Pressure solution occurs at the grain contacts, and it is defined as the enhanced dissolution of calcite in water that is caused by the additional stress on the grains. Hellmann et al. (2002) reported that time-dependent creep during long-term experiments is related to pressure solution.

Anders Nermoen et al. (2016) pointed out that stress driven dissolution is reduced with time. As illustrated in Figure 2.12, initially, grain contact areas are small relative to the total area and the external stress is distributed evenly over the rock surface. Then, when the contact stresses that are transmitted through the granular package get larger, the solid-solid contact areas increase accordingly due to localized dissolution. Further, as the grain contacts develop, the contact stresses will decline leading to reduced pressure solution effects with time.

$$\sigma_p = \frac{F}{A_{tot}}$$

External stress evenly distributed

Initial stress through grain contacts

Stress through evolved grain contacts

Stressed contacts

Dissolution at grain contacts

(a)   (b)   (c)
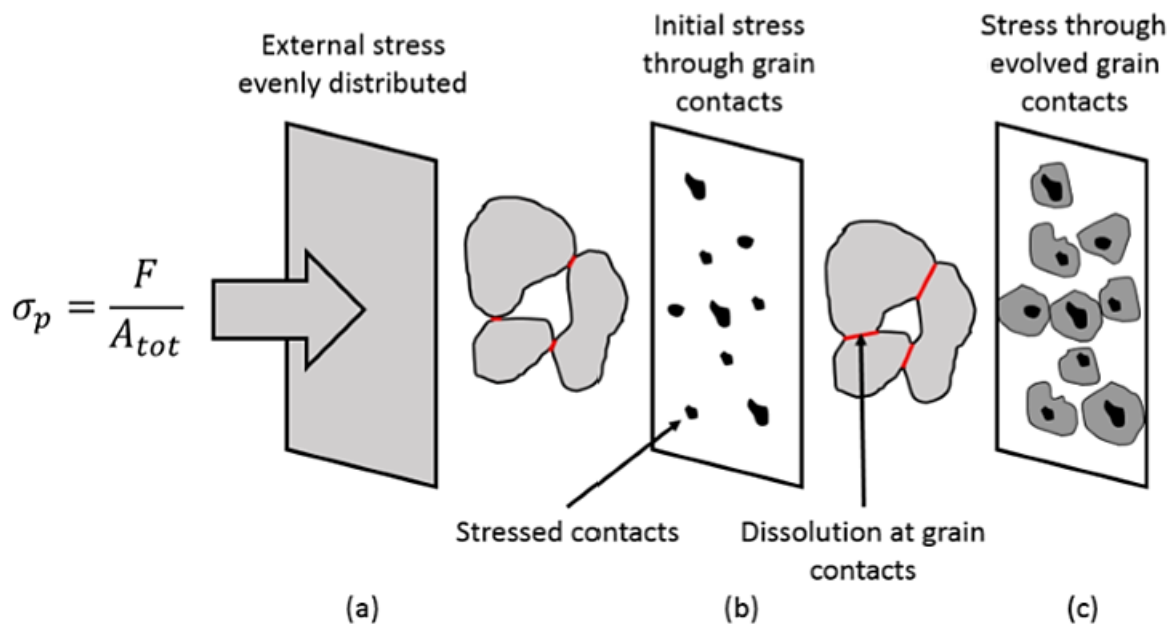
Figure 2.12 Schematic illustration of pressure solution (Anders Nermoen et al., 2016)

Chapter 3 Experimental Methodology

3.1 Core and brine preparation

3.1.1 Core sample preparation

The chalk samples from the Eldfisk field were drilled, cored and machined by an external handling contractor. Then, the test samples were brought to the laboratory where they have been prepared to be used in the tests.

To prevent the cores with fractures from breaking down when being cut, a shrinking sleeve were shrunk around the plug using a heating gun (Figure 3.1). Then, the cores were cut from the lower and upper ends to obtain parallel end faces using Struers Discotom-5 cutting machine displayed in Figure 3.2. After being cut, the dimensions were measured, and when it has been shown that the cores were not cut to have perfectly parallel ends because of the offset of the diamond saw caused by the hardness of the core, the dimensions were corrected by means of DELTA LF-350 grinding machine (Figure 3.3). Each end piece of the samples has been stored to be compared with the tested material.

Figure 3.1 Heating gun and shrinking sleeve   *Figure 3.2 Core cutting machine*   *Figure 3.3 Grinding machine*

A general rule of thumb in petroleum application, especially deviatoric testing, implies that the core length is twice the diameter (Fjaer et al., 2008). However, this requirement has not been met for this study because the received cores have limited lengths.

In this work, average core diameters are 37.93 and 37.98 mm with lengths of 52.40- and 53.00-mm. Table 3.2 illustrates the core diameters measured from the inlet, middle and outlet of the core. When core shaping process was finished, the cores were put in a heating chamber at 90°C to dry until the mass becomes constant before further porosity measurements. The drying conditions do not affect the calcite crystals (MacDonald, 1956).

Table 3.2 Measured diameters of the cores

Sample	E_2			E_3		
D_{inlet}	37.90	37.90	37.85	37.94	37.98	37.98
D_{middle}	37.94	37.99	37.95	37.98	37.94	37.97
D_{outlet}	37.92	37.97	37.96	37.99	38.01	38.03
$D_{average}$	37.93			37.98		

3.1.2 Fluids

Five different fluids have been used during the experimental work. These are distilled water (DW), 0.657 M Sodium Chloride (NaCl), 0.219 M Magnesium Chloride (MgCl2), 0.219 M Magnesium Chloride (MgCl2) combined with 0.130 M Calcium Chloride (CaCl2) and Synthetic Sea Water (SSW).

DW was employed to prepare 0.001 M water in equilibrium with calcite. After being prepared, equilibrium water with a concentration of 0.1 g/L have been filtrated, and almost all the calcite got retained by the 0.22µm filtrate paper. Filtration was done by the Millipore filtration apparatus shown in Figure 3.5. Then, the pH of the solution was measured by the calibrated pH meter to make sure that the value is above 7. DW was also used to clean the cores before ending the tests.
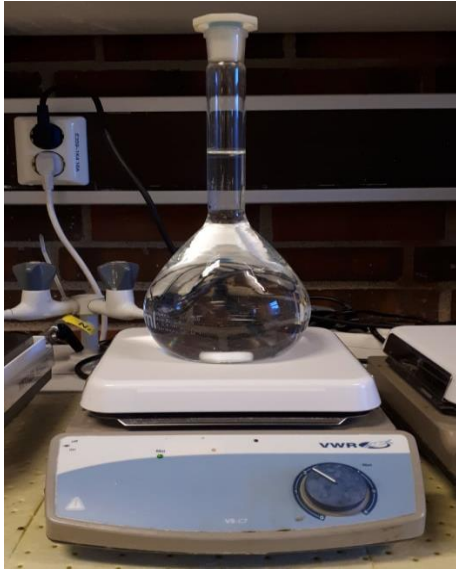
Figure 3.4 Magnetic stirrer

Figure 3.5 Filtration apparatus

0.657 M Sodium Chloride (NaCl) have been used as a saturation fluid for one sample (E2) and as a flooding brine for both samples used in this work. It was prepared by first adding 38.4 g NaCl to a 1 litre's volumetric flask containing about 0.8 L of the pre-prepared DW in equilibrium with calcite. Once the NaCl has dissolved completely, the equilibrium water was added until the final volume is brought to 1L. The brine was then mixed for more than one hour by a magnetic stirrer displayed in Figure 3.4. After being mixed, the brine was filtrated using the filtration apparatus (Figure 3.5) and 0.65 µm filtrate paper, and the pH of the final solution was measured to be around 9. The other brines were prepared following the same procedures according to the brine compositions summarized in Table 3.1.

Table 3.1 Compositions of brines injected during the mechanical tests

Compound	NaCl (g/l)	$MgCl_2$ (g/l)	$MgCl_2$+ $CaCl_2$ (g/l)	SSW (g/l)
NaCl	38.40	0.00	0.00	23.38
Na_2SO_4	0.00	0.00	0.00	3.41
$NaHCO_3$	0.00	0.00	0.00	0.17
KCl	0.00	0.00	0.00	0.75
$MgCl_2 \times 6H_2O$	0.00	44.50	44.50	9.05
$CaCl_2\, 2H_2O$	0.00	0.00	19.11	1.91

3.1.3 Core saturation

The pre-dried core (E2) was saturated with 0.657 M NaCl brine before testing according to the following steps. The core was partially covered with a shrinking sleeve and placed into a small plastic container, which was itself inserted into the vacuum chamber. The vacuum system, shown in Figure 3.6, is sealed by a rubber ring and a heavy lid on top. In addition, the vacuum system has two valves. One is connected to the atmosphere and it must be closed prior to opening and the second valve connects the chamber to the vacuum pump. The pump gear was switched on and vacuuming was started. When the pressure gauge indicated an inner pressure of 5 mbar, the chamber was properly vacuumed. The tube connected to the container containing NaCl was then pre-flushed and connected to the vacuum chamber. Thereafter, the valve connected to atmosphere was opened until the core became completely covered with the brine. The core was finally left for saturation for some time. This saturation procedure was only performed on one core (E2).
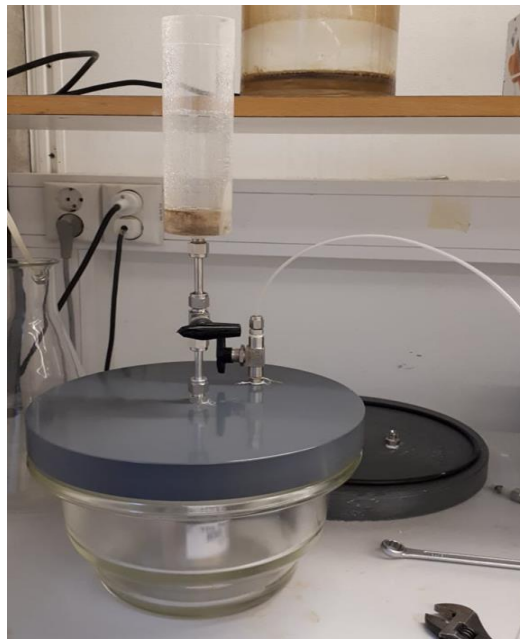
Figure 3.6 Vacuum apparatus

3.1.4 Porosity calculation

Pycnometry (Before and after testing)

The cores were taken out of the heating chamber and placed into a Dry-Seal vacuum desiccator (Figure 3.7) for a while to remove the moisture and to cool the cores down prior to porosity determination by pycnometry. The gas pycnometer (Figure 3.8) measures the amount of displaced helium gas within the porous sample placed into the volume chamber. Once the dry sample is placed in the enclosed chamber, helium gas molecules fill the chamber rapidly and penetrate in the pores of the sample. The chamber pressure is then measured by the device and the volume change is calculated from the pressure (P) and the chamber volume (V) by Boyle's law:

$$P_1 V_1 = P_2 V_2 \tag{3.1}$$

Figure 3.7 Dry-Seal vacuum desiccator   *Figure 3.8 Micromeritics Gas Pycnometer*

The volume of the dry rock material was measured by pycnometry. Together with the dimensions of the cores and the bulk weight, porosity was determined according to the following steps:

- The weight of the dry core (W_s) was first measured.

- The length (L) and the average diameter (D) of each core were measured in order to calculate the bulk volume (V_b) using equation (3.2)

$$V_b = \frac{1}{4}\pi D^2 L \qquad (3.2)$$

- The solid volume of the core material (V_s) was measured with a helium gas pycnometer (Micromeritics Gas Pycnometer model AccuPyc II 1340). A 100 cm^3 chamber represented the best fit with the samples and was therefore used.

- The pore volume was calculated from the bulk and matrix volumes using equation (3.3)

$$V_p = V_b - V_s \qquad (3.3)$$

- Then, the porosity (φ) was calculated by

$$\varphi = \frac{V_p}{V_b} \qquad (3.4)$$

- The mineral density was calculated as well by dividing the dry core mass by the solid volume read on the pycnometer.

$$\rho_s = \frac{W_{dry}}{V_s} \qquad (3.5)$$

Measurements and results involved in the porosity calculation are illustrated in Table 3.3.

Table 3.3 Properties of the cores

Sample	W_{dry}(g)	L(mm)	D(mm)	V_b(cm^3)	V_s(cm^3)	V_p(cm^3)	φ(%)	$\rho_s(g/cm^3)$
E-2	125.23	53.00	37.93	59.89	49.11	10.78	18.00	2.55
E-3	120.70	52.40	37.98	59.37	48.13	11.24	18.93	2.51

Saturation method (After testing)

After being tested, the saturated weight of each core, the drainage plates and the shrinking sleeve (W'_{sat}) were measured before being placed in a heating chamber to dry, and weighted several times until the dry masses have stabilized. The pore volume (V_p') was then calculated

from the difference between the wet and dry weights of the core, the drainage plates and the shrinking sleeve, (W'_{sat}) and (W'_{dry}) respectively, by means of equation (3.6), considering that the density of distilled water (ρ_w) is equal to 1.0 .

$$V'_p = \frac{W'_{sat} - W'_{dry}}{\rho_w} \tag{3.6}$$

Thereafter, the new length and diameter of each dry core were measured for calculation of the bulk volume (V_b), porosity (φ') and solid density (ρ_s') after testing according to equations (3.2), (3.4), and (3.5).

3.2 Test equipment

3.2.1 Triaxial test cell

Chalk mechanical tests in this work were performed in a hydraulically operated triaxial cell illustrated schematically in Figure 3.9. The design of the test cell is such that two high-pressure Quizix pumps control the applied pressure axially and laterally and a Gilson pump controls the flow of fluids. The core is mounted between the lower and upper steel pistons marked I on the same figure. The core is also surrounded by a steel skirt which makes up the confining chamber. An axial piston assembly, marked II, is mounted on top of the steel skirt to complete the pressure vessel in which the core is located.
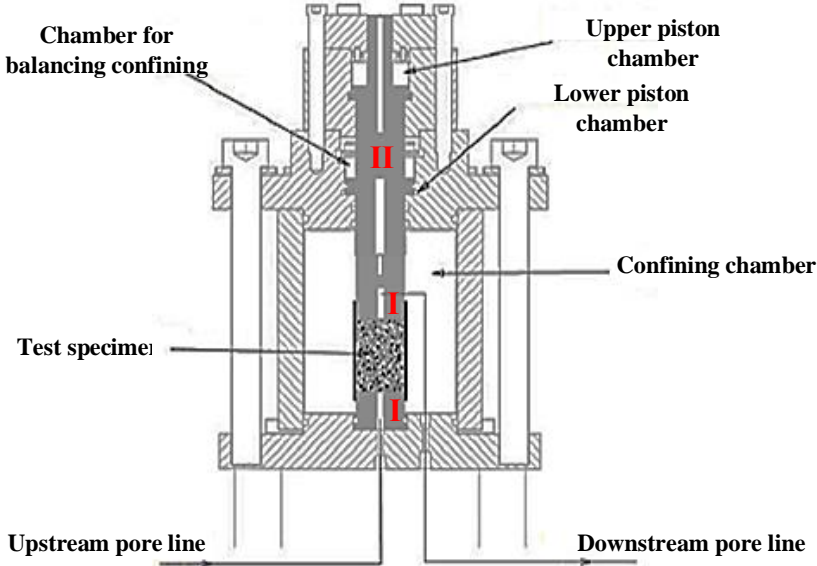
Figure 3.9 Triaxial cell illustration, modified after (Omdal, 2010)

The triaxial cell is designed so that the confining chamber is not only used to apply confining stress load. Yet, the confining pressure is also applied in the axial direction. This is due to the fluid in the confining chamber that can move up in the piston and into the chamber to balance the confining pressure. Besides, an additional axial load is required in order to overcome the friction between the cell and the piston and hence to enable the hydraulically operated piston to follow the deformation of the core. The friction can be calculated based on the piston area.

Two different systems are used to measure the core deformation. An outside Linear Voltage Displacement Transducer (LVDT) (uncertainty ±0.05mm) placed on the piston that follows the movement of the test specimen to measure the axial strain of the sample. When it comes to radial displacement, an extensometer, of type MTS model 632.92H-04, connected to a chain surrounding the core is utilized to detect any change of the circumference.

3.2.2 Pumps, gauges and software

Figure 3.10 Gilson pump

Figure 3.11 Quizix pumps

During the experiments, two different kinds of hydraulic high-pressure pumps are connected to the cell to control the injection flow rate, the confining pressure and the axial pressure. Two Quizix pumps (Figure 3.11) are operated by the Vindum Pump Program and are employed to supply the piston pressure and the confining pressure independently. The other pump type is

the Gilson pump (model 307 High Performance Liquid Chromatography HPLC) shown in Figure 3.10. It is used to control the flowrate. Together with a piston cell and a high-pressure piston pump, the upstream pore line, which is connected to the injection system, permits flooding of brines. The downstream pore line is connected to a back pressure regulating system (BPR-system). The BPR-system exhibited in Figure 3.12 maintains a stable pore pressure ($\pm$0.1 MPa) and allows the continuous collection of effluent.

The pore pressure and differential pressure along with the confining pressure and piston pressure are measured by digital pressure gauges shown in Figure 3.13. These pressure gauges manufactured by Emerson Rosemount, are connected to the LabView (Laboratory Instrument Engineering Workbench) program. This program records measurements in real time, monitors and controls parameters, one of which the flooding rate. Recorded measurements are written to a file that can be opened and observed on Microsoft Excel. Thus, the effect of injected brines and applied stresses on the mechanical behaviour of the samples can be monitored throughout testing.
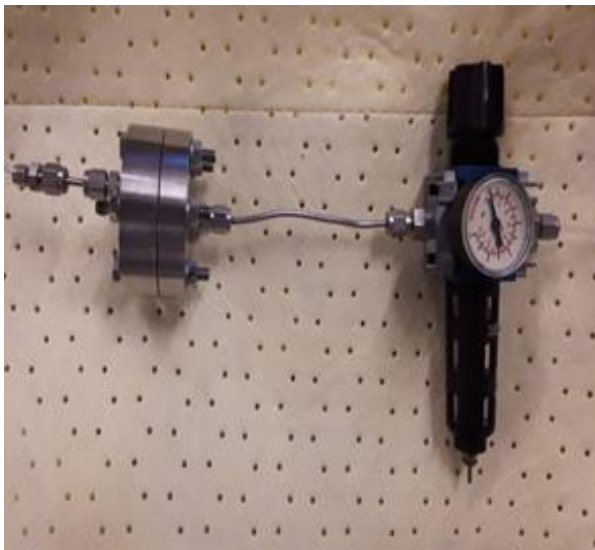
Figure 3.12 Back pressure regulator
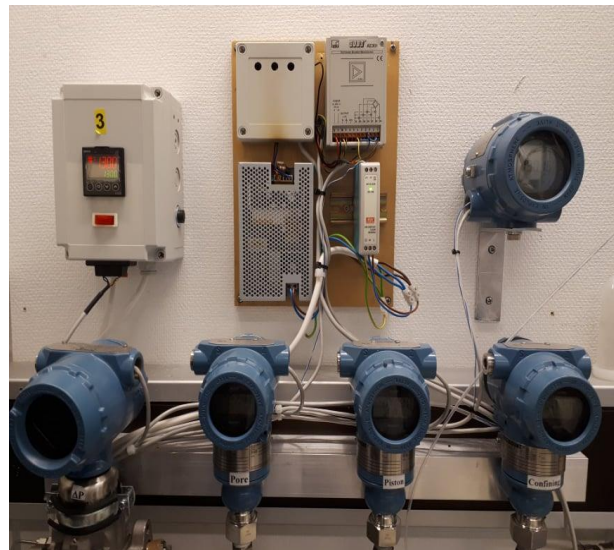
Figure 3.13 Gauges

3.2.3 Heating system

In the present work, the test temperature was set to 130°C. The cell is therefore connected to an external heat regulating system (Omron E5CN) that allows test temperatures up to 150°C. The cell is equipped with a heating jacket mounted outside the confining chamber to keep the temperature constant throughout the experiment. The temperature inside the cell is measured by a digital gauge (Figure 3.13) and a Pt-100 (Resistance Temperature Detector). Small

temperature fluctuations of ±0.2°C may be observed since the room temperature is not always stable and also because of the accuracy of the heating system.

3.2.4 Chemical analysis instruments

Samples of the effluents, or wastewater, that have been flooded through the core are collected for each experiment by a Gilson GX-271 Liquid Handler represented in Figure 3.14. The chemical composition of produced effluents and the injected brines are then compared in order to understand changes in the mineralogical composition of flooded cores. A dilution pump of the type Gilson (GX 271), shown in Figure 3.15, is firstly employed to dilute the sampled effluents and standard solutions with known concentrations with nanopure water. They are diluted 500 times in order to stay within the linear region of the calibration curve of the ion chromatograph. The ionic concentrations are analysed by means of a Dionex Ion Chromatography System (ICS)-5000$^+$ ion exchange chromatograph (Figure 3.16). The analyses are conducted using IonPac CS19 and IonPac AS20 are as cation and anion exchange columns, respectively.

| Figure 3.14 Sampling effluents | Figure 3.15 Diluting the sampled effluents | Figure 3.16 Ion chromatography apparatus |
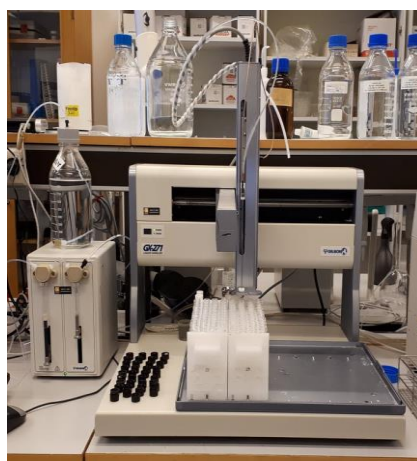
3.2.5 Field Emission Gun-Scanning Electron Microscope (FEG-SEM)

A Zeiss Supra 35 VP Field Emission Gun-Scanning Electron Microscope (FEG-SEM) (Figure 3.17) is employed to determine the mineralogical and elemental composition of the chalk core after mechanical flow-through experiments. The electron gun in this device accelerates electrons creating a focused electron beam, which scans the chalk samples. The beam can be adjusted and focused so that as small as possible spot of electrons on the surface of the sample

is produced. Thus, different energy signals that are collected by several detectors are produced or reflected from the surface when being hit by the beam.
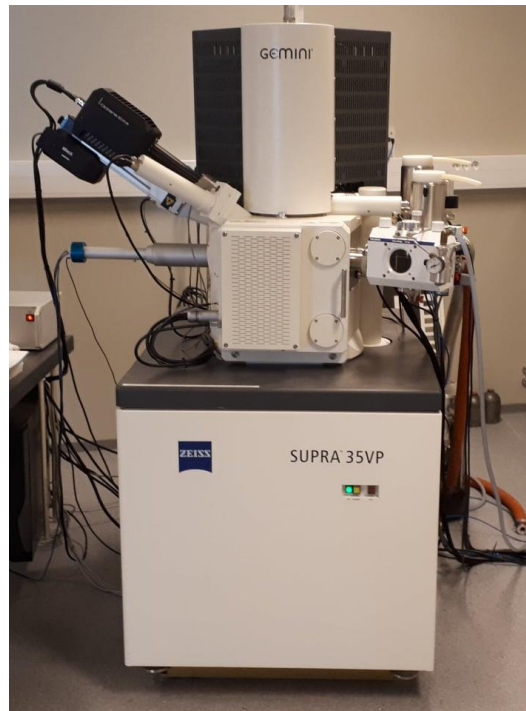
Figure 3.17 Zeiss Supra 35 VP (FEG-SEM)

3.3 Hydrostatic and creep tests

3.3.1 Hydrostatic test

Hydrostatic loading consists of exerting increased equal stresses in all directions on a sample. A hydrostatic test is performed by increasing the confining pressure while keeping the pore pressure constant and recording the sample deformations i.e. change in diameter and length of the core. With the design of the triaxial cell, the piston is balanced. In other words, the pressure of the confining oil hinders the progress of the piston by migrating to the upper chamber above the piston. However, the piston assembly needs to be in contact with the sample to measure the axial deformation. An additional axial load is then required to overcome friction, which makes the loading process not purely hydrostatic, but quasi-hydrostatic with an additional axial load typically around 0.3 MPa. In this work, it is beneficial to perform hydrostatic tests since they give good repeatability and less scatter in the data measurement and hence are useful when investigating the effect of different brines on the mechanical strength of chalk (Omdal, 2010).

3.3.2 Creep test

Creep test following the hydrostatic compression test was conducted under isotropic stress conditions. Creep is performed by simply keeping all pressures constant while measuring deformations continuously with time. The flooding rate of respective brines is kept constant as well throughout the creep period. In this work, creep during the first and second test were performed in periods of 61.6 and 25.6 days respectively and the deformation was mostly measured with a resolution time of 3 minutes.

3.5 Test procedures

3.5.1 Mounting the triaxial cell

At the beginning, the piston cell, introduced in Figure 3.18, was filled with 0.657 M NaCl brine. Afterwards, the brine was pumped into all tubes in order to displace air and saturate the test system with the brine. Then for more sealing between the confining chamber and the core, a high vacuum grease of the type DOW CORNING was used to smear the O-rings. After that, a filtrate paper and a drainage disk with the same diameter as the core were placed on the lower flooding piston (Figure 3.19) to inhibit the access of particles to flow tubings and to ensure that the fluid flow is evenly distributed across the core, respectively.
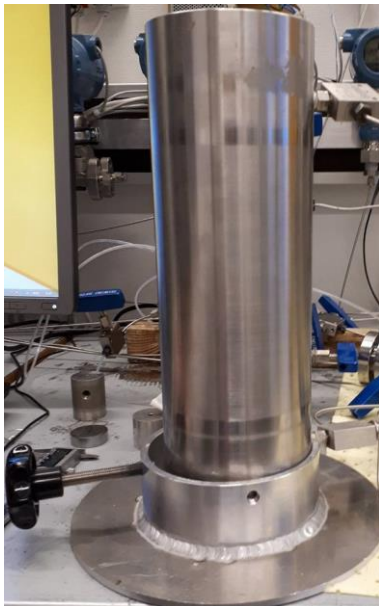
Figure 3.18 Piston cell   *Figure 3.19 Core mounting process (a)*   *Figure 3.20 Core mounting process (b)*
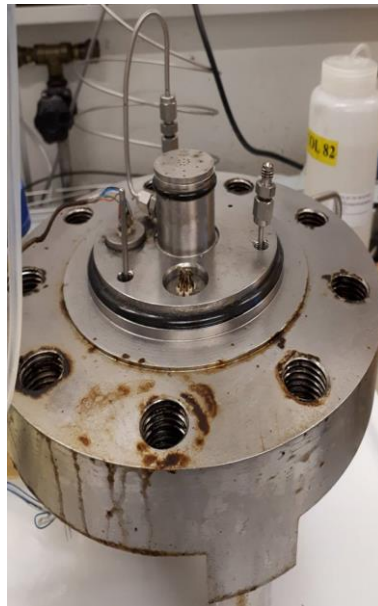
As exhibited in Figures 3.19 and 3.20, once the core is placed on top of the drainage disk, a second filtrate paper and drainage disk are put on top of it. In addition, a steel spacer with length

of 19.3 mm was placed on top of all in order to compensate for the limited core length. The specially polished rubber seals are attached around both the lower and the upper flooding piston and between the upper drainage disk and the steel spacer to provide additional sealing of the core. Thereafter, a heat shrinking sleeve is placed around the core prior to putting the upper flooding piston on top. The shrinking sleeve must be long enough so that it covers the rubber seals, the core, and the steel spacer as illustrated in Figure 3.22. Having covered the wires with a rubber that prevents damage by the heat, a heating gun is employed to shrink the sleeve tightly around the core to avoid that the confining oil leaks into the core. Next, an extensometer (Figure 3.23) that measures the radial deformation is positioned around the core.
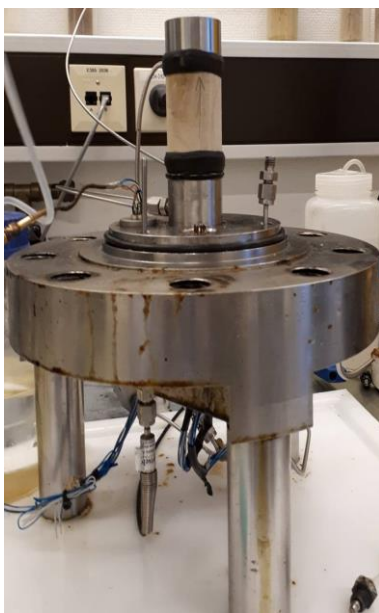
Figure 3.21 Core mounting process (c)
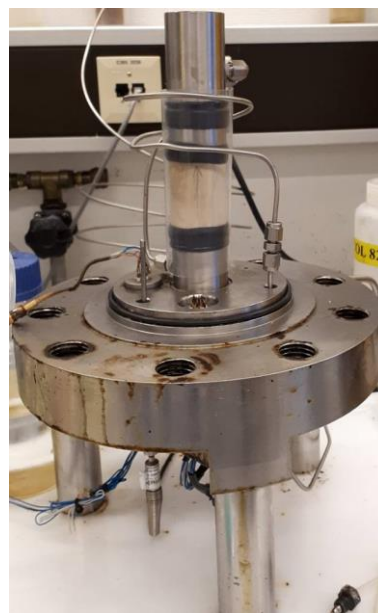
Figure 3.22 Core mounting process (d)
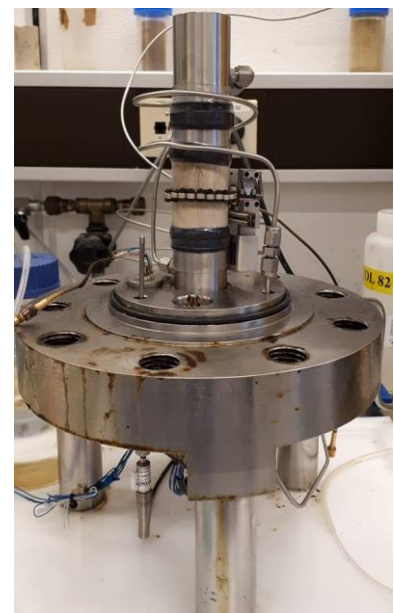
Figure 3.23 Core mounting process (e)

The core is now installed. A cylinder wall and a heating jacket (Figure 3.24) are then mounted on top of the bottom plate making up the confining chamber. The latter is filled with Marcol 82 oil after closing the drainage valve. The following steps are then to open the upper confining outlet valve to let excess oil leave the confining chamber, place the top part of the cell on top of the cylinder wall (Figure 3.25) and tighten the bolts placed between the top and bottom parts of the cell. The bolts are tightened by a torque wrench with a torque of 200 Nm shown in Figure 3.26.

| *Figure 3.24 Core mounting process (f)* | *Figure 3.25 Core mounting process (e)* | *Figure 3.26 Core mounting process (f)* |
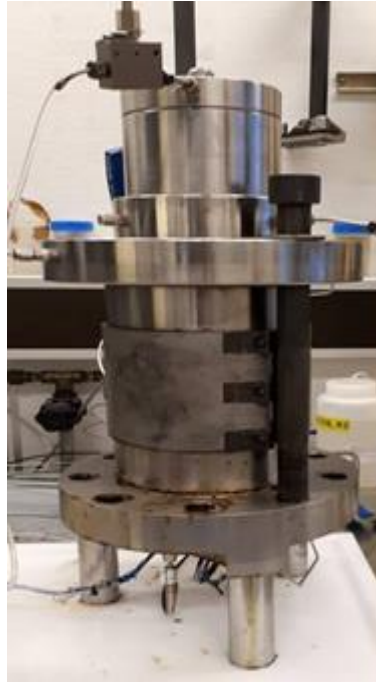
Mounting the triaxial cell is eventually finalized by placing the Linear Variable Differential Transformers (LVDT) on top of the cell to detect axial deformation of the core and making sure that the transducer can move easily during the piston movement.

3.5.2 Increasing confining pressure

The confining pressure is increased to 0.5 MPa before starting brine flooding into the system. Prior to pressure build-up, air inside the cell must be removed. This is done by opening the valve of the confining outlet and by starting the confining pump (pump 2 on Figure 3.27). Confining oil is then pumped through tubes towards the confining outlet passing by the confining chamber. When constant dripping of oil depleted of air bubbles is observed, the confining outlet valve can be closed. The confining pressure is then increased up to 0.5 MPa, with a flow rate at maximum 2.0 ml/min monitored by the constant delivery pump mode. After reaching 0.5 MPa, the confining pressure is kept constant by changing the pump mode.

Gauges:
G₁ = Differential pressure
G₂ = Pore pressure
G₃ = Piston pressure
G₄ = Confining pressure
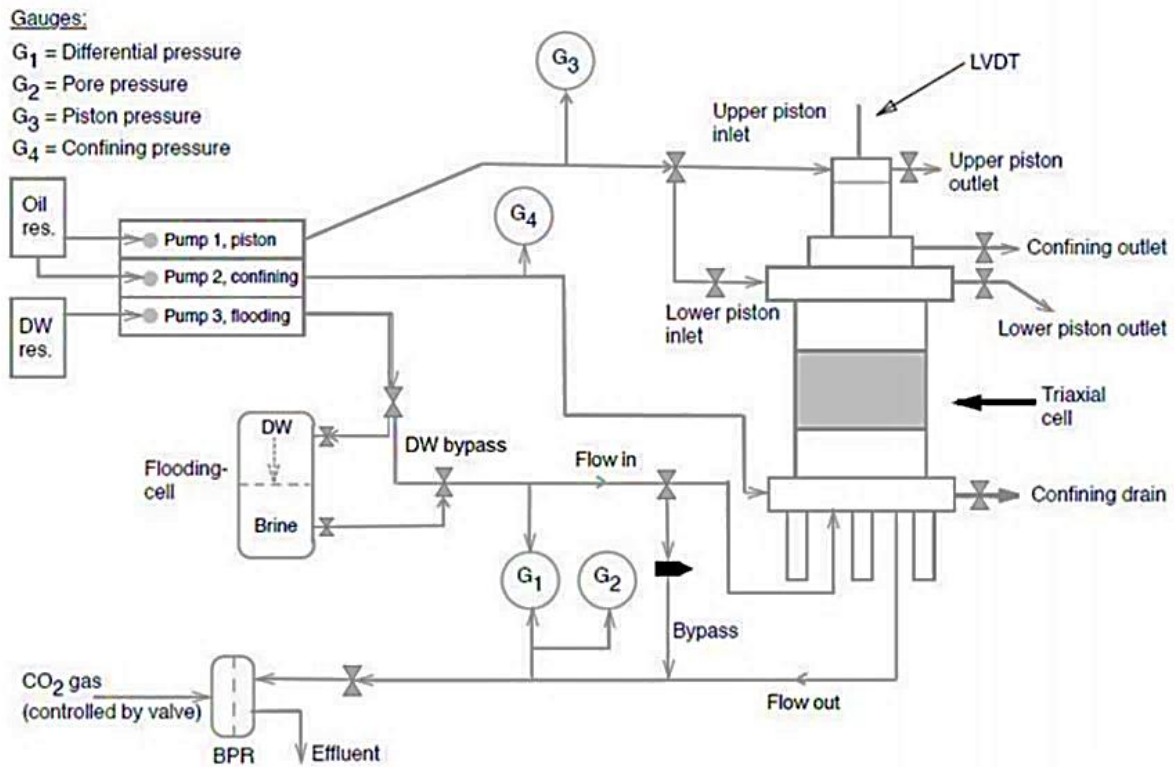
Figure 3.27 Illustration of experimental set-up (Anders Nermoen et al., 2016)

3.5.3 Moving down piston

After reaching the desired confining pressure, the piston is pushed down slowly and carefully until it meets the core. This is done by means of the piston pump (pump 1 on Figure 3.27) which exerts pressure on the piston assembling by pumping oil in the piston chamber. Prior to initiating the process, the lower piston inlet valve has to be closed, while it is required to open the upper piston inlet and the lower piston outlet valves. The valve of the upper piston outlet is kept open until air is displaced out of the piston chamber letting a continuous dripping of oil, then it is closed. When the piston lands on the core, the piston pressure increases noticeably in seconds, the pump is then immediately stopped, and the pump mode is switched from constant delivery to constant pressure mode. The extensometer shows higher values simultaneously with the pressure increase, which ensures that the piston have hit the core.

3.5.4 Flooding brine

The core is flooded by the test brine NaCl. The Gilson pump is started with an initial rate of 0.2 ml/min. The reactive brine from the piston cell is then displaced through the upstream pore line, flowing into the pores of the core sample and coming out via the downstream pore line. During this process, the differential pressure is not stable, and it may exceed the maximum limit of pressure difference, which is 260 kPa for the Rosemount gauges used in this work. Therefore,

40

to protect the gauge from being damaged, the flow rate should be regulated so that the differential pressure stays within the range of operating pressure difference.

3.5.5 Building up pressures

The pore pressure and the confining pressure are increased simultaneously to 0.7 and 1.2 MPa respectively. This is done stepwise so that the pore pressure is always 0.5 MPa lower than the confining pressure i.e. the effective pressure is constant and equal to 0.5 MPa. The pore pressure is adjusted with a backpressure regulator which is set to 0.7 MPa and the bypass valve should be open prior to that in order to accelerate this process. The confining pressure is increased by injecting oil from the confining pump into the confining chamber. When the pore pressure and the confining pressure reach the desired values, the bypass valve is closed, and the flooding rate is decreased to 0.023 ml/min, equivalent to approximately 3 pore volumes per day (PVs/day).

3.5.6 Increasing temperature

When the differential pressure becomes constant, the test temperature is set to 130°C and is kept constant throughout the experiment. As the temperature of the system is increased, the oil inside the confining chamber tend to expand causing an augmentation of the confining pressure. Therefore, a spring valve is connected to the valve at the confining outlet to regulate the confining pressure and keep it constant throughout the heating process. Furthermore, the confining pump is shut down during this process to avoid that oil with relative low temperature comes into the cell and affects the heating procedure.

3.5.7 Hydrostatic and creep loading

Prior to starting the hydrostatic loading, the spring valve used during the heating process is removed and the confining outlet valve is closed. The confining pressure is then increased from 1.2 MPa up to 50 MPa with a loading rate corresponding to 0.1 MPa/min. The pressure is not further increased since 50 MPa is a relatively high pressure, higher than that in the reservoir, and in addition to that the core did not tend to yield. When increasing the confining pressure, the friction associated to the piston rises simultaneously. The piston pressure is then increased from 0.6 MPa to 4.7 MPa with a loading rate of 0.0085 MPa/min to overcome the friction. Once, the desired piston and confining pressures are reached, the hydrostatic loading phase is ended, and the creep phase is initiated. The pressures are then kept constant throughout the creep period and the flooding rate is set to 0.023 ml/min. Radial and axial deformations are measured continuously during both hydrostatic- and creep phases.

3.5.8 Changing brines

The flooding cell contains distilled water (DW) in the upper chamber and the brine to be flooded through the core in the lower chamber as shown in Figure 3.28. The brine in the flooding cell is changed by first closing the inlet and outlet valves of the piston cell and stopping the Gilson pump. The flooding cell can then be disconnected from the flooding system and the brine change can be started. DW is initially emptied out of the DW chamber, not completely, and the lock is put on again. Then, after closing the valve from brine side and opening the valve from DW side, air is used to move the piston that separates the two chambers towards the upper one. When remained water comes out of the valve, the latter can be closed. Subsequently, the piston cell is turned upside down and the brine chamber is washed with distilled water and dried well to remove any remains from the previous brine. The brine to be circulated in the triaxial cell system is then filled in the brine chamber after collecting a sample of it to be chemically analysed. Afterwards, prior to starting the Gilson pump, the flooding cell is connected to the pump and the valve in between is opened. Likewise, it is connected to the triaxial cell, but the attached valve is kept closed. Meanwhile, the piston cell is kept inclined to clear out the air inside it. Eventually, the flooding pressure is increased to its value before starting brine changing and the valve associated to the triaxial cell upstream tubing is opened. The flooding process is then continued at the initial flow rate of 0.023 ml/min.
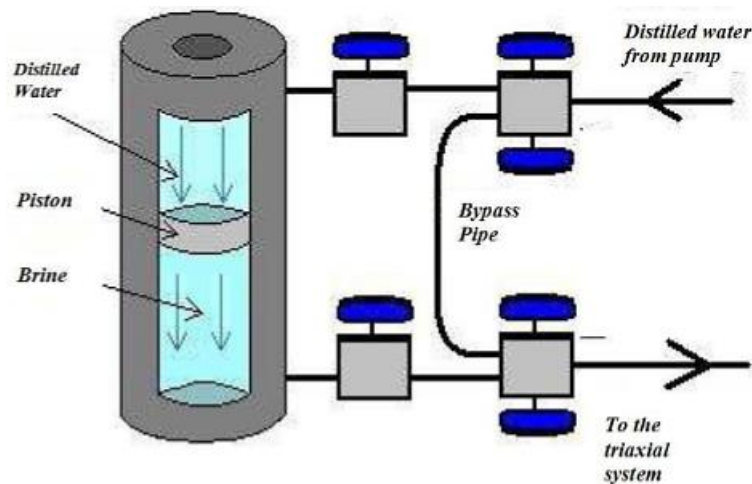
Figure 3.28 Schematic illustration of the flooding piston cell (Haddadi, 2013)

3.5.9 Flooding Distilled Water (DW) and dismantle of triaxial test setup

Before ending the test, the samples were cleaned by injecting 3 PVs per day of DW, which displaces the brine in the pores and thus avoids precipitation of any salts in the pore space when drying the core. The flooding fluid was switched to DW by closing the flooding in and out valves and opening the by-pass valves for the flooding piston cell (Figure 3.27). This cleaning procedure does not considerably change the geochemical properties of the chalk core (Mona Wetrhus Minde, 2018a). After minimum one day of core cleaning with DW, unloading is started. The by-pass of the triaxial cell is firstly opened such that the differential pressure is decreased to zero, and the temperature is turned off when the confining pressure and piston pressure have reached 1.2 and 0.6 MPa respectively. When the temperature is low enough, maximum 30°C, the inlet valve of the piston cell is closed, and the piston is lifted by pumping up oil in the lower piston chamber. The Gilson pump is stopped, and the confining- and pore pressures are reduced to 0.5 and 0 MPa respectively. When the pore pressure is zero, the confining pressure is taken down to zero by slowly opening the confining outlet valve. Next, after opening the confining drainage valve, compressed air is employed to squeeze out the oil from the confining chamber. Afterwards, the cell is dismounted, and the core is eventually taken out.

The saturated weights of the core, drainage plates and the shrinking sleeve were measured immediately after dismantling the cell. Then, they were dried in a heating chamber and weighted several times until stable dry masses were observed. The difference between the saturated and dry masses was used to estimate the new porosity and solid density of the core. The new porosity and density were also estimated by pycnometry as before testing.

3.5.10 Chemical analysis by Ion Chromatography (IC)

Prior to starting the chemical analysis, when the sampled effluents contained oil, the aqueous parts have been separated from the oily parts and transferred to new sampling glasses using syringes. Then, the effluent samples together with SSW and unflooded original brines are diluted to 500 times with DW by a Gilson dilution machine that is previously primed. Once a sample is diluted, a cap should be put on the original sampling glass collected from the cell to prevent evaporation or impurities getting inside it. Afterwards, diluted solutions to be analysed by the ion chromatograph are prepared by the following procedure:

- Diluted sample is shaken to get a more homogeneous and representative composition.

- Approximately 1 mL of the solution is extracted by use of a syringe, and the inner side of the syringe is wetted with the extracted solution.

- The syringe is emptied in the waste box and the remaining diluted solution is extracted by means of the same syringe.

- A filter is put on the syringe and the latter is emptied until there is around 1.5 mL left inside it.

- The remaining 1.5 mL of the solution is filled in an IC-glass, then the filter is removed, and the syringe is cleaned with about 2 mL nanopure water.

When the IC samples are ready, they are placed in the IC basket in a specific order. SSW and original brines are placed in the middle and at the end before the last row which comprises DW. Next, the Dionex Ion Chromatography System (ICS) is programmed to carry out the analysis.

3.5.11 Field Emission Gun-Scanning Electron Microscopy Coupled-Energy Dispersive X-Ray Spectroscopy

Fresh surfaces of the flooded material, from E3, were examined with Field Emission Gun-Scanning Electron Microscopy (FEG-SEM) to obtain visual images of the grains and the rock structure on μm scale. Besides, Energy-Dispersive X-Ray Spectroscopy (EDS) was applied to determine the mineralogical and elemental composition of the analysed chalk surfaces.

Electron microscopy requires oil-free samples. Oil residues in the core may cause a significant damage to the scanning electron microscope. Thus, when preparing the sample for electron microscopy, it is necessary to wash the plug carefully in order to imbibe as much as possible oil from the core. During the washing process, the core was injected with distilled water with a confining pressure of 0.5 MPa at room temperature. Then, the confining and pore pressures were increased to 1.2 and 0.7 MPa respectively. The temperature was increased as well to 92°C prior to methanol injection. Methanol is used as an intermediate injection brine due to its miscibility with distilled water and toluene to be injected. When flooding toluene through the core, oil residues were produced. This process continued until the colour of the effluent has gone from brown to completely colourless, meaning that no more oil is produced from the core. Methanol injection followed by distilled water injection were carried out prior to ending the cleaning process. After being cleaned, the sample was placed in the drying cabinet at 90°C.

Figure 3.29 Scheme of the sectioning of the core E3

After being dried, the core (E3) was cut to two halves, and the first half was further cut into four parts (P1, P2, P3, and P4). The inlet is at P1 and the outlet is at P4 as indicated by the arrow in Figure 3.29. Then, a small freshly broken piece from the inlet (P1) have been used for the analysis, and to ensure that the surface is electronically conductive upon analysis, it was coated by a conductive layer of palladium by means of an Emitech K550 sputtering device (Figure 3.30).

Figure 3.30 Emitech K550 sputtering device

The fresh surface broken from P1 of E3 was eventually imaged using a Zeiss Supra 35VP FEG-SEM in high vacuum mode with an accelerating voltage of 15 kV, aperture size of 30 µm, and a working distance between 8 and 9 mm. The field emission microscope is equipped with an EDS, which was calibrated using a dolomite standard from "Astimex Standards Limited" before the sample was analysed.

3.6 Data processing

Having completed the experimental work, the acquired results' data are processed to interpret the geo-mechanical behaviour of the Eldfisk chalk. First, the deformation of the core is interpreted by calculating the axial, radial and volumetric strains. Second, the effluent concentration of different ions is measured over time to monitor the difference in chemical flux in and out of the core and to estimate the evolution of the solid mass and volume and the change of density throughout the experiment.

3.6.1 The effective stress and stress-strain relations

The effective confining stress (σ'_{conf}) is calculated from the confining pressure (σ_{conf}), Biot coefficient (α) and the pore pressure (P_p) according to Biot effective stress relation represented previously by equation (2.5) in section (2.3.2). The effective stress coefficient (α) is set equal to unity since its exact value is not of high significance for low pore pressure values, as it is in this work (Anders Nermoen et al., 2016). Moreover, the effective confining stress is equal to effective radial stress, but not to effective axial stress (σ'_{ax}) since an additional piston pressure is applied. Thus, the effective axial stress is calculated, according to equation (3.7), from the confining stress (σ_{conf}), piston pressure (P_{pist}), friction pressure (P_{fric}), and an area factor (f_{area}) (Anders Nermoen et al., 2015).

$$\sigma'_{ax} = \sigma_{conf} + f_{area}\left(P_{pist} - P_{fric}\right) - \alpha P_p \qquad (3.7)$$

where the difference between the piston pressure and the friction pressure is equal to 0.3 MPa. The friction area factor for the cross area of the core and the piston- pressure chamber is dimensionless and generally it takes values between 1.2 and 1.3 depending on the diameter of the core and the setup design (Anders Nermoen et al., 2016). In this work, it is set to be 1.27 and it is equal for both tests since the same cell is used and because both tested cores have approximately the same diameter.

3.6.2 Ions concentrations estimates

The concentrations of anions and cations present in the samples of produced fluids were quantified and plotted against time by means of Ion Chromatography. The concentrations of Na^+, Cl^-, Mg^{2+}, Ca^{2+} and SO_4^{2-} are measured in this analysis. Carbonate (CO_3^{2-}) production is not reported since the concentrations of carbonate ions could not be measured. It is then assumed that carbonate ions are initially bounded to calcium and when magnesium is injected, the retained magnesium ions bind to carbonate to form other minerals such as dolomite or magnesite (Anders Nermoen et al., 2015). Assuming linear regime of chromatograph, the ionic concentrations were determined from the areas under the chromatographic curves and standard solutions with known concentrations of respective ions according to equation (3.8) (Jaspreet S. Sachdeva, Nermoen, Korsnes, & Madland, 2019a).

$$C_i = \frac{A_i}{A_{std,i}} * C_{std,i} \qquad (3.8)$$

where

C_i Concentration of the quantified ion in the effluent

         $C_{std,i}$ Concentration of the quantified ion in the standards

A_i Area under chromatographic curves of the quantified ion in the effluent

$A_{std,i}$ Area under chromatographic curves of the quantified ion in the standards

3.6.3 Constitutive relations for volume evolution

The bulk volume (V_b) of a porous chalk core, before and after testing, is given by the sum of the pore volume (V_p) and the solid volume (V_s). Thus, changes affecting the total volume are equal to the sum of changes in pore- and solid volumes i.e.:

$$\Delta V_b = \Delta V_p + \Delta V_s \qquad (3.9)$$

Before testing, the bulk volume of the specimen is given by the cylinder volume, while under hydrostatic stress conditions, the core was unevenly deformed with tendency to display radial contraction that is more significant on the bottom of the core as illustrated in Figure 3.31.
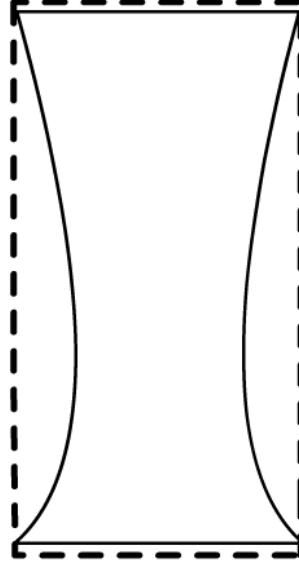
Figure 3.31 Volume change under hydrostatic stress conditions

Hence, the bulk volume of a non-uniformly deformed core is estimated from the sum of truncated circular cones with diameter D_i measured at height h_i along the core:

$$V_b = \sum_i \frac{\pi h_i}{12} \left(D_i^2 + D_{i+1}{}^2 + D_i D_{i+1} \right) \tag{3.10}$$

3.6.4 Estimating evolution of solid mass and volume

Since the chemical flux at both edges of the plug is monitored by measuring the concentrations of different ions over time, it is possible to estimate the change in the solid mass over a time interval δt. Given the difference in the ion concentration present in the injected and produced effluent $(c_{in,j} - c_{out,j})$, the flow rate (q) and the molar weight of ion j (M_{wj}), the evolution of the solid mass over time is given by equation (3.11) (Anders Nermoen et al., 2015)

$$\frac{\delta M_s}{\delta t} = \sum_j (c_{in,j} - c_{out,j}) \, q \, M_{wj} \tag{3.11}$$

The rock-fluid interactions are complex, thus the mass evolution of the core at any time t may be estimated by equation (3.12) (Anders Nermoen et al., 2015) assuming that overall geo-mechanical replacement is proportional to calcium production (Jaspreet S. Sachdeva et al., 2019a).

$$\triangle M_s(t) = \int_0^t \frac{\delta M_s}{\delta t'} dt' \tag{3.12}$$

Chapter 4 Experimental Results

In this section, the experimental results are presented for each of the tested cores E3 and E2 in the following order: strain measurements during hydrostatic loading, creep and unloading phases, effluent sample analysis using ion chromatography (IC), and Field Emission Gun-Scanning Electron Microscopy (FEG-SEM) for E3.

4.1 Test 1

4.1.1 Mechanical testing

Eldfisk reservoir core (E3) was tested mechanically in a triaxial cell at 130°C. It was initially loaded hydrostatically from a confining pressure of 1.2 MPa up to 50 MPa while flooding Sodium Chloride (NaCl). Thereafter, it was left to creep at constant stress with continuous flow of NaCl, $MgCl_2$, $MgCl_2$ combined with $CaCl_2$ and DW as illustrated in table 4.1. E3 was eventually unloaded to the initial confining pressure.

Table 4.1 Test scheme for core E3 at 130°C

	Hydrostatic loading	Creep at 50 MPa			
Brine	0.657 M NaCl	0.657 M NaCl	0.219M $MgCl_2$	0.219M $MgCl_2$+ 0.130 M $CaCl_2$	DW
Duration (days)	0.3	6.7	27.2	24.7	3.0

Hydrostatic loading phase

The isotropic loading phase was performed with flooding 0.657 M NaCl at a flow rate corresponding to 3 PVs/day. The axial stress versus axial and radial strains are plotted in Figure 4.1. As shown in Figure 4.1, the axial and radial strains reached 0.86 and 0.69 % respectively at the end of the isotropic loading phase. Rock mechanical properties under hydrostatic loading can be described by yield and bulk modulus. The yield point, which is the stress at which non-linear deformation initiates, was not observed for E3. However, the bulk modulus (K) could be calculated from the linear slope of axial stress versus volumetric strain within the elastic phase shown in Figure 4.2, and it is equal to 2.8 GPa.
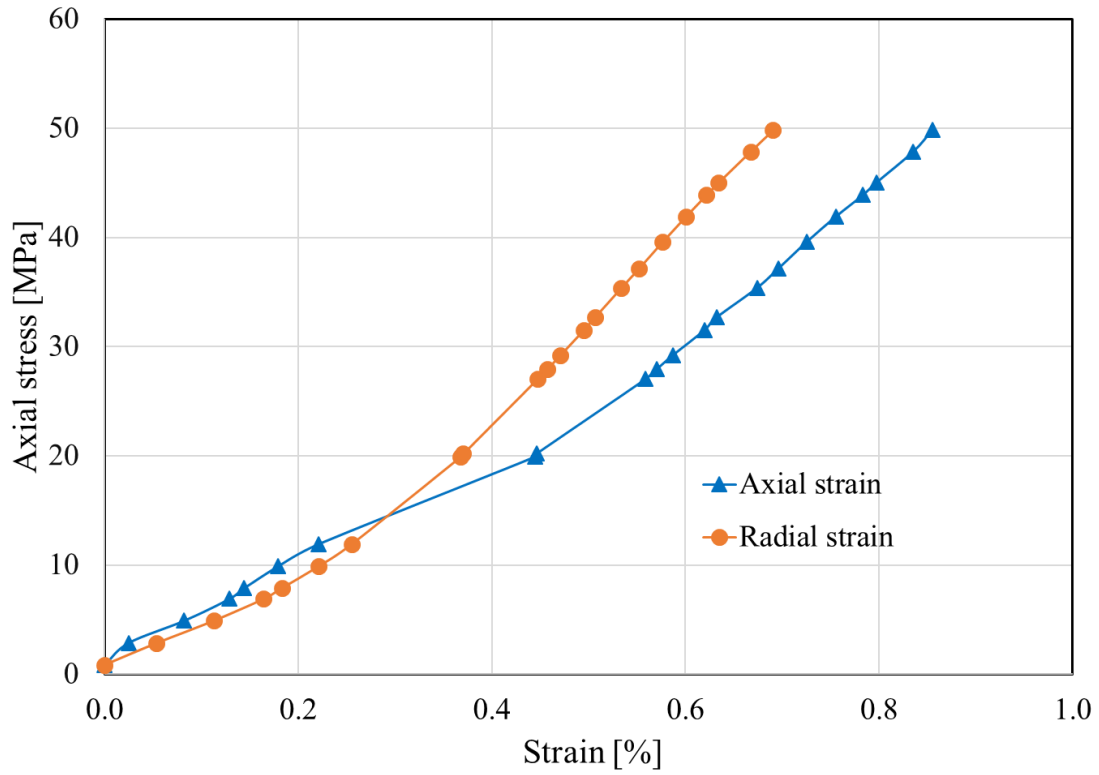
Figure 4.1 Axial stress [MPa] vs strain [%] for core E3 during hydrostatic loading
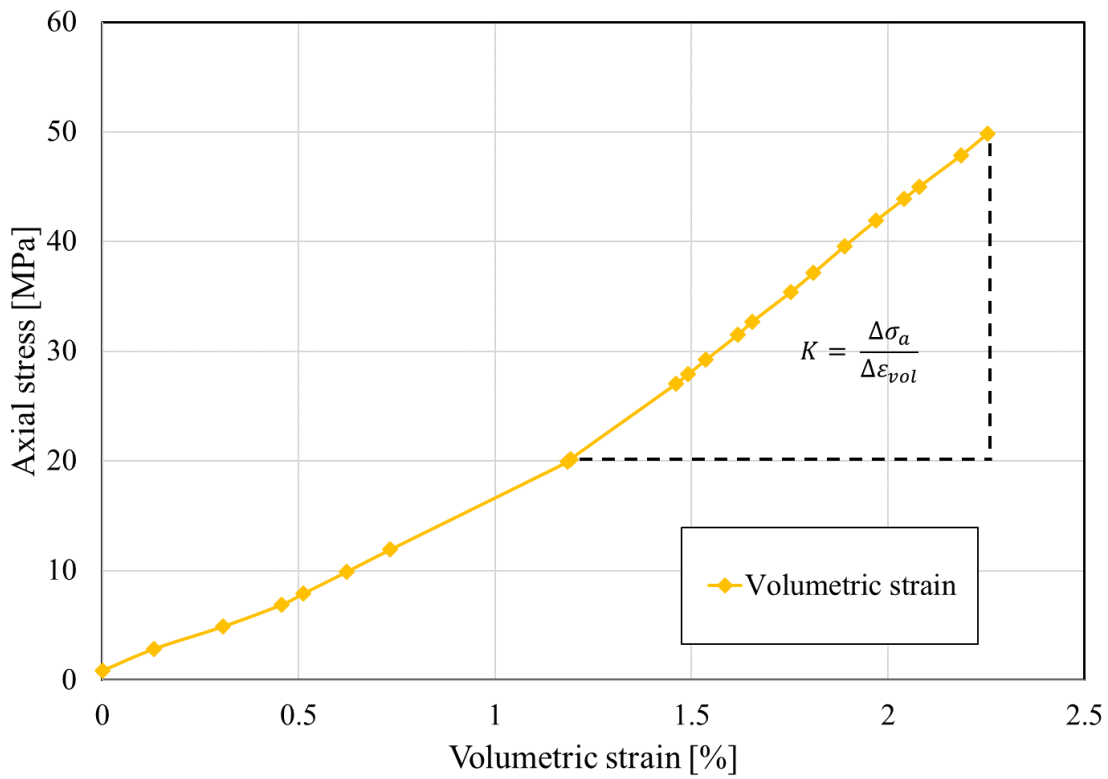
Figure 4.2 Axial stress [MPa] vs volumetric strain for core E3 during hydrostatic loading

Creep phase

The deformation of E3 at constant stress and pore pressure conditions, known as creep, lasted for 61.5 days with continuous logging of the axial and radial strains. The creep compaction profile of E3 is shown in Figure 4.3.

The core was initially flooded with 0.657 M NaCl for the first 6.7 days of creep before flow of 0.219 M $MgCl_2$ started. Creep axial and radial strains at the end of NaCl flow were around 0.5%. However, the flow of $MgCl_2$ led to an abrupt increase in the deformation rates, i.e. % strain per day, in both directions. This is shown in Figure 4.3, where the radial strain increased significantly especially until day 22 of creep, then it continued to increase but with a lower rate until a strain of 3.2% was recorded. At the same time, the axial strain increased continuously up to 2.1% at 34.7 days. During the period between day 34.7 and day 56.7 of creep, the injection of 0.219 M $MgCl_2$ together with 0.130 M $CaCl_2$, was followed by a reduction in the deformation rate. The axial creep strain increased only by 0.4% during this injection period, and the radial strain increased by 0.2% until day 54.8, then it showed a decreasing trend. Finally, distilled water was flooded leading to a drop in the radial strain and flattening of the axial strain curve.

The observed increase in the diameter when injecting distilled water, as the core was still exposed to a confining pressure of 50 MPa, may be explained by the increase in the pore pressure, which is probably caused by a blockage in the outlet tubing. The pore pressure increased from 0.7 when distilled water injection started up to 8.3 MPa after one day before it dropped to 5.4 MPa around 61 days of creep, resulting in a reduced effective stress and thus an increased core diameter.
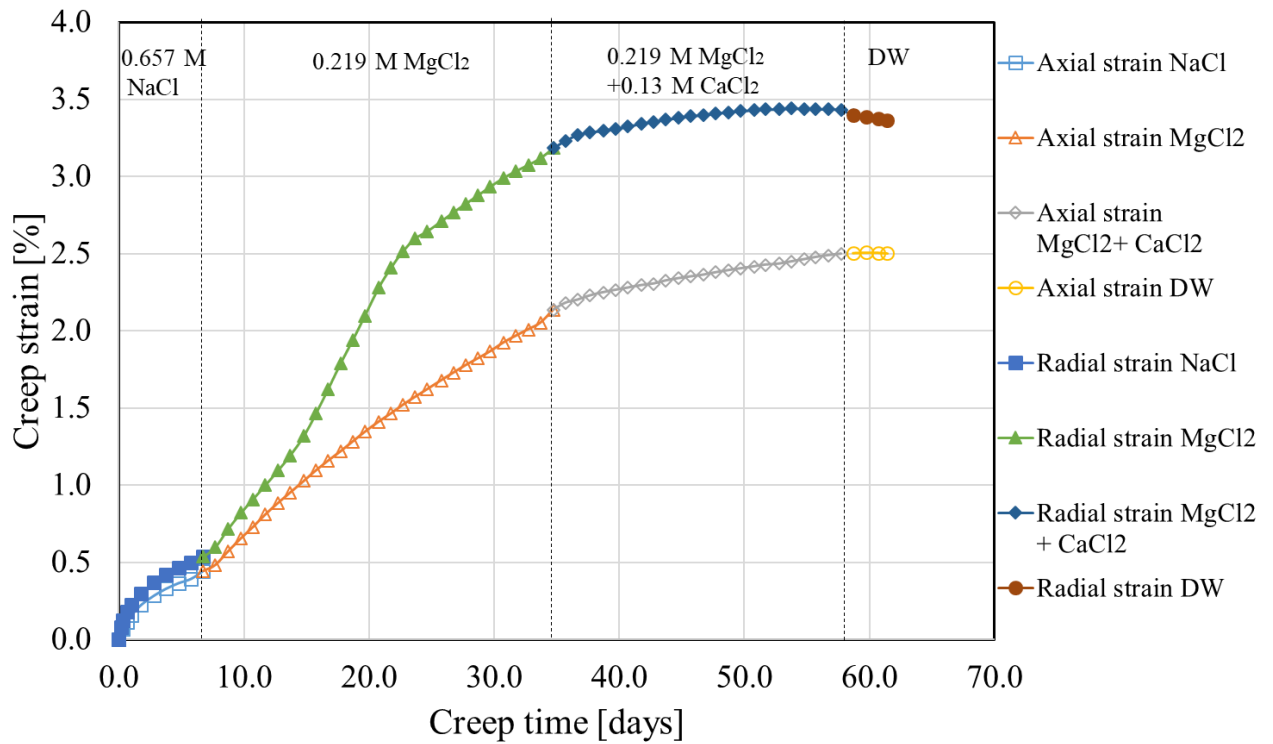
Figure 4.3 Axial and radial strain [%] vs creep time [days] for core E3 during creep phase at 50 MPa

From Figure 4.3, the creep curves show that the core E3 compacted more strongly radially than axially.

Unloading

Before ending the mechanical test, confining pressure and piston pressure are loaded back to 1.2 and 0.6 MPa respectively. The evolution of the confining pressure, piston pressure, radial strain and axial strain over unloading time are displayed in Figure 4.4. According to the unloading cycle, the radial and axial strains are decreased as the confining and piston pressures are reduced until slightly before 1 hour, indicating the expansion of the core. Between approximately 1 and 1.1 hour, the confining pressure and piston pressures kept constant resulting in flattening of the strain curves. Then, when unloading carried on, the radial and axial strains decreased down to 3.0 and 1.8 % respectively.
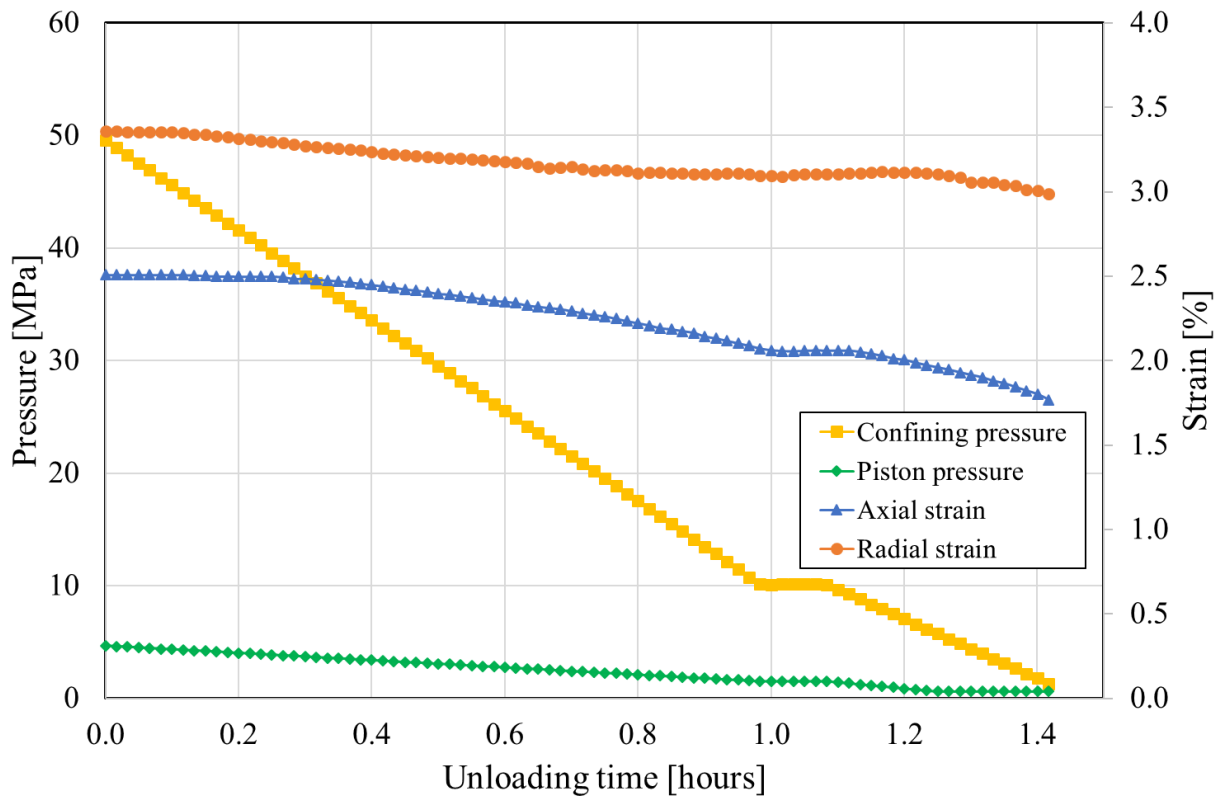
Figure 4.4 Axial and radial strain [%]and confining and piston pressure vs unloading time [hours] for core E3 during unloading

4.1.2 Chemical analysis E3

In this section, the results of ion chromatography analysis of the effluents are described. The changes in the ion concentrations between the injected and effluent brines indicate to which extent the rock-fluid interactions have occurred in the test specimen.

Ion Chromatography results

During the first experiment, the effluents were sampled regularly to measure the concentrations of sodium (Na^+) and chloride (Cl^-) ions and to produce effluent profiles based on the concentrations of magnesium (Mg^{2+}) and calcium (Ca^{2+}). When flooding with NaCl, the effluent concentrations of Na^+ and Cl^- are practically the same as the injected, i.e. 0.657 mol/L. Besides, only a small Ca^{2+} peak of 0.01 mol/L is found initially but it rapidly goes down towards zero as seen in Figure 4.5. The chemical analysis carried out throughout this experiment showed that chloride seems to be more or less inert to the chalk surface also when the core was flooded with the other test brines, illustrated in Figure 4.5, for which the concentrations of chloride quickly reach the original injected concentration values.

When changing from NaCl to $MgCl_2$, a transient behaviour in Ca^{2+} production and Mg^{2+} retention can be observed in Figure 4.5. A calcium peak starts, when introducing $MgCl_2$, at a concentration of ~ 0.003 mol/L before the production of calcium increases to a maximum value of 0.033 and stabilizes at ~ 0.026 mol/L around day 10 of creep. At the same time, a loss of magnesium is found as the concentration in the sampled effluent increases from 0 and stabilizes at ~ 0.190 mol/L which is clearly below the injected concentration of 0.219 mol/L.

When 0.130 M $CaCl_2$ was added to the flooding brine in the period between 34 and 59 days of creep, an immediate response in the calcium production and magnesium retention is brought out. As can be seen in Figure 4.5, the produced calcium concentration increases and exceeds 0.130 mol/L, then it gradually decreases the next ~15 days and the difference between the effluent calcium concentration and that of the injected brine becomes almost negligible. Complementary to calcium profile, a large peak in the magnesium effluent concentration with a maximum value of ~ 0.252 mol/L can be observed. Thereafter, the magnesium concentration decreases below the original concentration reflecting the profile of calcium, but with opposite directions.

Eventually, during distilled water flooding before ending the test, a fall in the calcium and magnesium concentrations to almost 0 is observed.
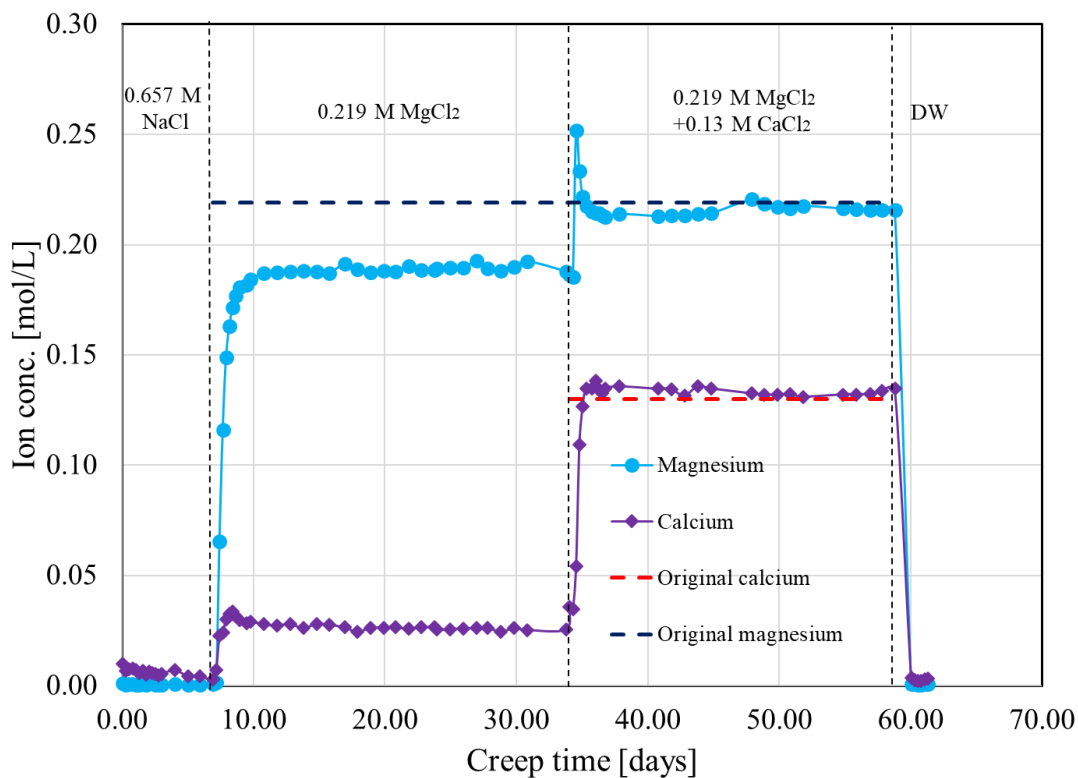
The differences in ion concentrations multiplied by the flow rates and the molar weights of magnesium and calcium i.e. 24.31 and 40.08 g/mol respectively, permits to calculate the production rates as depicted in Figure 4.6. Dissolution/retention profiles are plotted, such that produced calcium is expressed by positive numbers, while retained magnesium is shown on the negative scale. For the first 7 days of creep, during flow of NaCl a calcium dissolution peak is observed, initiating at a value of ~0.013 g/day and decreasing down to ~0.004 g/day. Then, when changing from NaCl to MgCl2, the rates of calcium dissolution and magnesium retention show a significant increase from ~0.004 up to 0.044 g/day before stabilizing around 0.035 g/day and from ~0.045 to around 0.025 g/day respectively. From 34 days, when adding calcium to the injected brine, a drop in the dissolution/retention rate, by approximately the same amount as the increases during the first brine change, is seen after that a fluctuation is found. From 35 to 59 days, the rate of calcium dissolution and magnesium retention show slight deviations before decreasing to ~0.003 and 0 g/day respectively when injecting DW.
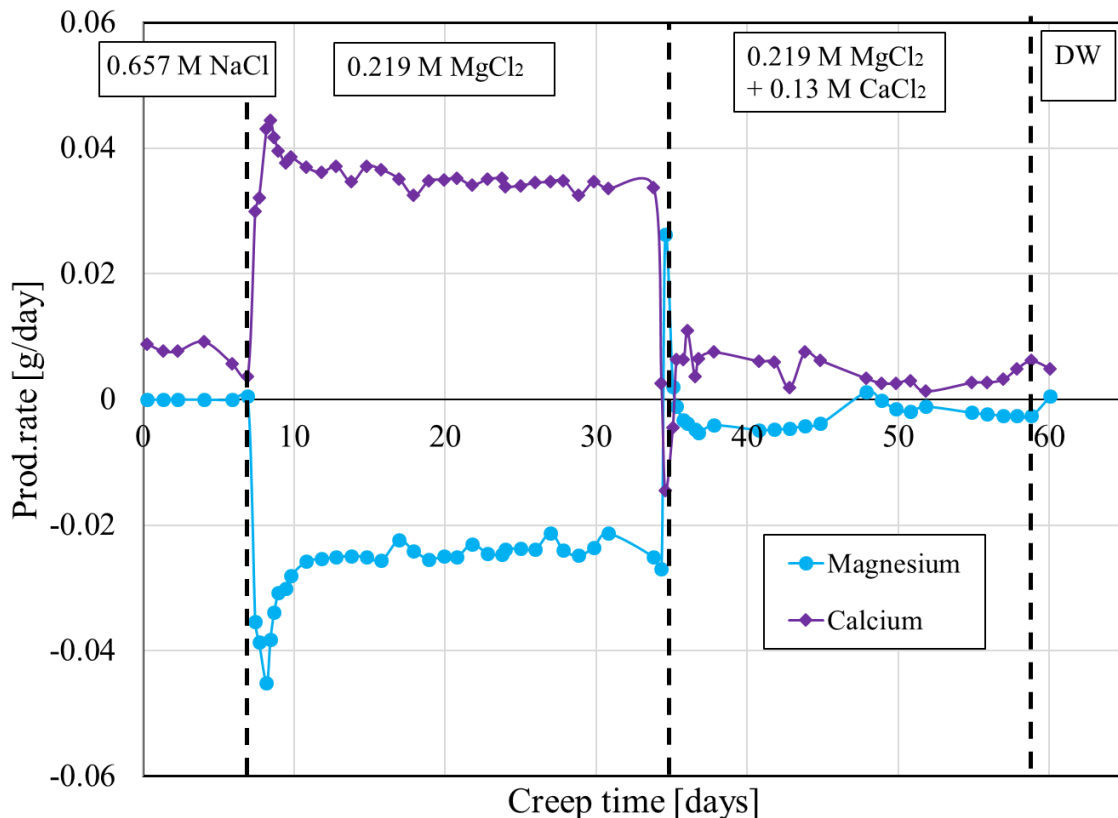
Figure 4.6 Evolution in the production rate of Mg^{2+} and Ca^{2+} [g/day] over creep time [days] for core E3

The rate of calcium production follows, more or less, the same trend as the magnesium retention within the core, which implies that the stoichiometric effects are of import in this system.

The solid mass and density of the core changed throughout the experiment. The mass decreased from 120.7 to 115.4 g, the density increased from 2.51 to 2.62g/cm^3 (measured by pycnometer) and 2.60 g/cm^3 (measured by saturation method). A decrease in the matrix volume was also measured from 48.13 to 43.89cm^3.

The integrated total calcium produced from the plug based on IC measurements was 1.13 g (0.028 mol) and the total retained magnesium was 0.75 g (0.031 mol). Hence, there is a clear deviation between the calculated and the measured mass change. A part of this deviation is probably due to the oil production during the hydrostatic loading phase. The weight of the produced oil, shown in figure 4.7, is 1.5 g, thereby, the weight loss due to oil production exceeds this value since a part of oil have not been sampled during the waste time.

Figure 4.7 Effluent glass sampled during the hydrostatic loading phase, containing 1.5g oil

Besides, the carbonate production has not been taken into account because of the inability to measure the CO_3^{2-} concentrations. Knowing that the carbonate ions are initially bounded to calcium, then when NaCl is injected, it is assumed that cumulative produced carbonates by calcite dissolution is equivalent to cumulative produced calcium (0.001 mol). Accordingly, the

mass loss due to carbonate production at the end of NaCl injection is equal to 0.09 g (0.001 mol). In addition, the tested Eldfisk cores are considered to be impure, hence, dissolved non-carbonate minerals may be produced and accordingly contribute in the solid mass change.

Table 4.2 Properties of the Eldfisk core (E3) before and after test

	W_{dry} (g)	L (mm)	D (mm)	V_b (cm^3)	V_s (cm^3)	V_p (cm^3)	φ (%)	φ' (%)	ρ (g/cm^3)	ρ' (g/cm^3)
Before Testing	120.70	52.40	37.98	59.37	48.13	11.23	18.92	-	2.51	-
After Testing	115.40	51.30	36.94	55.25	43.89	11.36	20.56	19.74	2.62	2.60

4.1.3 Field Emission Gun-Scanning Electron Microscopy (FEG-SEM) E3

Mineralogical and compositional analysis by Scanning Electron Microscopy (SEM) combined with Energy-dispersive X-ray spectroscopy (EDS) have been performed at the inlet of the Eldfisk core E3. FEG-SEM images from the flooded core are shown in Figures 8-12. Chemical alteration is clearly shown in Figure 4.8 by the occurrence of newly formed minerals in open pore spaces, mostly inside foraminifera shells. The crystals show a high magnesium content (Figure 4.9) and appear as cubic aggregates. Yet, it is difficult to interpret whether they consist of magnesite ($MgCO_3$) or dolomite ($CaMg (CO_3)_2$) due to their small sizes (~ 1µm).
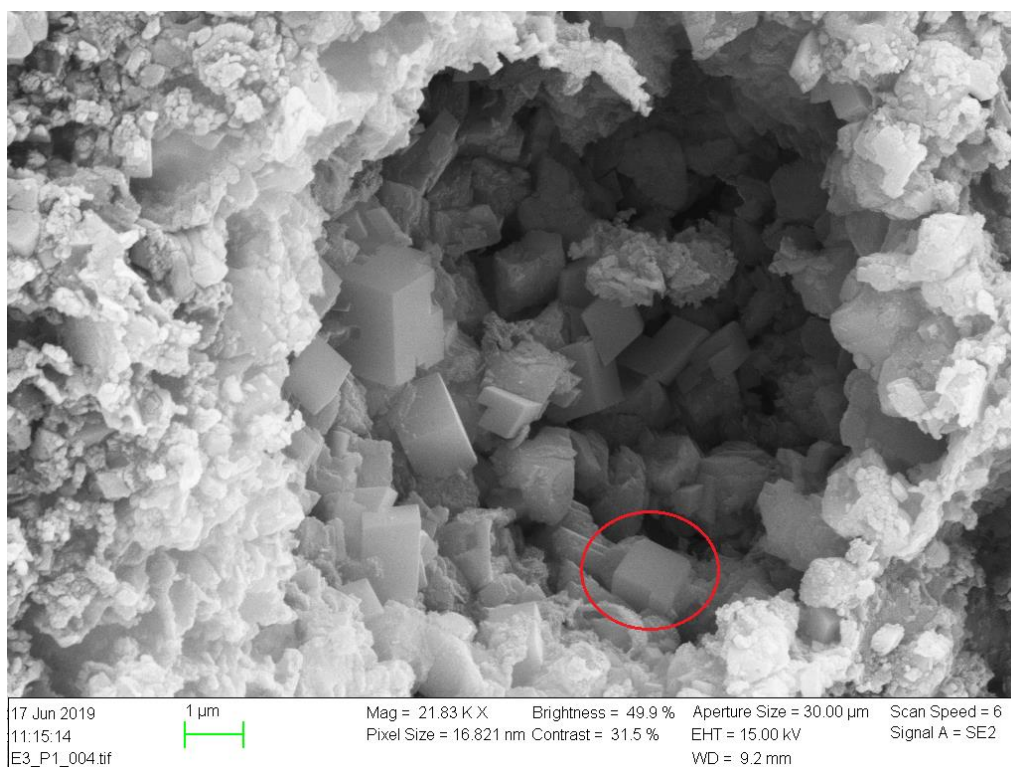
Figure 4.8 SEM image of flooded E3 (Inlet), the red circle shows Mg-rich crystal
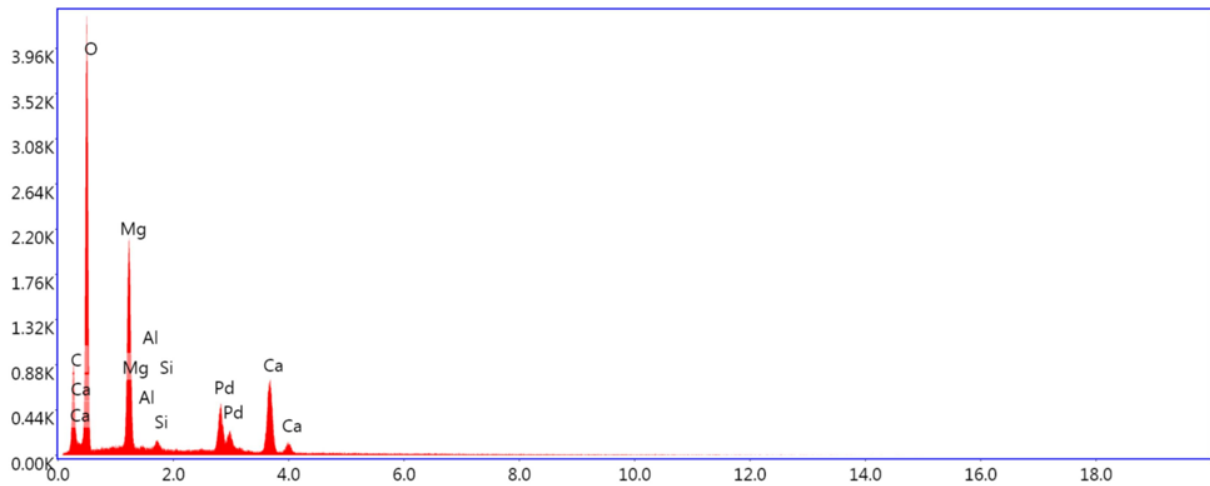
Figure 4.9 EDS analysis of the Mg-rich crystal (red circle in Figure 4.8)

In addition, the SEM image (red circle in Figure 4.10) and the EDS analysis (Figure 4.11) reveal the presence of clay minerals having a flake shape and containing both magnesium and silicon. These flake shaped Si-Mg-rich minerals are interpreted to be newly grown clay minerals as a result of injection of Mg-rich brines.

Although the SEM micrograph in Figure 4.10 also documents that unbroken microfossils are still present along with occurrence of clay minerals and quartz. A part of these clay minerals is believed to be kaolinite originally present in the core before flooding. This is indicated by the EDS analysis in Figure 4.12 which shows high aluminium and silicon weight percent around 23.4 and 24.3 % respectively, in addition to minor occurrence of magnesium, ~ 0.3 wt %, that is probably remained from flooding with $MgCl_2$.
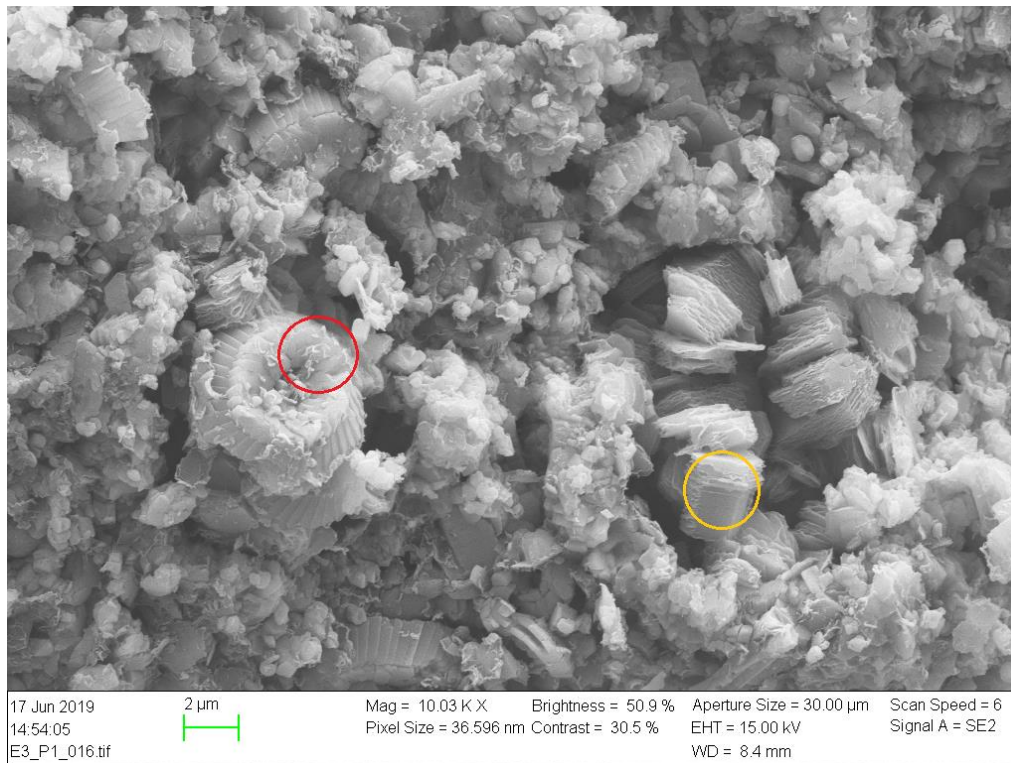
Figure 4.10 SEM image of flooded E3 (Inlet), the red circle shows Si-Mg-rich minerals and the yellow circle shows possible kaolinite mineral
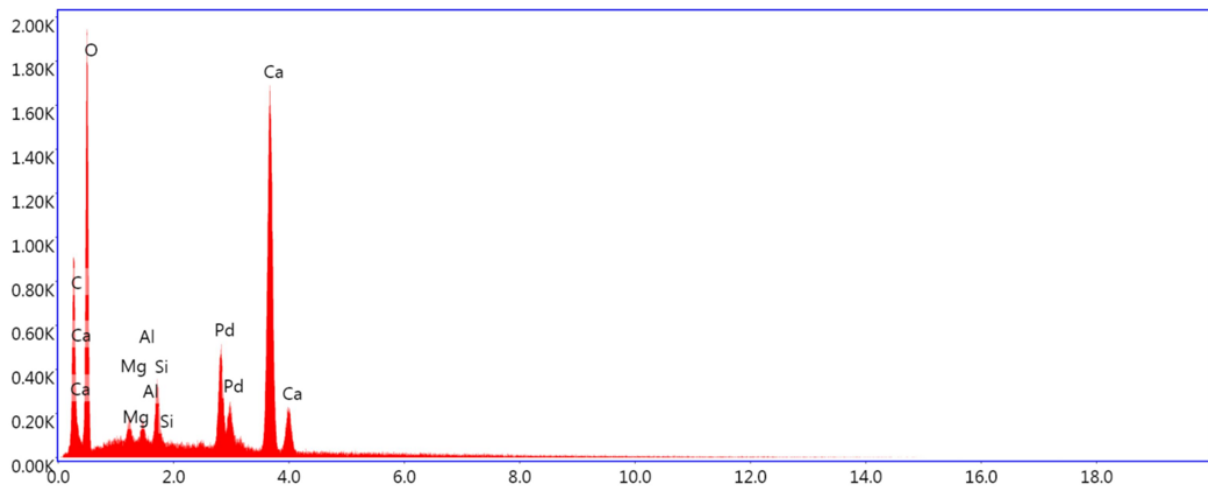
Figure 4.11 EDS analysis of Si-Mg-rich minerals (red circle in Figure 4.10)
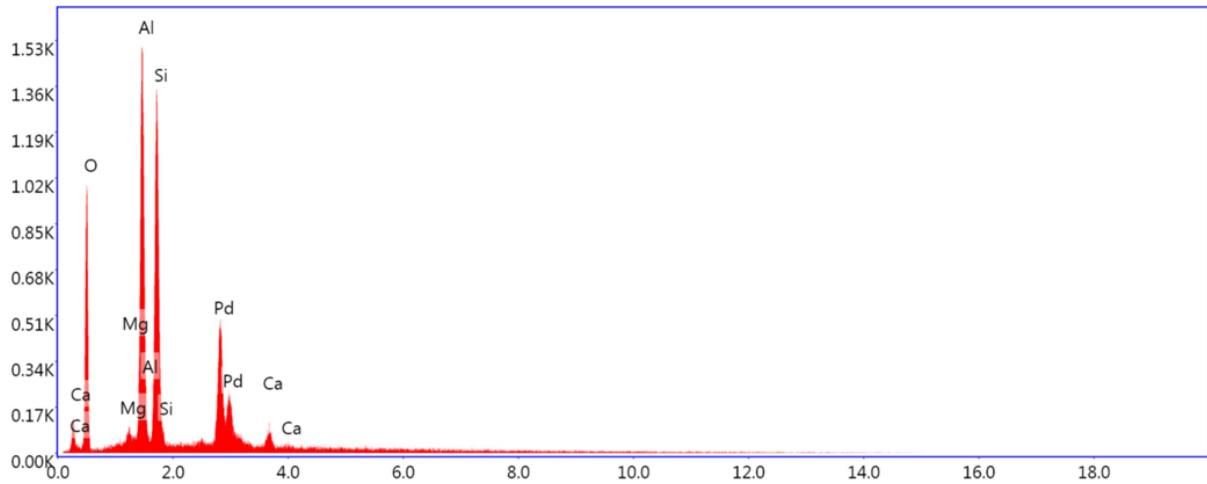
Figure 4.12 EDS analysis of possible kaolinite minerals (yellow circle in Figure 4.10)

4.2 Test 2

4.2.1 Mechanical testing

Eldfisk reservoir core (E2) was tested mechanically in the same triaxial cell as E3 at 130°C. It was initially loaded hydrostatically from a confining pressure of 1.2 MPa up to 50 MPa while flooding Sodium Chloride (NaCl). Thereafter, it was left to creep with continuous flow of NaCl followed by SSW as illustrated in table 4.3. E2 was eventually unloaded to the initial confining pressure.

Table 4.3 Test scheme for core E2

	Hydrostatic loading	Creep at 50 MPa	
Brine	0.657 M NaCl	0.657 M NaCl	SSW
Duration (days)	0.34	6.71	19.91

Hydrostatic loading phase

The Eldfisk reservoir core, E2, was loaded hydrostatically up to 50 MPa while flooding NaCl at an injection rate equal to 3 PVs/day. The axial stress versus axial strain and radial strain along with the axial stress against volumetric strain are plotted in Figures 4.13 and 4.14 respectively. As shown by Figure 4.8, the core compacted but did not yield, and the recorded axial and radial strains at the end of this phase were around 0.79 and 0.30 % respectively. The bulk modulus is calculated from the linear slope of axial stress against volumetric strain exhibited in Figure 4.14, and it was found to be equal to 3.9 GPa.
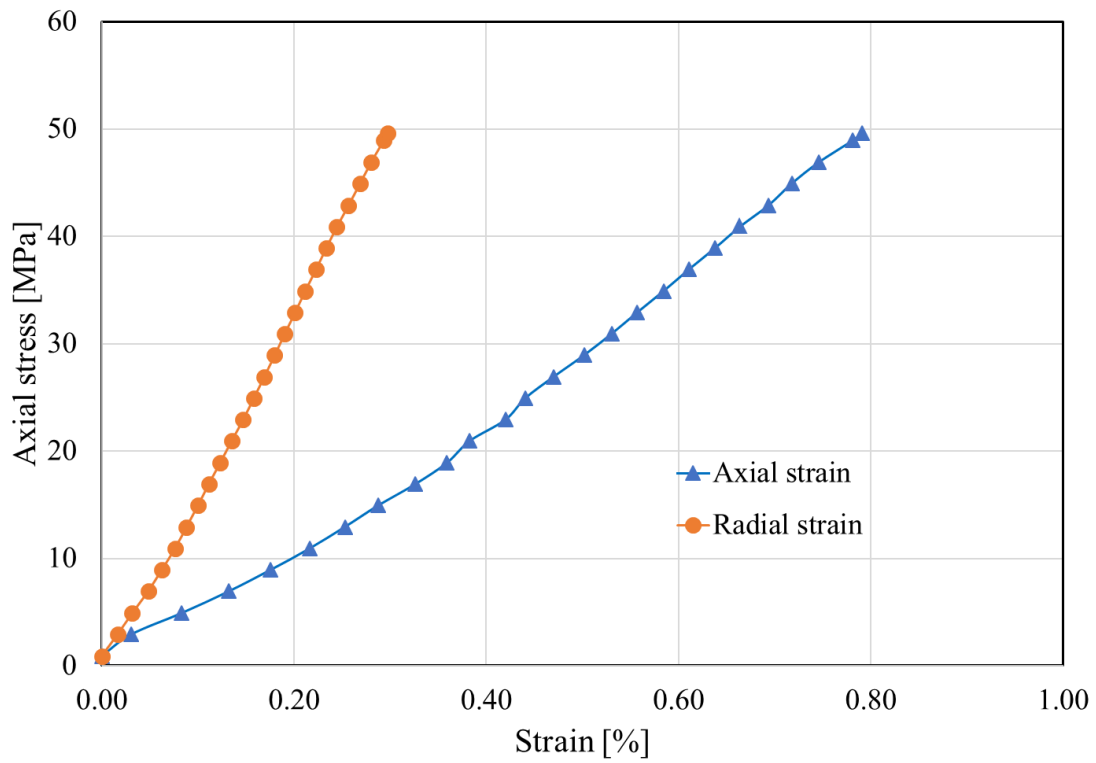
Figure 4.13 Axial stress [MPa] vs strain [%] for core E2 during hydrostatic loading
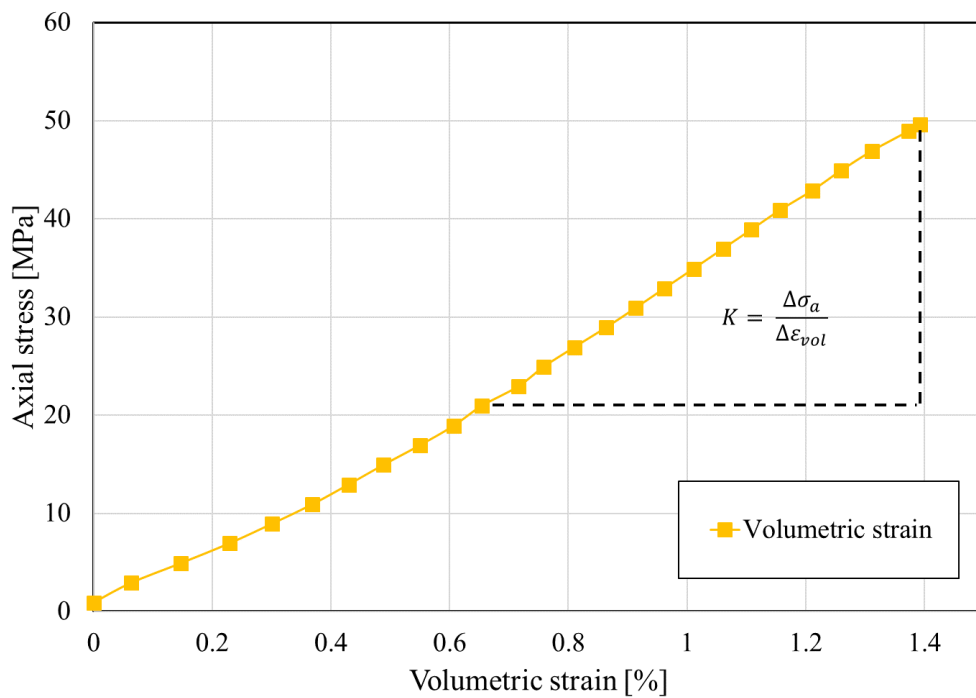
Figure 4.14 Axial stress [MPa] vs volumetric strain for core E2 during hydrostatic loading

Creep phase

The creep magnitude of core E2 through time is illustrated in Figure 4.15. Similar to the first test, 0.657 M NaCl was flooded during the first 6.75 days of creep. Nevertheless, the axial and radial creep strains were around 0.3%, which are 0.2% lower than creep strains recorded for E3. The flow of NaCl was followed by synthetic seawater (SSW) injection which lasted throughout the rest of the creep period. The compaction then accelerated, initiating a new period of continuous deformation, which varied until day 21 of creep. Then flattening of radial and axial creep strains during approximately 1 and 4 days respectively were observed as a result of clogging of the outlet tube. E2 displayed eventually an unexpected behaviour of increased radial strain possibly because of loosening of the chain of extensometer or due to weakening of the central part of the core. Opposite to E3 creep results, it can be seen from Figure 4.10 that E2 exhibited higher deformation in the axial direction compared to lateral during the first 23.7 days of creep, yet the radial creep strain exceeds the axial strain during the remaining creep period.
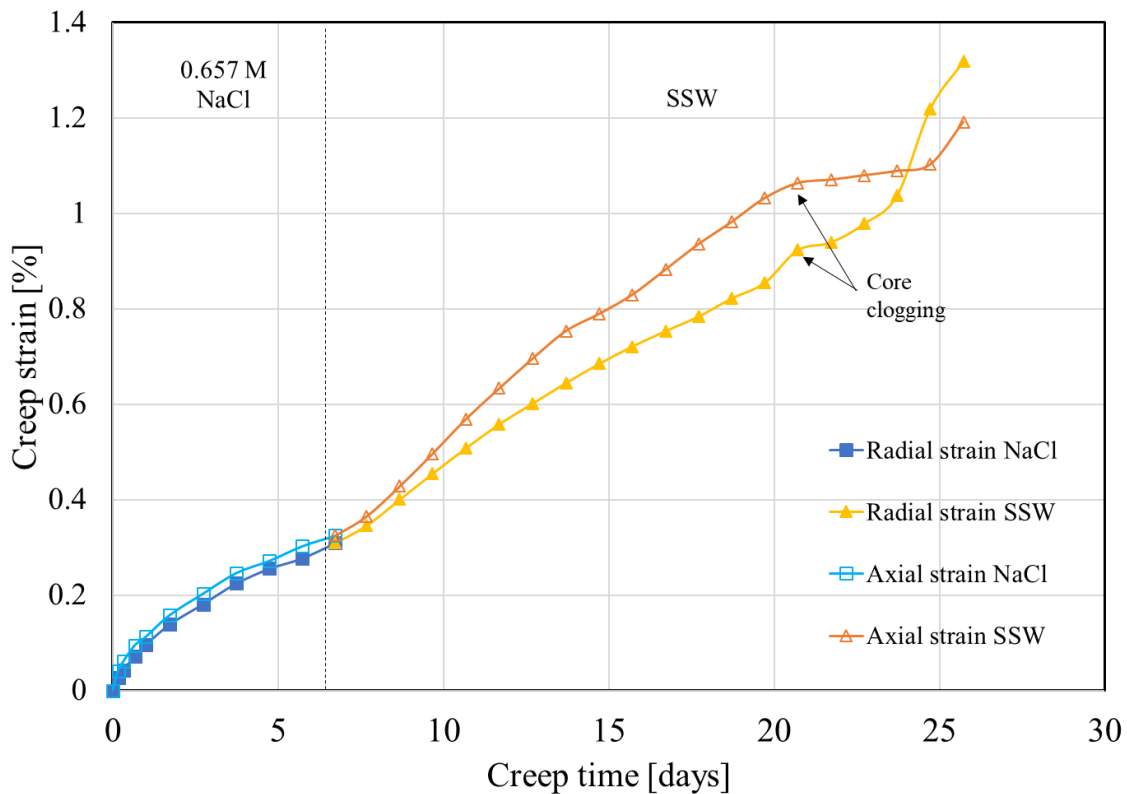
Figure 4.15 Axial and radial strain [%] vs creep time [days] for core E2 during creep phase at 50 MPa

Unloading

After a certain period of SSW injection during the creep phase, the steel tubing on the outlet side of the core got clogged due to precipitation in the system. Thereafter, the by-pass was opened to avoid pore pressure build up, and hydrostatic unloading started as shown in Figure 4.16. The piston pressure decreased smoothly from 4.7 to 0.6 MPa. While the confining pressure showed two major fluctuations at 0.7 and 2.2 hours when decreased from 50 to 1.2 MPa due to issues with the confining pump. At the same time when the fluctuations were found, the radial and axial strains followed approximately the same trend of these deviations. At 2.8 hours, the confining pressure continued to drop smoothly until 1.2 MPa was reached, and the axial strain decreased as well down to 1.3 %. However, the radial strain started to increase unexpectedly up to 2.0 % at to 7.75 hours and decreased by 0.1% in the last quarter of an hour.
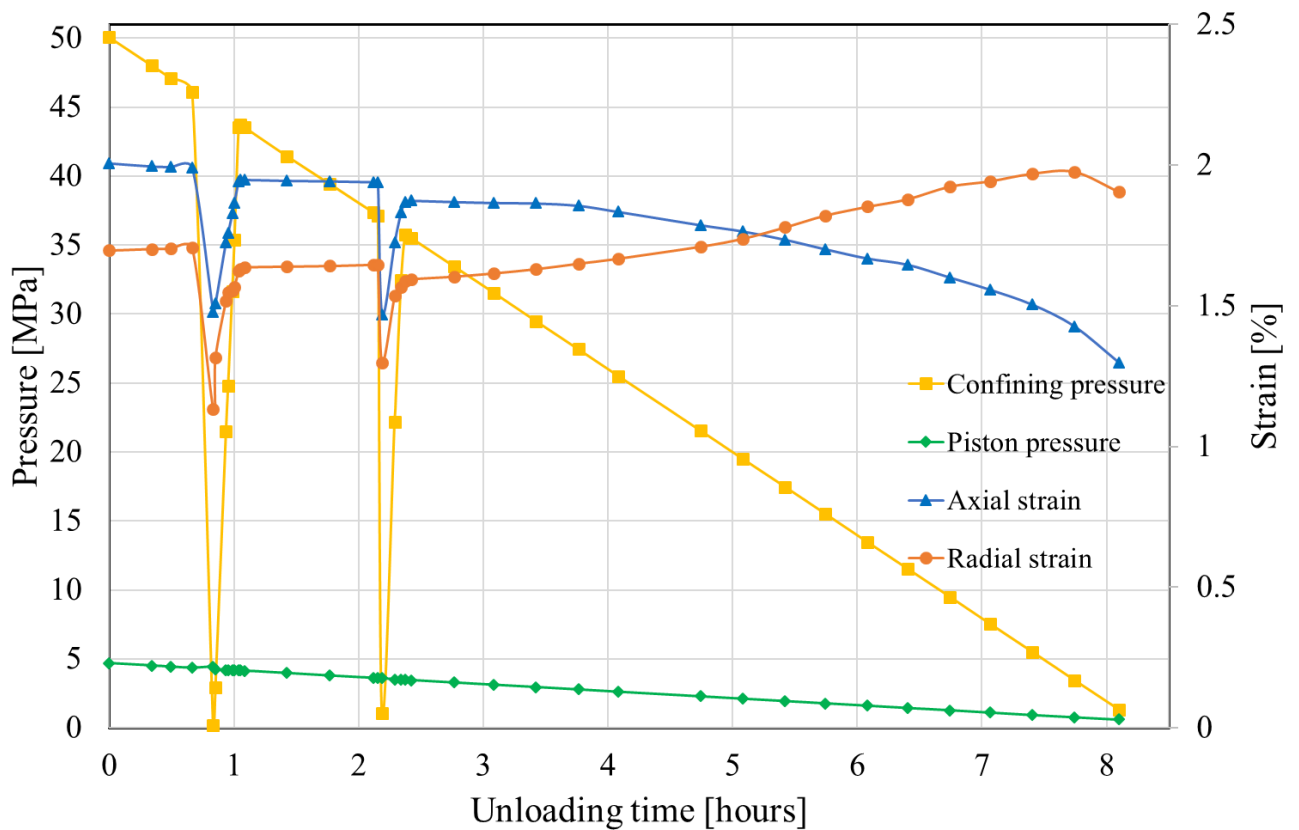
Figure 4.16 Axial and radial strain [%]and confining and piston pressure vs unloading time [hours] for core E2 during unloading

4.2.2 Chemical analysis E2

Ion Chromatography results

In the second experiment, the concentrations of sodium and chloride were measured like in the first experiment. Besides, the effluent profiles were produced based on the concentrations of the following ions: magnesium, calcium and sulphate. Figure 4.17 presents the ion chromatography analysis of E2 flooded with 0.657 M NaCl and SSW.

During NaCl flooding, the concentrations of sodium and chloride were generally stable throughout the whole experiment with values close to their original concentration, but some fluctuations have been found and they may possibly be caused by the dilution process. From the profile of E2, a small magnesium peak of ~ 0.002 mol/L and a larger calcium peak of ~ 0.01 mol/L are observed initially. The magnesium peak is followed by a decreasing trend until the concentration stabilizes. The calcium concentration also decreases down, but it shows a second peak with a maximum value of 0.005 mol/L which starts at day 3 and ends right before day 6 when it stabilizes at ~ 0.003 mol/L.

When the Synthetic Seawater (SSW) flooding commenced, a loss of magnesium is detected, where the effluent concentration increases gradually up to 0.035 mol/L at day 10, and with smaller fluctuations it increases over the next 4 days to around 0.037 mol/L. Then, two fluctuations with a value of 0.04 mol/L are followed by an increase in the magnesium concentration due to by-pass opening. Thus, the original concentration of 0.045 mol/L is slightly exceeded at the end of the test. On the other hand, upon SSW flow, calcium is produced immediately as its concentration displayed an increasing trend up to 0.018 mol/L, from day 8 to day 10, exceeding the original concentration of 0.013 mol/L, Thereafter, a decrease in the calcium concentration, down to ~ 0.014 mol/L at day 20, was found and followed by a stabilised production during three days, a further reduction to the original concentration of 0.013 mol/L, and eventually a slight augmentation due to by-pass opening. The evolution of sulphate concentration over time follows almost the same trend as that of calcium. The sulphate concentration in the effluent is below that of SSW during testing, and it exceeds the concentration of 0.024 mol/L when the by-pass is opened.
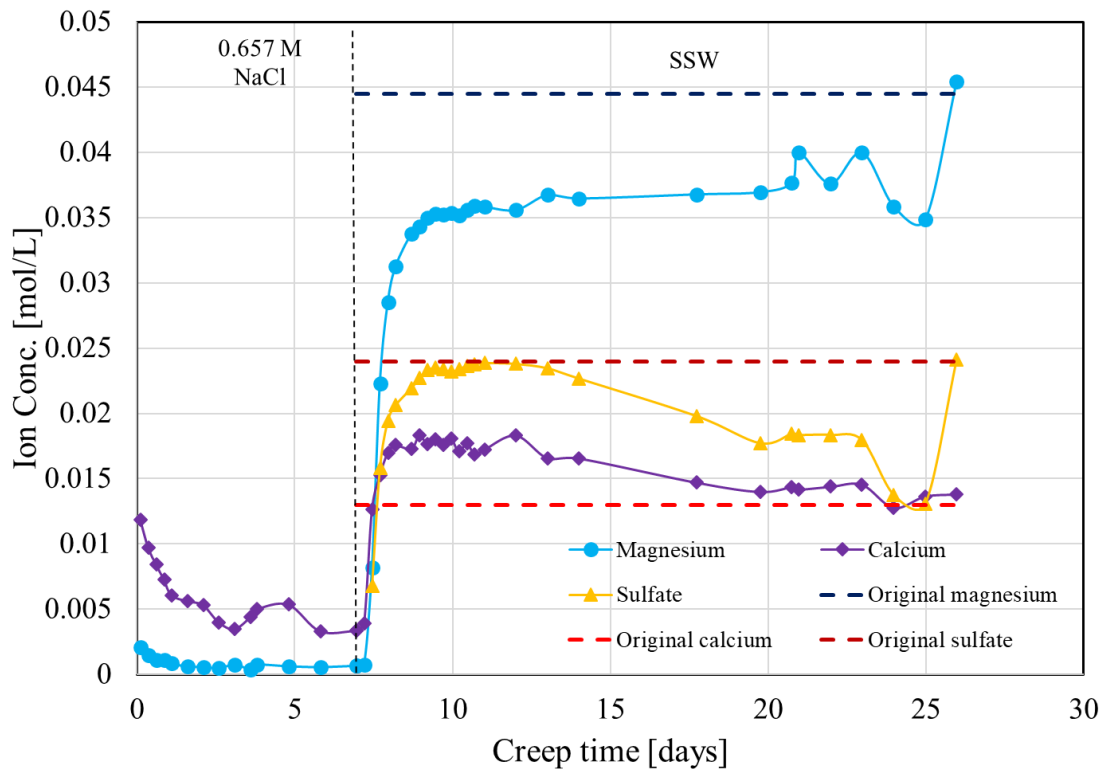
Figure 4.17 Chemical composition of effluents [mol/L] vs creep time [days] for core E2

Figure 4.18 displays the evolution in the ion concentration in (g/day) during the creep period until just before opening the by-pass. Calcium and magnesium production rates are calculated as in the first test. Additionally, the sulphate retention rate, which is expressed by negative numbers is calculated by multiplying the difference in ion concentrations, the flow rates and the molar weight of sulphate equal to 99.06 g/mol. The dissolution rate of calcium decreased by a factor of 4 from the start of NaCl injection until before changing the flooding brine.

Then, when SSW flooding commenced, the rates of calcium dissolution, as well as magnesium and sulphate retention, showed peaks, taking values of ~0.008, ~0.011 and ~0.02 g/day respectively. Thereafter, the weights of magnesium retained- and calcium produced per day decreased gradually and showed eventually an increase up to 0.001 and 0.008 g/day at 24 and 23 days respectively. The sulphate retention rate, however, decreased from the peak value of ~0.02 g/day down to almost zero after 11 days of creep, and started to increase again to a maximum value of 0.036 g/day.
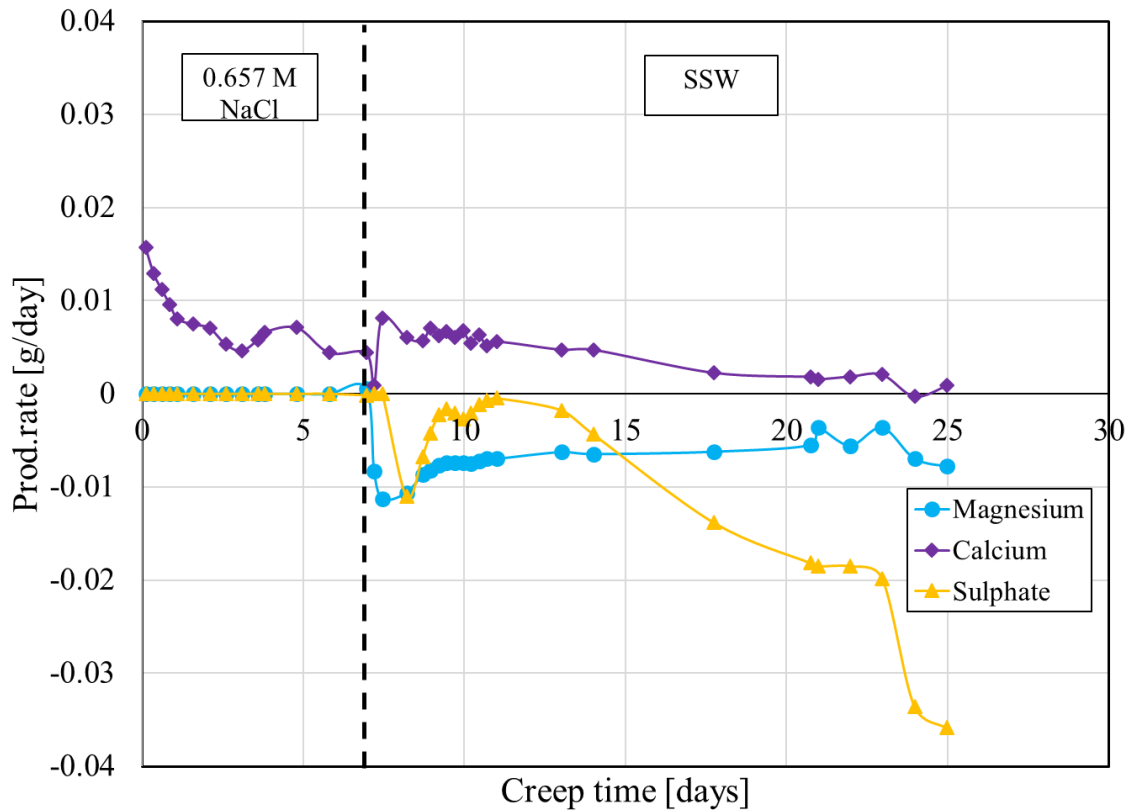
Figure 4.18 Evolution in the production rate of Mg^{2+} and Ca^{2+} [g/day] over creep time [days] for core E2

The integrated total magnesium and sulphate retained in the core based on the IC analysis were 0.12g (0.005 mol) and 0.25g (0.003 mol) respectively. Similarly, the integrated total calcium produced was 0.13g (0.003 mol). Thus, the theoretical mass change is around 0.24 g. However, this change is not in accordance with the measured difference in the mass before and after testing (table 4.4), which is equal to 4.36 g. A part of this deviation may be caused by the oil produced from the core. Besides, it is probably due to sulphate retention, not in the core, but in the outlet tubing, where anhydrite have precipitated and caused clogging. Furthermore, since the core is impure, silicate minerals may also have been produced.

Table 4.4 Properties of the Eldfisk core (E2) before and after test

	W_{dry} (g)	L (mm)	D (mm)	V_b (cm^3)	V_s (cm^3)	V_p (cm^3)	φ (%)	φ' (%)	ρ (g/cm^3)	ρ' (g/cm^3)
Before Testing	125.23	53.00	37.93	59.89	49.11	10.78	18.00	-	2.55	-
After Testing	120.87	52.52	37.58	58.22	45.06	13.16	22.61	23.20	2.68	2.70

Chapter 5 Discussion

In this section, based on mechanical tests and chemical analysis of effluents, results are discussed from geo-mechanical aspects point of view .The main issues range from explaining the compaction behaviour of hydrocarbon-producing chalk reservoirs in response to injected reactive brines in mechanical flow-through experiments to comparing the geo-mechanical behaviour of the reservoir core with previous results from onshore outcrop chalk.

5.1 Reservoir chalks -Hydrostatic loading

Hydrostatic loading followed by a hydrostatic creep phase were carried out during both tests so that the test results are as comparable as possible relative to each other and relative to previous tests performed on outcrop chalk. Experimental results from the isotropic loading of E2 and E3 showed nonlinear stress-strain relations when subjected to increased pressure. This can be seen from Figure 5.1, where the ratios of stress to strain are not constant for all pressures (Fjaer et al., 2008). The nonlinear behaviour is commonly noticed in rocks under large stresses, and it arises from many factors. One of which, is the presence of cracks in different sizes, particularly microcracks. As, the confining pressure increases, the microcracks are compressed to be closed resulting in a relatively increased initial strain. At a certain stress level, the cracks are closed, and the compression of the core becomes more difficult, thus, the rate of deformation becomes lower promoting a new elastic phase of linear stress-strain from which the bulk modulus is estimated.
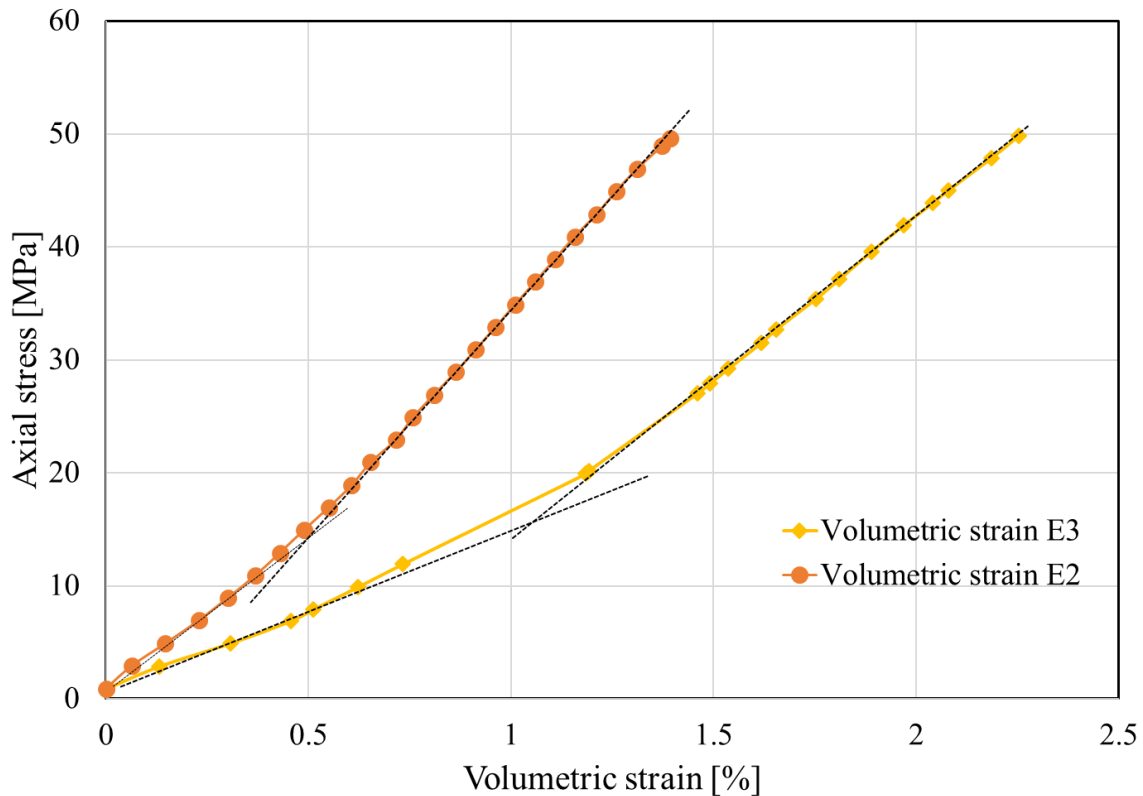
Figure 5.1 Axial stress [MPa] vs volumetric strain for cores E2 and E3 during hydrostatic loading

Even though both cores E2 and E3 are of the same type and they were flooded at the same temperature and with the same fluid, they showed different K-modulus values estimated to 3.9 versus 2.8 GPa. This dissimilarity is clarified by the difference in the magnitude of the radial strains. As reported by Figures 4.1 and 4.8, the radial strain of E3 is higher than that of E2 by a factor of 2.3, and this may be caused by the brusque and quick increase in the piston pressure while moving the piston down on core E3 prior to hydrostatic loading. The piston pressure jumped from 0.55 to 4.8 MPa in few seconds causing an increase in the diameter and shortening of core E3. Another possible reason back the difference in the volumetric strains may be the occurrence of cracks with different degrees in the two cores. As shown in Figures 5.2 and 5.3, the sample E3 contains more vertical cracks compared to E2 before testing, which may have a significant effect on the elastic properties of the material. Common for both tests is that the linear trends indicate that both cores showed notable resistance against the applied stresses. Moreover, they did not yield throughout the loading phase despite the sufficiently high confining pressures. However, the chalk material of the test specimen is not perfectly elastic, and it suffered a permanent deformation since the loading path and the unloading path were different. This is effect is known as hysteresis (Fjaer et al., 2008), and it is due to the dissipation

of some of the strain energy in the rock material. Hence the work done upon loading is not completely released upon unloading.

Figure 5.2 Core E2 before test

Figure 5.3 Core E3 before test

5.2 Reservoir chalks - Creep phase

5.2.1 NaCl

During flooding of E2 and E3 with NaCl, there were tiny dissolution of calcite as detected by ion chromatograph analysis. The calcium concentration in the effluents decreased down to 0.003 mol/L in both tests before changing the injected brine (Figures 5.4 and 5.5), implying that NaCl is weakly reactive towards the chalk surface. Likewise, previous studies showed that the interaction between outcrop chalk and NaCl is negligible. Andersen et al. (2018) observed that the concentration of produced calcium when flooding NaCl through Stevens Klink, Liège and Aalborg cores at 130°C stabilised at 0.002, 0.003 and 0.004 mol/L respectively. For Obourg Saint Vaast chalk, a production of 0.003 mol/L calcium was found at the same temperature (Abubeker, 2013). Moreover, previous NaCl experiments at 130 °C revealed that no new minerals were observed using geochemical analysis (M. Madland et al., 2011; M. Megawati et al., 2015; Mona W Minde et al., 2018b; Wang et al., 2016), and only smoothened corners and edges were found in some crystals (Andersen et al., 2018). With reference to Gautier, Oelkers,

and Schott (2001), the morphological changes affecting the calcite surfaces, such as grain rounding, can be activated by dissolution. Moreover, these changes in the calcite grains may lower the mechanical intergranular friction, and consequently enhance the creep development with time (Megawati Megawati et al., 2011).

5.2.2 MgCl₂

MgCl2 represents a simplified aqueous chemistry of seawater, and it is injected to specially investigate the effect of magnesium ions on the mechanical strength of chalk. When the chalk core, E3, is injected with MgCl2, a clear physical response is observed. The chemically induced creep deformation is reflected in the plot of axial strain along with the effluent concentration profiles as a function of creep time (Figure 5.4). A steady considerable amount of calcium, ~0.026 mol/l, was produced, while a substantial amount of magnesium, around 0.03 mol/l, was retained in the core as the MgCl2 flooding commenced. At the same time a continuous strain enhancement was found as response to the non-equilibrium nature of the rock-fluid interface. This enhanced creep have been proved in multiple earlier studies on outcrop chalk (Andersen et al., 2018; M. Madland et al., 2011; M. Madland et al., 2008; M. Megawati et al., 2015; Mona W Minde et al., 2018b; Wang et al., 2016). There are most probably several active mechanisms that play a major role in the compaction of chalk cores during MgCl2 flooding, yet according to earlier studies, dissolution of calcite and precipitation of magnesium bearing minerals are considered as the underlying processes at play. In line with dissolution/precipitation, the growth of magnesium-bearing minerals such as magnesite and the depletion of calcite have been detected and reported posterior to MgCl2 injection at 130°C (R. Korsnes et al., 2013; Zimmermann et al., 2015). Newly precipitated magnesium-bearing minerals have also been detected in the inlet of E2 by SEM-EDS analysis. The crystals were too small to identify, yet according to previous studies, some of these minerals seem to be magnesite (Figure 4.8).

Magnesium-rich minerals have higher densities than calcite, thereby, less space is occupied in the core as magnesite and other magnesium-bearing minerals precipitate at the expense of calcite. This contributes most likely in the enhancement of creep strain.

In addition to mineral replacement through dissolution/precipitation processes, the interaction between the pore fluid and the chalk surface may be attributed to adsorption and desorption of surface-active ions (Ahsan & Fabricius, 2010; Jaspreet S. Sachdeva et al., 2019a). When MgCl2 brine is flooded through chalk, chemical reactions are induced due to non-equilibrium between the brine and the calcite surface. Thereby, a new equilibrium is established as the magnesium

ions adsorb on available chalk surface sites and as calcium ions desorb from the internal surface. (Anders Nermoen et al., 2018; Jaspreet S. Sachdeva et al., 2019a) pointed to that adsorption give rise to lower internal force at granular contacts by the increased disjoining pressure, which governs the grain movement. When time comes to play, adsorption and desorption are considered as limited processes that occur only within the few first pore volumes of the injected reactive brine because of the finite number of available surface sites(Jaspreet Singh Sachdeva et al., 2019b). Thereafter, the changes in magnesium and calcium concentrations in the effluents are dominated by the dissolution and precipitation processes.
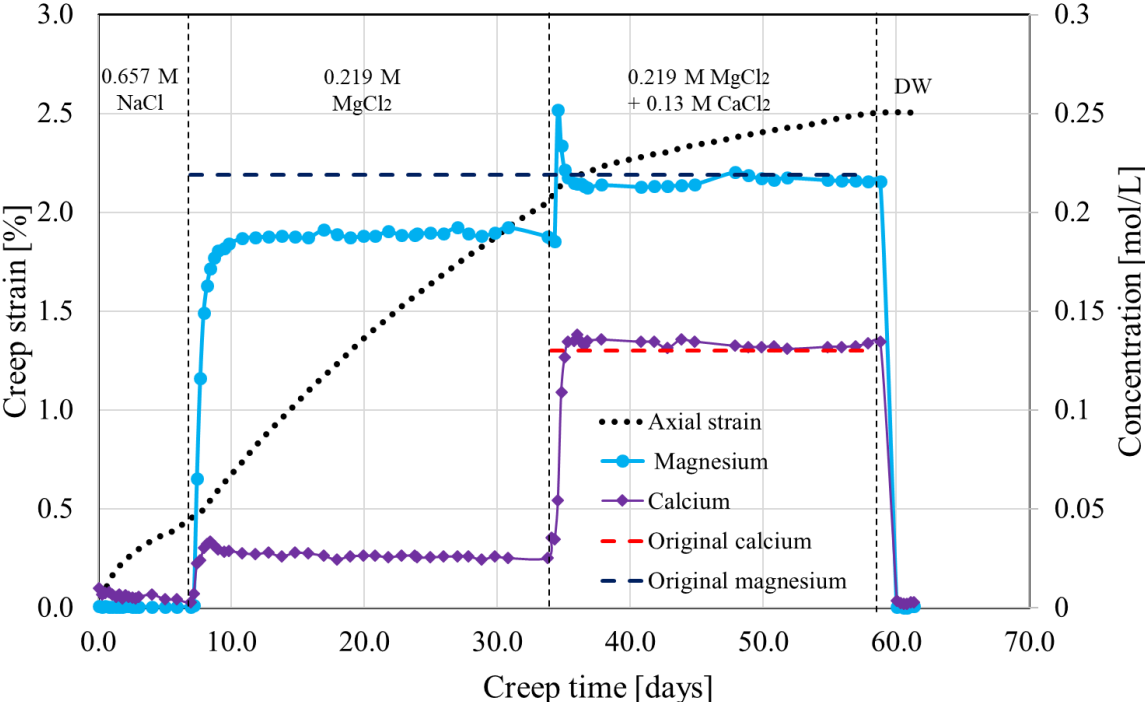
Figure 5.4 Schematic representation of axial creep strain and chemical composition of effluent vs time for core E3

It should be mentioned that, when starting MgCl$_2$ flooding, the Gilson pump showed a pressure value of 1.7 MPa, and the pore pressure was equal to 0.7 MPa, which it remained stable. However, the Gilson pressure did not remain constant, and started to increase, up to 6.3 MPa at the end of the MgCl$_2$ injection. However, the differential pressure, measured by the Gilson pump, seems not to affect the whole core significantly by affecting the creep behaviour. One hypothesis is that, only the inlet of the core is influenced by the reduced effective stress resulting from increased differential pressure. Supposing that rock-brine interactions at the inlet of the core create a flow barrier, then the rest of the core will be slightly influenced by the increased

differential pressure. This hypothesis is reasonable only if there is clogging at the inlet of the core due to chemical interplay between the chalk and the injected brine.

5.2.3 $CaCl_2$

Based on the chemical calculations performed by M. Madland et al. (2011), it is likely that the fluid in the pores is undersaturated with respect to calcium, while at the same time the aqueous solution is supersaturated with some other minerals, which precipitate out. Thus, the total produced calcium, which exceeds the limited number of surface sites indicates that the ion exchange or substitution does not prevail indefinitely, and that dissolution is the dominating mechanism. Then, adding sufficiently high calcium concentration to the $MgCl_2$ brine, will shift the under-saturation state, and consequently hinder the calcite dissolution. This hypothesis has been investigated by Megawati Megawati et al. (2011) by adding 0.130 mol/L $CaCl_2$, containing ten times the calcium concentration present in seawater, to 0.219 mol/L $MgCl_2$.

The effect of calcium addition to the magnesium rich brine on the calcite dissolution and consequent creep compaction is studied in this thesis as well. As seen from Figure 5.4, during the period when $CaCl_2$ is added to the $MgCl_2$ brine, the magnesium and calcium concentrations lay steady around the ion concentrations of the injected brine as expected, indicating limited additional calcium production by dissolution of calcite and magnesium loss by precipitation. Consequently, the creep compaction rate showed a clear reduction, however, it did not stop as in the study by Megawati Megawati et al. (2011). The study by Megawati Megawati et al. (2011) showed that calcite dissolution ceased when the Liège chalk was flooded by $MgCl_2$ combined with $CaCl_2$ (Figure 5.7b) at a constant pressure of 11.6 MPa, which is consistent with the observed results for the reservoir core E2. However, the outcrop chalk showed severe reduction in the creep rate compared to the Eldfisk reservoir core most probably due to the difference in the effective pressures during creep.

It is noticed that when injecting the calcium saturated brine, the Gilson pressure increases further from 6.3 MPa to 9.9 MPa, which means it increased only by 3.6 MPa versus 6.3 MPa when $MgCl_2$ was injected. Thus, the exerted effective stress on the core when injecting $MgCl_2$ should result in lower creep strain due to higher effective stress, but this is not the case. The creep strain is much higher when only $MgCl_2$ is injected without calcium, which indicates the significance of chemical interactions at the chalk surface and how the time-dependent behaviour is controlled by the chemical composition of the injected brines.

2.2.4 Distilled Water (DW)

During DW injection to clean core E3, calcium and magnesium concentrations dropped significantly to almost zero. Accordingly, the axial creep strain fell drastically or actually stopped since minor to negligible chemical interactions take place. Jaspreet S. Sachdeva et al. (2019a) demonstrated such behaviour: Both unaged water-wet and aged mixed wet Kansas chalk samples were flooded with DW after being injected with $MgCl_2$, which led to a fall in the magnesium and calcium concentrations, and hence an immediate drop in the strain rate to almost zero. However, for E3, an increase in the diameter have been observed, as the core was still exposed to a confining pressure of 50 MPa. This may be explained by the increase in the pore pressure, which is probably caused by a blockage in the outlet tubing. The pore pressure increased from 0.7 MPa when distilled water injection started up to 8.3 MPa after one day before it dropped to 5.4 MPa around 61 days of creep, resulting in a decreased effective stress and thus an increased core diameter.

5.2.5 Synthetic Seawater (SSW)

Further, the effect of the major divalent ions i.e. magnesium, calcium and sulphate, on the mechanical response of the Eldfisk core E2, have been emphasised during the continuous flow of seawater throughout the creep phase. In Figure 5.5, both the axial creep strain and the concentrations of the potential determining ions in seawater (Mg^{2+}, Ca^{2+}, and SO_4^{2-}) present in the effluents are plotted versus creep time for core E2.

As seen in Figure 5.5, the test specimen shows a lower strength than when injected with NaCl. This is measured by the increase in the creep strain, as magnesium ions are retained in the core and calcium ions are produced. In interpreting the excess production of calcium and the loss of magnesium, the dissolution of calcite and precipitation of magnesium-bearing minerals are seemingly the ongoing processes during seawater injection.

Additionally, the concentration of sulphate ions decreased when flooding the core with seawater at 130°C. This decrease in sulphate ions, together with clogging in the outlet steel tubing after ~ 20 days of SSW injection, point toward the precipitation of new minerals such as anhydrite, $CaSO_4$ (Heggheim et al., 2005; Hiorth et al., 2008; M. Madland et al., 2008).To further check the strength of this assumption, the measured magnesium concentration and the additional amount of calcium ions in the effluent are summed up. The sum of magnesium and calcium concentrations have shown to be lower than the magnesium concentration of the injected brine, i.e. 0.0445 mol/L, indicating the occurrence of anhydrite precipitation, which is in accordance

with results acquired by (M. Madland et al., 2011). Following to anhydrite formation, the fluid in the pores would be undersaturated with respect to calcium, which promotes calcite dissolution.
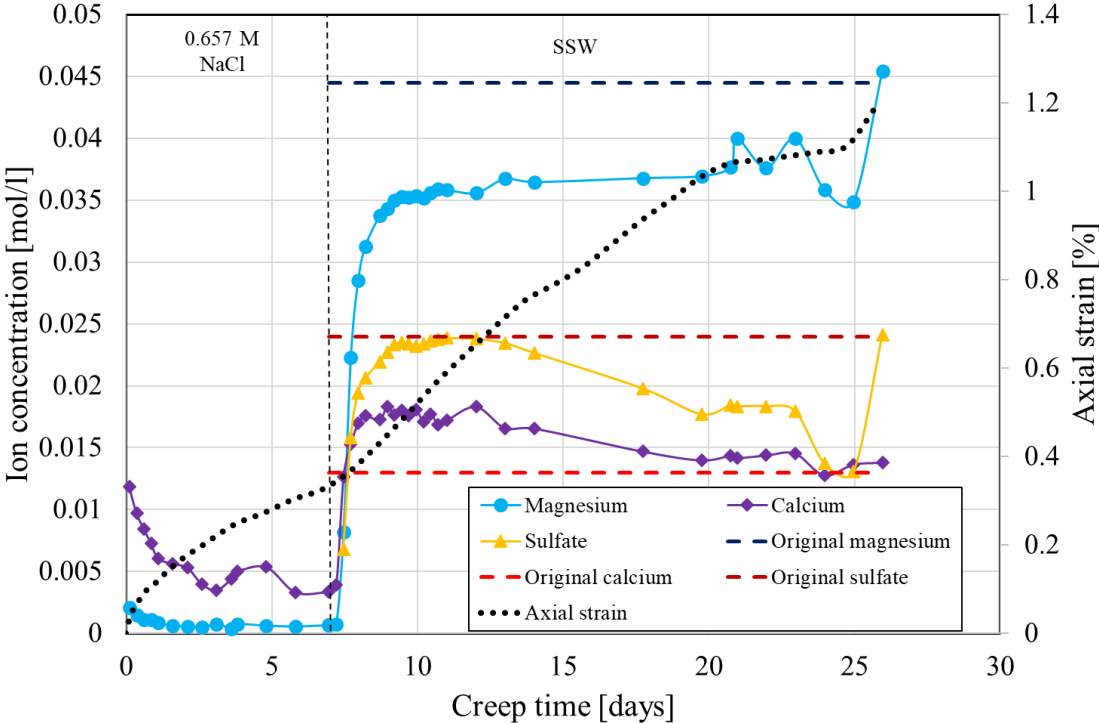
Figure 5.5 Schematic representation of axial creep strain and chemical composition of effluent vs time for core E2

In interpreting the loss of sulphate, another possible mechanism rather than calcite dissolution and anhydrite precipitation is also discussed. The retention of sulphate during the first pore volumes of SSW flooding may be explained in terms of adsorption (Hiorth et al., 2010; M Megawati et al., 2013). Sulphate ions adsorb to the calcite surface and generate a negative surface charge. When the negatively charged surfaces approach each other, significant repulsive forces known as the total disjoining pressure are created close to the granular contacts. The disjoining pressure resulting from rock-fluid interactions due to sulphate adsorption is a suggested key driving force for creep compaction. A study by M Megawati et al. (2013) showed that reduced strength of chalk cores exposed to sulphate-rich brine at 130 °C is attributed to adsorption of sulphate ions, this is valid, not only in the creep phase, but also during the hydrostatic loading phase. Thus, a combination of effects related to dissolution/precipitation and adsorption processes are suggested as the ongoing water wakening mechanisms during SSW flooding at 130°C.

An additional explanation of the creep behaviour when injecting SSW, is that the differential pressure measured by the Gilson pump increased throughout injection with SSW due to clogging in the outlet tubing. When the tubing got clogged around 21 days of creep, the pore pressure increased in the entire core from being initially equal to 0.7 MPa to a maximum of 15 MPa after ~23 of creep days resulting in reduced effective stress, and hence lower creep strain. Then, in order to reduce the pore pressure in the core, the by-pass valve was opened around day 25 of creep. Eventually, the pore pressure decreased, and hence the axial creep compaction increased as shown in Figure 5.5.

5.3 Comparison with outcrop chalk

Most of the previous experiments have been carried out on chalk from exposures, and rarely on offshore reservoir rocks from hydrocarbon deposits in the North Sea. Several outcrops around the world are considered as suitable analogues to North Sea reservoir chalk. However, a question that need to be answered is to which extent are the previous geo-mechanical studies, performed on onshore chalks, valid when comparing to reservoir chalk.

In an attempt to evaluate the feasibility of previous laboratory tests, results gained from injection of outcrop chalks with fluids containing potential determining ions are compared with the experimental results obtained from Eldfisk reservoir cores flooded with the same brines. Three kinds of outcrop chalks have been selected to be compared with the reservoir cores; Mons, Obourg St Vaast, and Liège outcrops.

Mons outcrop chalks are characterized by an extremely high carbonate content, higher than 99% (Andersen et al., 2018; M. Megawati et al., 2015) with only scares occurrence of quartz and possibly talc. The porosity of these chalks is in the range of 36 to 44% (Gaviglio et al., 1999). Chalk samples from Mons have been considered as good analogues to Ekofisk, Valhall and Dan reservoir chalks (Mona Wetrhus Minde, 2018a). Obourg Saint Vaast outcrop chalk samples are collected from the Saint Vast formation of the Mons basin, however they are relatively impure with calcite content ranging from around 90 to 95% (Anders Nermoen et al., 2016), and the porosity lies in the range of 40 to 42% (Abubeker, 2013). Liège chalks are also used as good analogues to Ekofisk chalks with regards to their mechanical behaviour (Collin et al., 2002). The outcrop chalk from Liège contains 95% carbonate minerals, and the remaining 5% consists of quartz, feldspar, smectite, mica and pyroxene as well as clinoptilolite, apatite and titanium oxide (M. L. Hjuler & Fabricius, 2009). The chalks from Liège have porosity

values between 40 and 43% (M. Madland et al., 2011; Risnes, Gjesdal, Landaas, & Madland, 1994; Schroeder, Bois, Maury, & Halle, 1998).

When it comes to the reservoir cores, as mentioned in section 2.2, the Eldfisk chalk samples from the Tor formation belonging to Bravo have shown intervals rich in non-carbonate minerals, and these intervals are characterised by low porosities between 20 and 25 %, which is almost found to match the porosity of the Eldfisk chalk samples studied in this work. E2 and E3 cores had porosities close to 20%. Even though the Eldfisk reservoir cores tested in this thesis and those studied by Madsen (2010) are sampled from different formations, Ekofisk and Tor respectively, the low porosity may E2 and E3 may correlate with high contents of kaolinite and quartz. This assumption is enforced by the SEM-EDS analysis of flooded E2, which show the occurrence of these minerals in the flooded core sample.

When introducing reactive brines, outcrop chalk samples, similar to Eldfisk reservoir core, generally follow a trend where the mechanical strength decreases as the water weakening effect is activated by the divalent ions present in the injected brine (R. Korsnes et al., 2006; M. Madland et al., 2011; Megawati Megawati et al., 2011). However, it is difficult to compare the degree of creep deformation because of the difficulty of finding laboratory experiments carried out with a high confining pressure as in this experiment. Yet, the change in the individual ion concentrations in the sampled effluents can be compared.

5.3.1 $MgCl_2$

In a previous master thesis, Veen (2012) demonstrated the dissolution of calcite and precipitation of magnesium-bearing minerals during flooding of $MgCl_2$ through Mons chalk (MS4), which has a porosity of 43.3%. The time evolution of the ion concentration of magnesium and calcium as well as the axial creep strain for MS4 at 130℃ during the creep phase at 12 MPa is plotted in Figure 5.6b.

In another master thesis, Obourg Saint Vaast chalk cores (OB SV), have been studied by Abubeker (2013) to understand which effects the flooding brines and the presence of fractures have on the mechanical properties of chalks. Thereby, an intact OB SV6 and a fractured OB SV4 have been injected by a magnesium-rich brine at 130℃ during the creep phase at a constant pressure of 12 MPa (Figures 5.6c and 5.6d). Prior to testing the cores had porosities of 40.8 and 40.5% respectively.

Figure 5.6 Axial strain and chemical composition of effluents [mol/L] vs creep time [days] for the reservoir core (a) E3 and outcrops (b) MS4 from (Veen, 2012), (c) OB SV6, and (d) OB SV4 from (Abubeker, 2013)

As Shown in Figure 5.6, all cores have been injected for periods between 5 and 7 days of creep with NaCl prior to $MgCl_2$ flow. This procedure is typically carried out in order to create baseline results used to lower or eliminate the impact of chemical effects. The reservoir core (Figure 5.6a) and the outcrops showed minute dissolution of calcite when flooding NaCl.

Then, when flooding with the Mg-rich brine, the results shown in Figure 5.6 fall into two groups, pure chalk group consisting of MS4 and impure chalk group consisting of the reservoir core and OB SV cores. Clean chalk from Mons displayed a delayed response with a low compaction rate followed by creep enhancement and higher compaction rates later on. The time-dependent behaviour is reflected in the effluent profile (Figure 5.6b), which shows decreasing calcium effluent concentration during the creep delay period and increasing calcium production until reaching a stable states during the creep acceleration period. Accordingly, the magnesium showed an opposite behaviour compared to the calcium profile, i.e. the magnesium concentration showed a peak before stabilizing during the creep delay period and the accelerated creep respectively.

For impure E3, OB SV 4 and OB SV6, dissolved calcium concentration showed an immediate increase, which is reflected in the creep strain. The time-dependent behaviour displayed an immediate enhancement and continuous compaction with no delay or acceleration phases.

From these observations, it is clear that pure chalks require higher amount of calcite to dissolve so that any creep acceleration can be found, while for impure chalks, the non-carbonate content is obviously involved in the chemical alteration resulting in an immediate creep development. Thus, the water weakening effect seem to be governed by the rock mineralogy in addition to the ionic composition of the injected brines. Thereby, it is essential to select the appropriate substitute for reservoir chalks when studying water weakening in reservoir chalks.
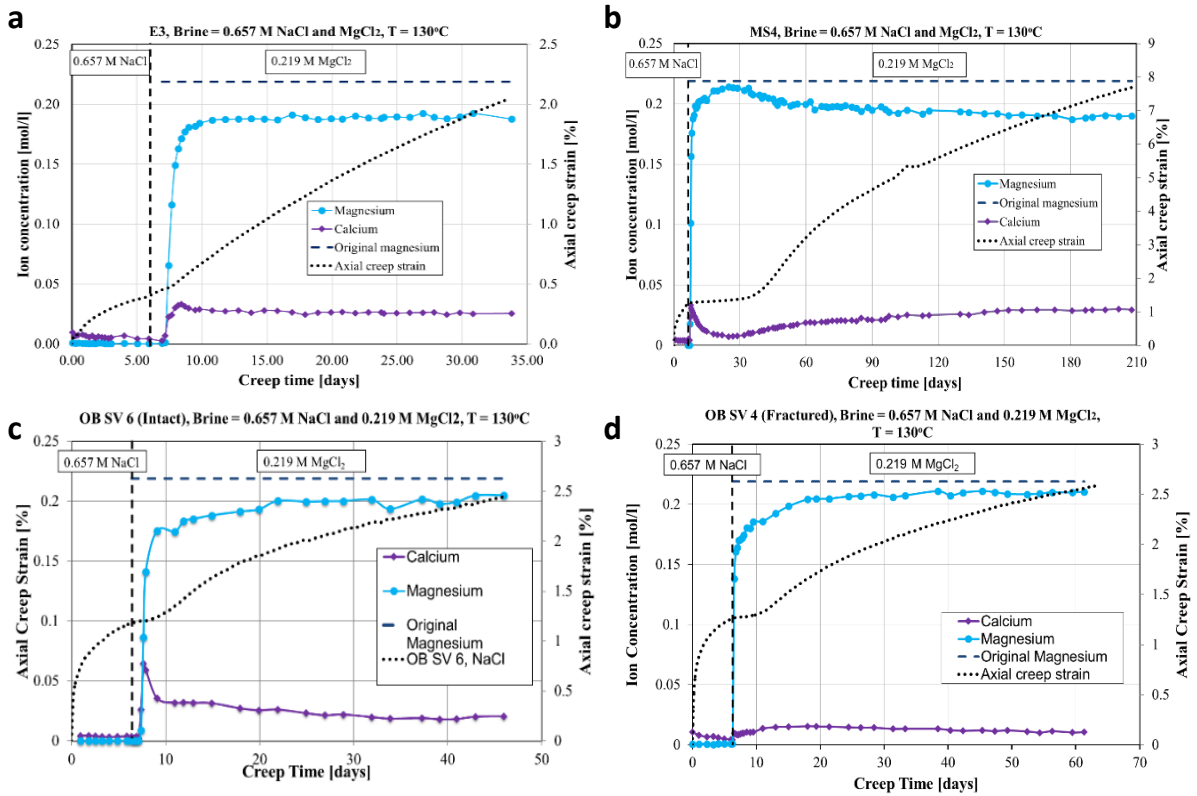
5.3.2 CaCl$_2$

Figure 5.7 Axial strain and chemical composition of effluents [mol/L] vs creep time [days] for the reservoir core (a) E3 and outcrop core (b) LEM3 modified after (Megawati Megawati et al., 2011)

The study by Megawati Megawati et al. (2011) demonstrated from the effluent analysis that the calcite dissolution and mineral precipitation ceased when the Liège chalk (LEM3), with porosity equal to 43%, was flooded by MgCl$_2$ combined with CaCl$_2$ at 130°C (Figure 5.7b), which is consistent with the observed results for the reservoir core E3 (Figure 5.7a). However, the outcrop chalk showed a severe reduction in the creep rate compared to the Eldfisk reservoir core. This may possibly be attributed to the mineralogy difference between Eldfisk and Liège cores. The difference in the creep rate may also be caused by the high constant creep stress in this work, 50 MPa versus only 11.6 MPa in the experiment performed by (Megawati Megawati et al., 2011).

5.3.3 Synthetic Seawater (SSW)

In addition to studying the effect of MgCl₂ injection on the water weakening of chalks, (Abubeker, 2013) did also investigate the effect of SSW on Intact and fractured Obourg St Vaast cores, OB SV 9 and OB SV 12 accordingly, at the same temperature and creep pressure mentioned previously, i.e. 130℃ and 12 MPa. It should also be mentioned that both cores had an initial porosity of 41.3%.

The significance of synthetic seawater weakening at high temperature, 130℃, has also been addressed by Reidar Inge Korsnes in 2012, but this work has not been published. The experiment consisted of testing the geo-mechanical behaviour of a Liège chalk core (L7), with porosity equal to 41.2%, during the creep phase at a confining pressure of 11 MPa.
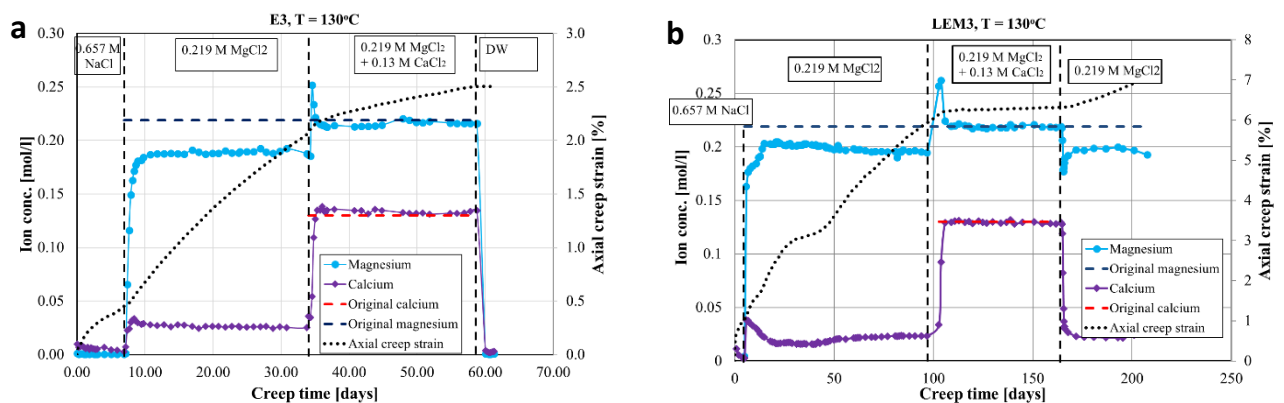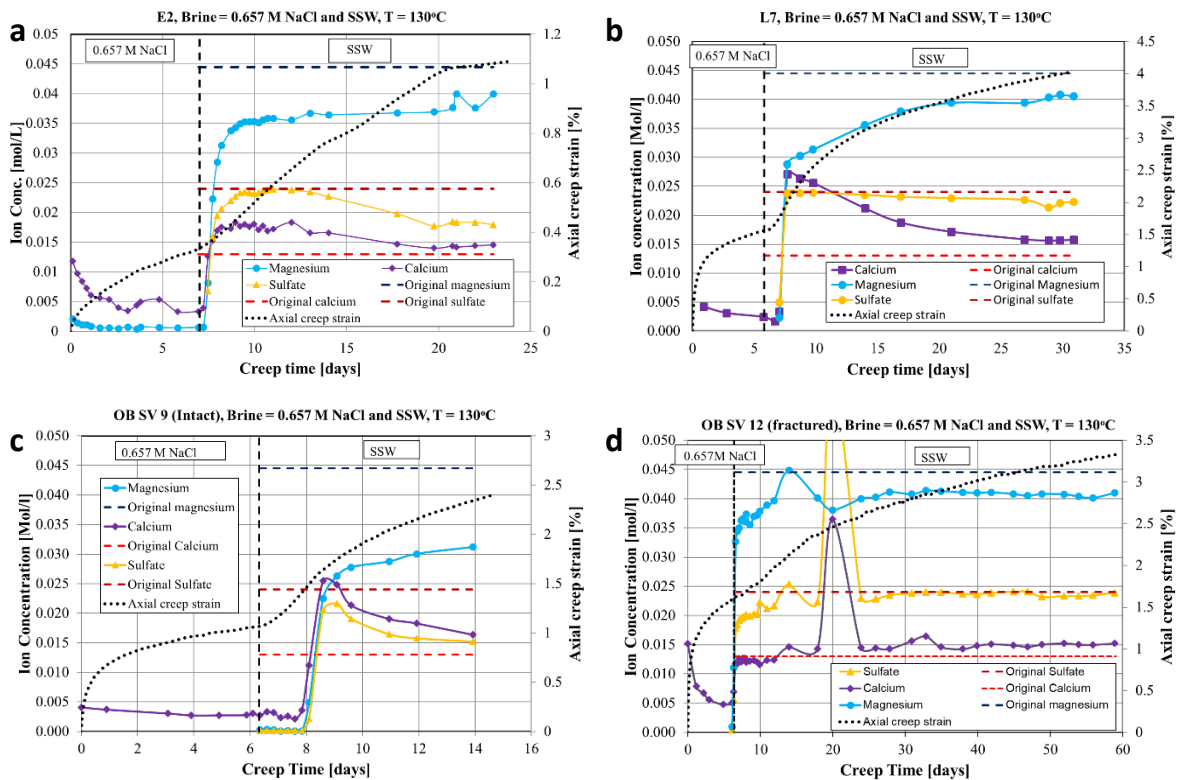

Figure 5.8 Axial strain and chemical composition of effluents [mol/L] vs creep time [days] for the reservoir core (a) E2 and outcrops (b) L7 from Reidar Inge Korsnes (2012), (c) OB SV 9, and (d) OB SV 12 from(Abubeker, 2013)

Figure 5.8 displays the observations of changes in the calcium, magnesium and sulphate concentrations when injecting SSW during the creep phase for Eldfisk reservoir core (E2) and outcrop chalk cores from Liège core (L7) and Intact and fractured Obourg St Vaast cores (OB SV9) and (OB SV12) respectively, as well as the corresponding time-dependent axial strains. When flooding with SSW, the concentrations of calcium, magnesium, and sulphate starts to increase for the reservoir core E2 and the outcrops, and the interplay between the chalks and ions in the SSW is immediately reflected in the creep deformation. The axial strain is immediately enhanced, and it develops over time. Thus, these results indicate the coupled nature of the brine chemistry and the corresponding creep.

However, some differences in the effluent concentrations may be seen. For instance, for Liège (L7) and the fractured Obourg St Vaast (OB SV 12), the sulphate concentration stay close to its original concentration, but this is not the case for the intact OB SV 9 and E3 for which the concentrations started to increase to the original concentration before clear drops are observed (Figure 5.8). In addition, high amounts of magnesium are retained in E2, higher by a factor of 1.9, compared to L7 and OB SV 12, but the magnesium loss in E2 is lower by a factor of 1.7 relative to OB SV 9 during the same time span. These observations probably indicate that precipitation of anhydrite do not occur with the same degree for the studied cores.

5.4 Active factors in brine-rock systems

When subjected to different aqueous chemistry, there seems to be a clear physical response for both reservoir and outcrop chalk cores. This is in line with the results reported by (Abubeker, 2013; Megawati Megawati et al., 2011; Veen, 2012) and the present work. However, the water-induced strain is not only governed by the ionic composition of the injected brine. Research have shown that also the diagenetic processes, the primary mineralogical composition of rocks, porosity, the presence of fractures, and effectives stresses seem to be active factors in controlling the chemo- mechanical interactions.

5.4.1 Effect of non-carbonate content

Several authors (Andersen et al., 2018; Fabricius & Borre, 2007; Morten Leth Hjuler & Fabricius, 2007; M. L. Hjuler & Fabricius, 2009; M. Madland et al., 2011; Mona W Minde et al., 2018b; Strand et al., 2007) have empathized the significance of investigating the effect of the non-carbonate content on the brine-chalk system. Non-carbonate minerals are often associated with silicate-bearing minerals such as quartz and different forms of clay, and they commonly fill the intergranular space and hold the calcite minerals together by acting as contact

cement. M. Madland et al. (2011) observed, while flooding Liège cores with $MgCl_2$ for ~ 17 days, that silicate minerals dissolved and re-precipitated to form a new phase of silicates. This observation is supported by geochemical analyses performed by Zimmermann et al. (2015) on Liège cores flooded during a longer period of 516 days with $MgCl_2$. with reference to Fabricius and Borre (2007), the formation of new phases of silicate minerals containing calcium may give rise to enhanced solubility of calcite. Moreover, sliding off of the support carried by the granular contact points may result from the dissolution of non-carbonate minerals, hence the chalk deformation is furthered (M. Megawati et al., 2015).

For pure chalk from Mons (Figure5.6b), there is minute contribution from the dissolution of non-carbonate minerals, thereby, the creep development is characterized by a time lag (Veen, 2012). The delayed response is possibly associated with the time required for calcite to dissolve and overcome the intergranular friction. This is not the case for the impure chalk from Eldfisk, which is characterised by an immediate creep compaction induced by dissolution/precipitation processes when magnesium-rich brines are injected. It can be concluded that the knowledge of the primary mineralogy of outcrop cores is indispensable when predicting the geo-mechanical behaviour of reservoir rocks.

5.4.2 Effect of fractures and porosity

The degree of water weakening is not only controlled by the mineralogical composition of rocks, but it is also affected by the presence of fractures and the amount of available pore spaces. For fractured chalk, the flow is initially focused within the fractures, and within the next time interval, it is in these regions the chemical interactions and compaction occur. Mona W Minde et al. (2016) showed that the presence of fractures may affect the fluid flow, and in turn the distribution of newly formed minerals. It was observed that the new grown fracture minerals showed a high concentration of magnesium, silicon, and aluminium relative to the surrounding matrix, which is most probably due to precipitation of crystals in the fractures.

For intact cores, contrarily, the injected brines flow through the entire core matrix allowing the occurrence of significant chemical reactions between the brine and the chalk surface. This is compatible with the results from the study by Abubeker (2013), which clearly shows that the loss of magnesium (Figures 5.6c and 5.8c), and sulphate (Figure 5.6d and 5.8d) by precipitation as well as the dissolution of calcite are higher for intact OB SV cores flooded entirely with $MgCl_2$ or SSW compared to fractured cores.

The influence of reactive brines on rock deformation have also been associated with porosity. Similar to fractures, the pore voids represent free spaces in which the flow is focused and chemical effects promoting deformation occur. In line with the porosity effect, it has been observed that compaction increases with increased porosity (Johnson, Rhett, & Siemers, 1989; Reidar I Korsnes et al., 2008). The Eldfisk cores studied in this thesis have a relatively low porosity, while the outcrop chalks presented in section 5.3 have porosities that are almost higher by a factor of two and they displayed much higher creep strain than the reservoir core even though four to five times lower creep stress are used.

Chapter 6 Conclusion

When searching for an optimized injection brine with the best-suited water composition for Enhanced Oil Recovery purposes, it is of great importance to study the fluid-rock interplay and induced changes in the geo-mechanical properties of the rock. For this objective, mechanical flow-through reservoir core experiments have been carried out during creep, the ion concentrations of the effluent water samples have been analysed chemically, and a sample from a tested core has been analysed by SEM-EDS. Thereafter, the geo-mechanical behaviour of Eldfisk cores have been compared with previous results obtained from onshore outcrop chalks. The main conclusions can be summarized as follows:

- The creep rate depends on the flooding brine

  - Synthetic seawater (SSW) and modified seawater ($MgCl_2$) enhanced the water weakening of Eldfisk cores compared to NaCl.

  - Adding calcium to $MgCl_2$ results in diminution of the creep strain.

- Retention of magnesium and production of calcium from the core in the case of SSW and $MgCl_2$ are discussed in terms of precipitation of secondary Mg-bearing minerals and dissolution of primary calcite. For SSW, anhydrite is also formed due to the presence of sulphate ions. However, for brines saturated with calcium dissolution is inhibited.

- Dissolution and precipitation processes are the key driving mechanisms for chemical creep compaction in these reservoir cores flooding experiments. This effect is attenuated when injecting with brines with excess calcium.

- Results gained from previous studies on water wet outcrop chalks seem to be valid also for reservoir cores in terms of the brine-rock chemical interactions and geo-mechanical behaviour.

Chapter 7 Future Work

This work is a part of a study which shows that results obtained from previous studies on water-wet chalks from exposures are also valid for reservoir cores such as Eldfisk cores. Thus, this work improves the understanding of reservoir chalk behaviour. Additional investigations regarding the behavior of reservoir rocks needs to be continued to enhance the accuracy of prediction of the reservoir behavior, and eventually contribute to find more efficient and smarter IOR techniques for the future.

Based on what have been observed, the amount of non-carbonate content in chalks do affect the degree of water weakening. Future work in this respect is thus to analyse the mineralogical composition and to quantify the non-carbonate content in unflooded pieces of the reservoir cores. This have not been carried out due to the presence of oil in the test specimens, which may cause severe damage to the electron microscopy tools. However, this limitation might be solved if the unflooded pieces of the cores are successfully washed, for example by the Soxhlet method.

SEM and EDS analysis have identified precipitations of magnesium-bearing minerals at the inlet of the Eldfisk core injected with Mg-rich brine, but most of the newly grown minerals have small grain sizes. Microscopic description on nano scale can therefore be useful to further specify the nature of these minerals, and thus better understand the water weakening mechanisms.

Moreover, the time frame of the experiments in this work have been limited. Thus, longer-term geo-mechanical testing of reservoir chalks is suggested in order to investigate the time dependency of rock-fluid interplay, as well as the propagation of the front of mineralogical alteration. The front propagation along the entire core might also be studied by electron microscopy.

Last but not least, the discrepancy between the mass loss estimated from ion chromatography analysis and the measured mass loss estimated from weight measurements before and after testing strengthens the necessity of a more detailed analysis of the effluent brines. A more specified analysis would help to determine whether non-carbonate minerals are produced, and to quantify the production of additional ions such as aluminium, silicon and iron if any is at play.

References

Abubeker, E. A. (2013). *Water weakening of chalks: comparison of intact and fractured cores*(Vol. 2013).

Ahsan, R., & Fabricius, I. L. (2010). *Sorption of magnesium and sulfate ions on calcite.* Paper presented at the 72nd EAGE Conference and Exhibition incorporating SPE EUROPEC 2010.

Andersen, P., Wang, W., Madland, M., Zimmermann, U., Korsnes, R., Bertolino, S. R. A., . . . Gilbricht, S. J. T. i. p. m. (2018). Comparative study of five outcrop chalks flooded at reservoir conditions: chemo-mechanical behaviour and profiles of compositional alteration. *121*(1), 135-181.

Biot, M., & Willis, D. J. J. a. M. (1957). The elastic coeff cients of the theory of consolidation. *24*, 594-601.

Biot, M. A. (1941). General theory of three-dimensional consolidation. *12*(2), 155-164.

Bjørlykke, K. (2014). Relationships between depositional environments, burial history and rock properties. Some principal aspects of diagenetic process in sedimentary basins. *Sedimentary Geology, 301*, 1-14. doi:https://doi.org/10.1016/j.sedgeo.2013.12.002

Bjørlykke, K., Høeg, K. J. M., & Geology, P. (1997). Effects of burial diagenesis on stresses, compaction and fluid flow in sedimentary basins. *14*(3), 267-276.

Carlberg, B. L. (1973). *Solubility of Calcium Sulfate in Brine*. Paper presented at the SPE Oilfield Chemistry Symposium, Denver, Colorado. https://doi.org/10.2118/4353-MS

Charlez, P. A. (1991). *Rock mechanics: theoretical fundamentals* (Vol. 1): Editions Technip.

Collin, F., Cui, Y. J., Schroeder, C., & Charlier, R. (2002). Mechanical behaviour of Lixhe chalk partly saturated by oil and water: experiment and modelling. 897-924. doi:10.1002/nag.229

Croize, D., Renard, F., & Gratier, J.-P. (2013). Compaction and porosity reduction in carbonates: A review of observations, theory, and experiments. In *Advances in Geophysics* (Vol. 54, pp. 181-238): Elsevier.

Delage, P., Schroeder, C., & Cui, Y. J. J. a. p. a. (2008). Subsidence and capillary effects in chalks.

Fabricius, I. L., & Borre, M. K. (2007). Stylolites, porosity, depositional texture, and silicates in chalk facies sediments. Ontong Java Plateau – Gorm and Tyra fields, North Sea. *Sedimentology, 54*(1), 183-205. doi:10.1111/j.1365-3091.2006.00828.x

Fjaer, E., Holt, R. M., Horsrud, P., Raaen, A. M., & Risnes, R. (2008). *Petroleum related rock mechanics* (Second edition ed. Vol. 53). Amsterdam.

Gautier, J.-M., Oelkers, E. H., & Schott, J. J. G. e. C. A. (2001). Are quartz dissolution rates proportional to BET surface areas? *, 65*(7), 1059-1070.

Gaviglio, P., Vandycke, S., Schroeder, C., Coulon, M., Bergerat, F., Dubois, C., & Pointeau, I. (1999). Matrix strains along normal fault planes in the Campanian White Chalk of Belgium: structural consequences. *Tectonophysics, 309*(1), 41-56. doi:10.1016/S0040-1951(99)00131-6

Gutierrez, M., Øino, L., Høeg, K. J. R. M., & Engineering, R. (2000). The effect of fluid content on the mechanical behaviour of fractures in chalk. *33*(2), 93-117.

Haddadi, D. (2013). An investigation of permeability and porosity evolution of Kansas chalk under in-situ conditions. In: University of Stavanger, Norway.

Hardman, R. F. P. (1982). *Chalk reservoirs of the North Sea*.

Heggheim, T., Madland, M., Risnes, R., Austad, T. J. J. o. P. S., & Engineering. (2005). A chemical induced enhanced weakening of chalk by seawater. *46*(3), 171-184.

Hellmann, R., Renders, P. J., Gratier, J.-P., Guiguet, R. J. W.-r. i., ore deposits,, & Crerar, e. g. A. t. t. D. A. (2002). Experimental pressure solution compaction of chalk in aqueous solutions. Part 1. Deformation behavior and chemistry. *7*, 129-152.

Hermansen, H., Landa, G. H., Sylte, J. E., & Thomas, L. K. (2000). Experiences after 10 years of waterflooding the Ekofisk Field, Norway. *Journal of Petroleum Science and Engineering, 26*(1), 11-18. doi:https://doi.org/10.1016/S0920-4105(00)00016-4

Hermansen, H., Thomas, L. K., Sylte, J. E., & Aasboe, B. T. (1997). *Twenty Five Years of Ekofisk Reservoir Management*. Paper presented at the SPE Annual Technical Conference and Exhibition, San Antonio, Texas. https://doi.org/10.2118/38927-MS

Hiorth, A., Cathles, L., Kolnes, J., Vikane, O., Lohne, A., & Madland, M. (2008). *Chemical modelling of wettability change in carbonate rocks.* Paper presented at the 10th Wettability Conference, Abu Dhabi, UAE.

Hiorth, A., Cathles, L., & Madland, M. J. T. i. p. m. (2010). The impact of pore water chemistry on carbonate surface charge and oil wettability. *85*(1), 1-21.

Hiorth, A., Jettestuen, E., Cathles, L., & Madland, M. J. G. e. C. A. (2013). Precipitation, dissolution, and ion exchange processes coupled with a lattice Boltzmann advection diffusion solver. *104*, 99-110.

Hjuler, M. L., & Fabricius, I. L. (2007). *Diagenesis of Upper Cretaceous onshore and offshore chalk from the North Sea area*: DTU Environment.

Hjuler, M. L., & Fabricius, I. L. (2009). Engineering properties of chalk related to diagenetic variations of Upper Cretaceous onshore and offshore chalk in the North Sea area. *Journal of Petroleum Science and Engineering, 68*(3), 151-170. doi:https://doi.org/10.1016/j.petrol.2009.06.005

Japsen, P. (1998). Regional velocity-depth anomalies, North Sea Chalk; a record of overpressure and Neogene uplift and erosion. *AAPG Bulletin, 82*(11), 2031-2074. doi:10.1306/00AA7BDA-1730-11D7-8645000102C1865D

Japsen, P., & Bidstrup, T. J. B. o. t. G. S. o. D. (1999). Quantification of late Cenozoic erosion in Denmark based on sonic data and basin modelling. *46*, 79-99.

Japsen, P. J. C. (2000). Fra Kridthav til Vesterhav. Nordsøbassinets udvikling vurderet ud fra seismiske hastigheder. *24*, 165-173.

Jarvis, I. (2006). The Santonian-Campanian phosphatic chalks of England and France. *Proc. Geol. Assoc., 117*, 219-237.

Johnson, J. P., Rhett, D. W., & Siemers, W. T. (1989). Rock mechanics of the Ekofisk reservoir in the evaluation of subsidence. *JPT. Journal of Petroleum Technology, 41*(7), 717-722. doi:10.2118/17854-PA

Kennedy, W., Brooks, J., & Glennie, K. (1987). Sedimentology of Late Cretaceous–Palaeocene chalk reservoirs, North Sea Central Graben. *Petroleum Geology of North West Europe. Graham & Trotman, London, 469*, 481.

Korsnes, R., Madland, M., & Austad, T. (2006). *Impact of brine composition on the mechanical strength of chalk at high temperature.* Paper presented at the Eurock.

Korsnes, R., Strand, S., Hoff, Ø., Pedersen, T., Madland, M., & Austad, T. (2006a). *Does the chemical interaction between seawater and chalk affect the mechanical properties of chalk.* Paper presented at the Eurock.

Korsnes, R., Zimmermann, U., Madland, M., Bertolino, S., Hildebrand-Habel, T., & Hiorth, A. (2013). *Tracing Fluid Flow in Flooded Chalk under Long Term Test Conditions.* Paper presented at the 75th EAGE Conference & Exhibition incorporating SPE EUROPEC 2013.

Korsnes, R. I. (2007). *Chemical Induced Water Weakening of Chalk by Fluid-rock Interactions: A Mechanistic Study*: University of Bergen.

Korsnes, R. I., Madland, M. V., Austad, T., Haver, S., Røsland, G. J. J. o. P. S., & Engineering. (2008). The effects of temperature on the water weakening of chalk by seawater. *60*(3-4), 183-193.

Liteanu, E., Spiers, C., & De Bresser, J. J. T. (2013). The influence of water and supercritical CO2 on the failure behavior of chalk. *599*, 157-169.

Lockner, D. A. J. R. p., & constants, p. r. A. h. o. p. (1995). Rock failure. *3*, 127-147.

Lykke, M. M. (2005). Displacement of oil by waterflooding in fractured chalk. In: BYG DTU.

MacDonald, G. J. F. (1956). Experimental determination of calcite-aragonite equilibrium relations at elevated temperatures and pressures*. *American Mineralogist, 41*(9-10), 744-756. Retrieved from http://dx.doi.org/

Madland, M., Hiorth, A., Omdal, E., Megawati, M., Hildebrand-Habel, T., Korsnes, R., . . . Cathles, L. J. T. i. p. m. (2011). Chemical alterations induced by rock–fluid interactions when injecting brines in high porosity chalks. *87*(3), 679-702.

Madland, M., Midtgarden, K., Manafov, R., Korsnes, R., Kristiansen, T., & Hiorth, A. (2008). *The effect of temperature and brine composition on the mechanical strength of Kansas chalk.* Paper presented at the International Symposium SCA.

Madland, M. V., & Risnes, R. (2005). *Water weakening of chalk: A mechanistic study.* University of Stavanger, Norway, University of Stavanger.

Madsen, H. (2010). Silica diagenesis and its effect on porosity of upper Maastrichtian chalk - an example from the Eldfisk Field, the North Sea. *Geol. Surv. Den. Greenl. Bull.*(20), 47-50.

Megawati, M. (2015a). *Geochemical aspects of water-induced compaction in high-porosity chalks.* (no. 247). University of Stavanger, Faculty of Science and Technology, Department of Petroleum Engineering, Stavanger.

Megawati, M., Andersen, P. Ø., Korsnes, R. I., Evje, S., Hiorth, A., & Madland, M. V. J. P. F. I. E. n. P., Nov. (2011). The effect of aqueous chemistry ph on the time-dependent deformation behaviour of chalk experimental and modelling study. 16-18.

Megawati, M., Hiorth, A., Madland, M. J. R. m., & engineering, r. (2013). The impact of surface charge on the mechanical behavior of high-porosity chalk. *46*(5), 1073-1090.

Megawati, M., Madland, M. V., & Hiorth, A. (2015). Mechanical and physical behavior of high-porosity chalks exposed to chemical perturbation. *Journal of Petroleum Science and Engineering, 133*, 313-327. doi:https://doi.org/10.1016/j.petrol.2015.06.026

Minde, M. W. (2018a). Mineral Replacements in Flooding Experiments Linked to Enhanced Oil Recovery in Chalk. In M. V. Madland & U. Zimmerman (Eds.): University of Stavanger, Norway.

Minde, M. W., Wang, W., Madland, M. V., Zimmermann, U., Korsnes, R. I., Bertolino, S. R., . . . Engineering. (2018b). Temperature effects on rock engineering properties and rock-fluid chemistry in opal-CT-bearing chalk. *169*, 454-470.

Minde, M. W., Zimmermann, U., Madland, M. V., Korsnes, R. I., Schulz, B., & Audinot, J.-N. (2016). *Fluid–flow during EOR experiments in chalk: insights using SEM–MLA, EMPA and Nanosims Applications.* Paper presented at the International Symposium of the Society of Core Analysts. Colorado, USA.

Nermoen, A., Korsnes, R., Haug, S. A., Hiorth, A., & Madland, M. (2014). *The dynamic stability of chalks during flooding of non-equilibrium brines and CO2.* Paper presented at the Fourth EAGE CO2 Geological Storage Workshop.

Nermoen, A., Korsnes, R. I., Aursjø, O., Madland, M. V., Kjørslevik, T. A. C., & Østensen, G. (2016). How Stress and Temperature Conditions Affect Rock-Fluid Chemistry and Mechanical Deformation. In (pp. 2). Lausanne.

Nermoen, A., Korsnes, R. I., Madland, M. V., & Hiort, A. (2015). Porosity and permeability development in compacting chalks during flooding of nonequilibrium brines: Insights from long-term experiment. doi:https://doi.org/10.1002/2014JB011631

Nermoen, A., Korsnes, R. I., Storm, E. V., Stødle, T., Madland, M. V., & Fabricius, I. L. J. G. (2018). Incorporating electrostatic effects into the effective stress relation—Insights from chalk experiments. *83*(3), MR123-MR135.

Newman, G. H. J. J. o. P. T. (1983). The effect of water chemistry on the laboratory compression and permeability characteristics of some North Sea chalks. *35*(05), 976-980.

Norwegian Petroleum Directorate, Ekofisk Field, viewed on 2nd February, 2019

Omdal, E. (2010). *The mechanical behavior of chalk under laboratory conditions simulating reservoir operations.* (no. 104). University of Stavanger, Faculty of Science and Technology, Department of Petroleum Engineering, Stavanger.

Powell, B. N., & Lovell, G. L. (1994). *Mechanisms of chalk compaction.* Paper presented at the Rock Mechanics in Petroleum Engineering.

Risnes, R. (2001). Deformation and yield in high porosity outcrop chalk. *Phys. Chem. Earth Pt. A-Solid Earth Geod., 26*(1-2), 53-57.

Risnes, R., Flaageng, O. J. O., science, G., & technology. (1999). Mechanical properties of chalk with emphasis on chalk-fluid interactions and micromechanical aspects. *54*(6), 751-758.

Risnes, R., Gjesdal, S. A., Landaas, T. L., & Madland, I. (1994). *Changes in mechanical properties of chalk caused by deformation and by pore pressure*. Paper presented at the Rock Mechanics in Petroleum Engineering, Delft, Netherlands. https://doi.org/10.2118/28136-MS

Risnes, R., Haghighi, H., Korsnes, R., & Natvik, O. J. T. (2003). Chalk–fluid interactions with glycol and brines. *370*(1-4), 213-226.

Risnes, R., Madland, M., Hole, M., Kwabiah, N. J. J. o. P. S., & Engineering. (2005). Water weakening of chalk—Mechanical effects of water–glycol mixtures. *48*(1-2), 21-36.

Sachdeva, J. S., Muriel, H., Nermoen, A., Korsnes, R. I., Madland, M. J. E., & Fuels. (2019b). Chalk Surface Area Evolution during Flow of Reactive Brines: Does Oil Play a Role?

Sachdeva, J. S., Nermoen, A., Korsnes, R. I., & Madland, M. V. (2019a). Impact of Initial Wettability and Injection Brine Chemistry on Mechanical Behaviour of Kansas Chalk (Book review). In.

Scholle, P. A. (1977). Chalk diagenesis and its relation to petroleum exploration; oil from chalks, a modern miracle? *AAPG Bulletin, 61*(7), 982-1009. doi:10.1306/C1EA43B5-16C9-11D7-8645000102C1865D

Scholle, P. A., & Kinsman, D. J. J. (1973). Diagenesis of upper Cretaceous chalks from North Sea, England and Northern Ireland. *The American Association of Petroleum Geologists Bulletin, 57*(4), 803-804. doi:10.1306/83D90C6E-16C7-11D7-8645000102C1865D

Schroeder, C., Bois, A. P., Maury, V., & Halle, G. (1998). *Water/Chalk (or Collapsible Soil) Interaction: Part II. Results of Tests Performed In Laboratory On Lixhe Chalk to Calibrate Water/Chalk Models*. Paper presented at the SPE/ISRM Rock Mechanics in Petroleum Engineering, Trondheim, Norway. https://doi.org/10.2118/47587-MS

Sheng, J. (2010). *Modern Chemical Enhanced Oil Recovery: Theory and Practice*: Elsevier Science.

Skempton, A. (1961). Effective stress in soils, concrete and rocks-Pore pressure and suction in solis. Conference of the British National Society. In: Butterworths London.

Stoddart, D. P., Hall, P. B., Larter, S. R., Brasher, J., Li, M., & Bjorøy, M. (1995). The reservoir geochemistry of the Eldfisk Field, Norwegian North Sea. *Geological Society,*

London, Special Publications, 86(1), 257-279. doi:10.1144/GSL.SP.1995.086.01.15 %J Geological Society, London, Special Publications

Strand, S., Hjuler, M. L., Torsvik, R., Pedersen, J. I., Madland, M. V., & Austad, T. (2007). Wettability of chalk; impact of silica, clay content and mechanical properties. *Petroleum Geoscience, 13*(1), 69-80. doi:10.1144/1354-079305-696

Strand, S., Høgnesen, E. J., & Austad, T. (2006). Wettability alteration of carbonates—Effects of potential determining ions (Ca2+ and SO42−) and temperature. *Colloids and Surfaces A: Physicochemical and Engineering Aspects, 275*(1), 1-10. doi:https://doi.org/10.1016/j.colsurfa.2005.10.061

Sulak, A. M., & Danielsen, J. (1988). *Reservoir Aspects Of Ekofisk Subsidence*. Paper presented at the Offshore Technology Conference, Houston, Texas. https://doi.org/10.4043/5618-MS

Terzaghi, K. J. C. o. t. p. i. o. c. f. h. t. c. S. A. d. W., Vienna. (1923). Die berechnung deer durchlässif-keitsziffer des tones aus dem verlauf der hydrodynamischen spannungserscheinungen. *132*.

Teufel, L. W., Rhett, D. W., & Farrell, H. E. (1991). *Effect of Reservoir Depletion And Pore Pressure Drawdown On In Situ Stress And Deformation In the Ekofisk Field, North Sea*. Paper presented at the The 32nd U.S. Symposium on Rock Mechanics (USRMS), Norman, Oklahoma. https://doi.org/

Teufel, L. W., & Warpinski, N. R. (1990). *Laboratory determination of effective stress laws for deformation and permeability of chalk*. Retrieved from

Veen, S. H. v. D. (2012). Water induced compaction of chalks with varying non-carbonate content : the effect of Mg2+ and pH of the injected brines. In: University of Stavanger, Norway.

Wade, J. M., Hough, E. V., Harrington, T. R., Valdal, J., & Pedersen, S. H. (1998). *Case History of Oil Well Performance Monitoring and Production Optimization in the Eldfisk and Ekofisk Fields, Norwegian North Sea*. Paper presented at the SPE International Oil and Gas Conference and Exhibition in China, Beijing, China. https://doi.org/10.2118/48847-MS

Wang, W., Madland, M. V., Zimmermann, U., Nermoen, A., Korsnes, R. I., Bertolino, S. R. A., & Hildebrand-Habel, T. (2016). Evaluation of porosity change during chemo-mechanical compaction in flooding experiments on Liege outcrop chalk. *Special Publication - Geological Society of London, 435*. doi:10.1144/SP435.10

Zhu, X., Mosher, C., Brewer, J., Gundersen, A., Scheepens, C., & Cao, J. (2012). *Geologic-to-seismic Modelling for Eldfisk SOA Reservoir Characterization-An Integrated Study*. Paper presented at the 74th EAGE Conference and Exhibition incorporating EUROPEC 2012.

Zimmermann, U., Madland, M. V., Nermoen, A., Hildebrand-Habel, T., Bertolino, S. A., Hiorth, A., . . . Grysan, P. J. A. B. (2015). Evaluation of the compositional changes during flooding of reactive fluids using scanning electron microscopy, nano-secondary ion mass spectrometry, x-ray diffraction, and whole-rock geochemistryCompositional Changes during Flooding. *99*(5), 791-805.